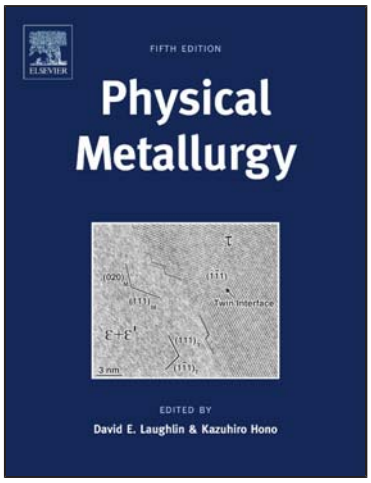

From Raabe, D., 2014. Recovery and Recrystallization: Phenomena, Physics, Models, Simulation. In: Laughlin, D.E., Hono, K. (Eds.), Physical Metallurgy, pp. 2291–2397.
ISBN: 9780444537706

Elsevier

23 Recovery and Recrystallization: Phenomena, Physics, Models, Simulation

Dierk Raabe, Max-Planck-Institut für Eisenforschung, Düsseldorf, Germany

23.1 Phenomena, Terminology, and Methods: Recovery and Recrystallization

23.1.1 Basic Phenomena and Terminology

In engineering processing terms, severe plastic cold working is typically carried out for changing the shape of a metallic work piece. In physical metallurgy terms, cold deformation leads to the increase of the internal stored energy. This increase in the stored energy is microstructurally associated with the accumulation of lattice defects. More specific, the majority of the internal energy that is stored due to cold working of metals can be attributed to dislocations (Orowan, 1934; Taylor, 1934; Polanyi, 1934). Point defects such as vacancies and interstitials as well as interfaces arising from athermal processes such as deformation twinning or martensite formation contribute only a minor portion to the stored energy (Wever, 1924; Swan et al., 1963; Keh and Weissman, 1963).

During plastic straining only a relatively small fraction of the total deformation energy imposed through the tool actually remains stored in the material. The main part of this energy is dissipated as heat during cold working. This is also the reason why heavily cold-worked metallic alloys can become very hot upon plastic deformation with up to several 100 K of temperature increase when strained at high rates. Yet, the defect density that remains stored in heavily cold-worked metals is still high enough to serve as driving force for a number of nonequilibrium transformation phenomena that are usually summarized as recovery, recrystallization, and grain coarsening (Kalisher, 1881; Sorby, 1886, 1887; Stead, 1898; Rosenhain, 1914; Ewing and Rosenhain, 1899, 1900a, 1900b; Alterthum, 1922; Carpenter and Elam, 1920; Czochralski, 1927; Burgers and Louwerse, 1931). Typically, for these processes to occur, the total amount of cold working has to be above a certain critical threshold value, namely, typically 30–50% thickness reduction or above.

For many metals and alloys, the dislocation density increases from values of 10^{10}–10^{11} /m^2 in the annealed state to 10^{12}–10^{13} /m^2 after modest deformation and even up to 10^{16} /m^2 after very heavy deformation at low temperatures. When translating these values into an average spacing among the dislocations, we obtain 1 μm for weakly deformed materials and 10 nm for heavily deformed metals.

These high-lattice defect densities lead to changes in a number of properties, such as the electrical resistivity, hardness, strength, toughness, and ductility with the amount of cold working. Also, the corrosion behavior is altered since the potential changes around dislocations render deformed zones preferred attacking points to oxidation phenomena.

At the light optical scale, i.e. at a mesoscopic observation regime, the grains become elongated along the direction of cold working and their shapes are distorted. Often shear bands that are oblique mesoscopic inhomogeneities of high local deformation appear at higher stages of the plastic deformation. At an electron optical scale complex dislocation cell (DC) arrangements and twinning substructures evolve. The latter microstructure features are an essential characteristic when the stacking fault energy is low (of the order of 20–40 mJ/m^2). For materials with yet lower stacking fault energy deformation-induced martensitic transformations can take place. This is for instance the case for Cu-30 wt.% Zn brass (mechanical twinning), many highly alloyed austenitic Cr–Ni stainless steels and high-Mn containing TWIP (twinning-induced plasticity) and transformation-induced plasticity steels.

For the further downstream manufacturing of heavily cold-worked metals, the high strength and hardness that are also associated with a drop in ductility and toughness typically requires to first restore the original soft state of the material (Burke and Turnbull, 1952; Smith, 1948; Beck and Hu, 1966; Haessner, 1978; Humphreys and Hatherly, 1995, 2004; Doherty et al., 1997; Doherty, 2005).

In that context, recovery, recrystallization, and competitive grain coarsening are the most important and effective thermomechanical processing methods to render cold-worked metallic materials back into a softer and hence easily formable state (Kalisher, 1881; Sorby, 1886, 1887; Stead, 1898; Rosenhain, 1914; Ewing and Rosenhain, 1899, 1900a, 1900b; Alterthum, 1922; Carpenter and Elam, 1920; Czochralski, 1927; Burgers and Louwerse, 1931). Correspondingly, the microstructure as well as the mechanical and electrical properties of the crystalline materials observed after heavy plastic deformation can be restored back into their original states before conducting further manufacturing steps.

Static primary recrystallization starts when heating deformed metals to an elevated temperature (**Figure 1**). In practical terms this usually means holding the cold deformed materials at a temperature above about 1/3 of their respective absolute melting point for a certain period of time, typically 1 h. Higher recrystallization temperatures require in most cases much shorter annealing times. The relationship between plastic deformation, annealing temperature, and the resulting grain size is for specific alloys for practical applications often presented in terms of recrystallization diagrams (**Figure 2**) (Kalisher, 1881; Sorby, 1886, 1887; Stead, 1898; Rosenhain, 1914; Ewing and Rosenhain, 1899, 1900a, 1900b; Alterthum, 1922; Carpenter and Elam, 1920; Czochralski, 1927; Burgers and Louwerse, 1931). It should be noted though that in such diagrams the influence of chemical alloy variations and specifically also of the annealing time is often not taken into consideration. This means that even for practical purposes such recrystallization diagrams can only serve as a rough first guideline for assessing an appropriate softening heat treatment.

The term dynamic recrystallization refers to all recrystallization phenomena that occur during the plastic deformation (Doherty et al., 1997; Humphreys and Hatherly, 2004; Gifkins and Coe, 1951; Tamhankar et al., 1958; Rossard and Blain, 1960; Rossard, 1963; Sellars and Tegart, 1966; Drube and Stüwe, 1967; Stüwe, 1968; McQueen et al., 1976; Fritzmeier et al., 1979; Luton and Sellars, 1969; McQueen, 1968; Jonas et al., 1969; McQueen and Jonas, 1975; Sellars, 1978). Such phenomena hence typically occur when hot deforming the material at temperatures greater than about half of the absolute melting point.

The kinetics associated with the softening process during such an annealing treatment can be grouped into three main stages, namely, recovery, recrystallization, and competitive grain coarsening.

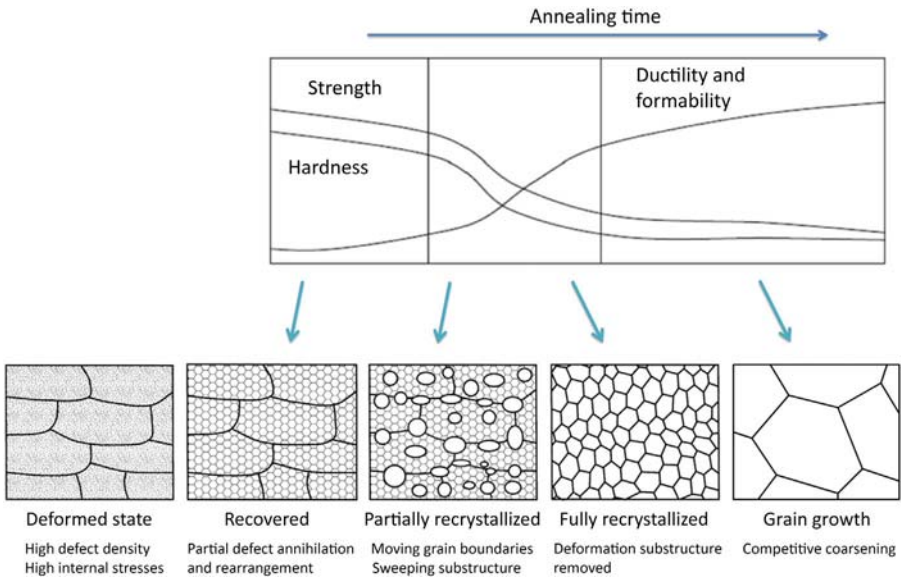

Figure 1 Schematical diagram illustrating the most generic steps during recovery, static primary recrystallization, and grain growth.

The latter mechanism is also referred to as grain growth (Carpenter and Elam, 1920; Burke and Turnbull, 1952; Doherty et al., 1997; Humphreys, 1997; Miodownik, 2002; Himmel, 1962; Cahn, 1965, 1966).

Recovery usually occurs at low temperatures and involves the thermally activated motion, condensation, and annihilation of point defects and specifically the annihilation and rearrangement of dislocations (Burgers and Louwerse, 1931; Doherty et al., 1997; Humphreys and Hatherly, 2004; Himmel, 1962). Owing to the high self-ordering tendency among dislocations recovery hence results in the formation of pronounced subgrain structures consisting of tilt and twist low-angle grain boundaries. With ongoing recovery, further dislocation annihilation and particularly competitive subgrain growth takes place (Humphreys, 1997). This mechanism overlaps with the onset of recrystallization, which is characterized by discontinuous nucleation phenomena (**Figure 3**). In some materials, recrystallization nucleation can result from discontinuous subgrain growth where some of the subgrains accumulate a sufficiently high misorientation relative to the as-deformed surrounding microstructure (Burgers, 1941; Doherty et al., 1997; Humphreys and Hatherly, 2004; Humphreys, 1997; Himmel, 1962).

Recovery leaves the grain topology of the deformed crystals usually unaffected as it does not involve the motion of high-angle grain boundaries. Instead the dislocation rearrangements described above occur within the as-deformed grains. Relatively small and continuous changes in hardness occurring during static recovery are essentially due to the gradual decrease in the elastic distortion of the material, which is attributed to the reduction in the dislocation density, to the formation of low-energy DC structures, and to the growth of these subgrains (Clarebrough et al., 1955) (**Figure 4**).

While static recovery thus describes the thermally activated formation and reorganization of dislocation substructures in a deformed material, recrystallization is concerned with those phenomena where the formation and subsequent motion of new high-angle grain boundaries is involved. The

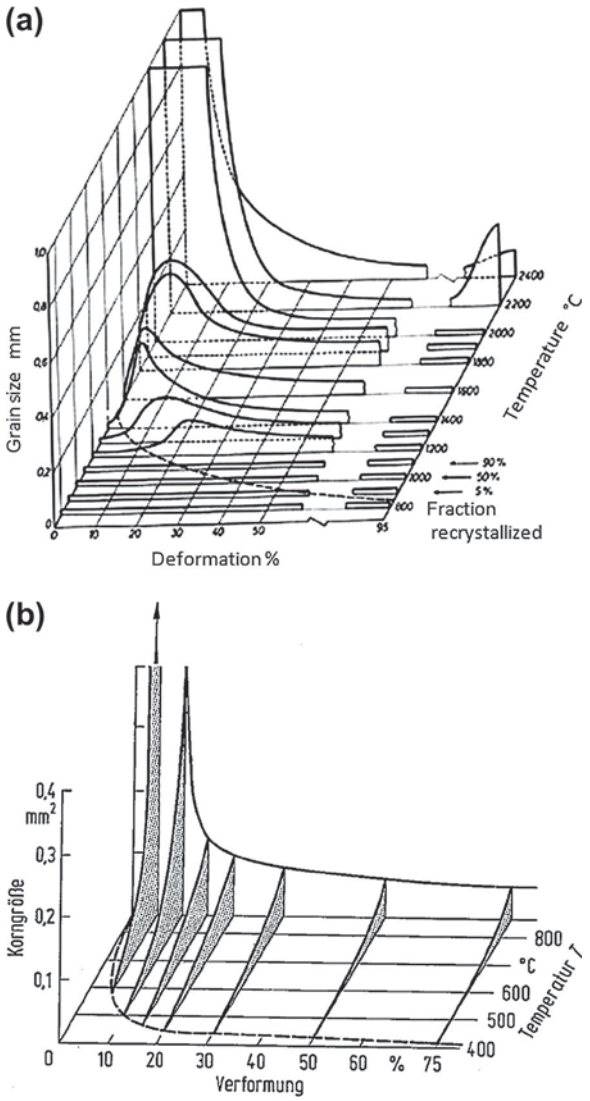

Figure 2 Recrystallization diagram of molybdenum (a) (grain size, deformation, temperature, recrystallized volume fraction) and (b) pure iron (Burgers, 1941; Doherty, 2005; Humphreys and Hatherly, 2004).

newly formed interfaces discontinuously sweep the inherited deformation substructure and lead to a softened polycrystal microstructure.

Recrystallization starts when sufficient thermal activation is available to lead to nucleation and growth of strain-free new grains in the plastically deformed matrix (Kolmogorov, 1937). Since newly formed grains sweep the deformation microstructure discontinuously, recrystallization nucleation can be described as a process leading to a local strain-free zone in the deformation matrix. This newly formed strain-free region is mainly surrounded by newly formed or bulged mobile high-angle grain

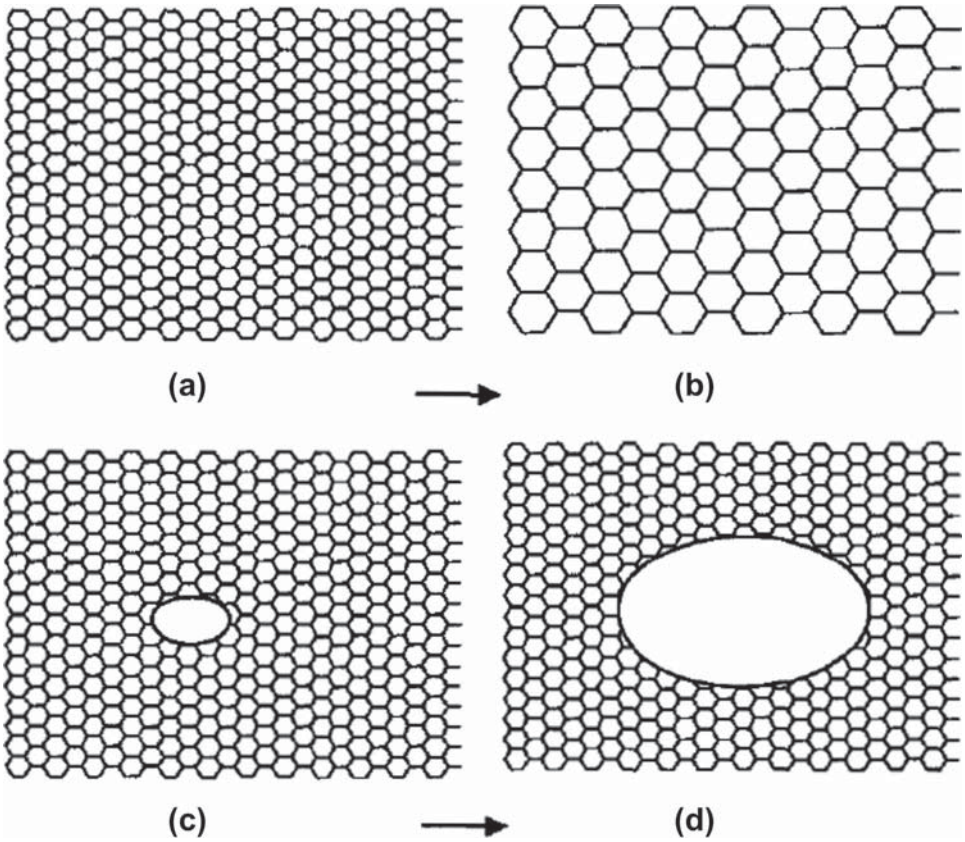

Figure 3 Schematic illustration of (a–b) continuous, and (c–d) discontinuous subgrain-coarsening phenomena during annealing (Humphreys, 1997).

boundaries (Beck and Hu, 1966; Humphreys and Hatherly, 1995; Humphreys, 1997; Himmel, 1962; Cahn, 1965, 1966; Kolmogorov, 1937; Johnson and Mehl, 1939; Avrami, 1939, 1940; Doherty and Cahn, 1972; Humphreys and Ferry, 1997; Faivre and Doherty, 1979; Bhatia and Cahn, 1978; Srolovitz et al., 1986a; Sebald and Gottstein, 2002; Engler et al., 1996; Engler, 1997; Humphreys, 1992a).

During recrystallization the strength and hardness both decrease considerably and often at much higher rates than during recovery. During the recrystallization process, the original ductility that the metal had prior to cold deformation is restored. The lowest temperature at which newly formed stress-free grains appear in the microstructure of a previously plastically deformed metal is termed the recrystallization temperature. This depends upon the grain size, the severity of plastic deformation, the strain path, and the presence of solute atoms or second-phase particles. The recrystallization temperature is usually 1/3–1/2 the absolute melting point of the material in Kelvin.

Recrystallization is finished when all originally deformed grains are swept by mobile grain boundaries. After that and locally also during the ongoing recrystallization grain growth, i.e. competitive capillary driven grain-coarsening begins. This phenomenon changes the strength of the material further owing to the increase in the average grain size and the associated reduction in Hall–Petch strengthening. Grain growth is thermodynamically driven by the reduction of the total grain-boundary area. While

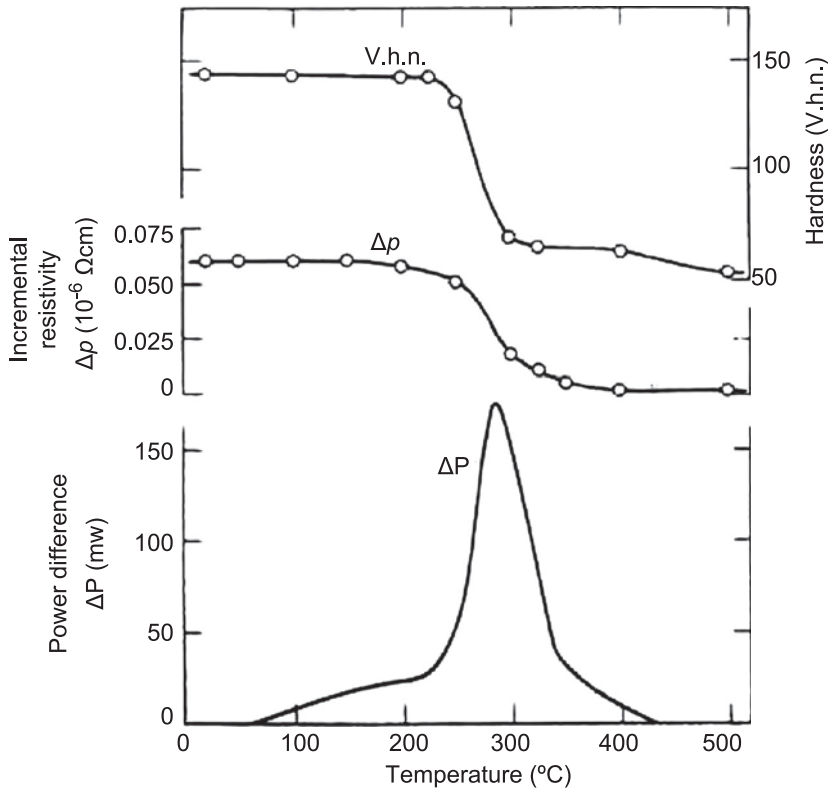

Figure 4 Changes in hardness, release in energy, and change in electrical resistivity upon isothermal heating of a copper rod (Clarebrough et al., 1955).

recovery and grain growth are relatively slow processes, recrystallization follows in most cases sigmoidal-type kinetics, i.e. it can proceed very fast after an initial more sluggish nucleation period.

23.1.2 Historical Notes

Many of the technical terms associated with phenomena such as recovery, recrystallization and grain growth are older than the knowledge that we have today about them.

This means that some of the terminology that is commonly used in this field is often a bit imprecise at first view. An example is the term "recrystallization". It describes the removal of the deformation substructure obtained from cold working via the formation and thermally activated motion of high-angle grain boundaries. The notion "recrystallization" seems odd since deformed metals remain, as a rule, crystalline upon plastic deformation because the elementary deformation carriers, the dislocations, proceed via translational shear increments. In other words the material is (usually) not rendered amorphous upon straining, hence, "recrystallization" is not a correct term as the crystalline state of the material is not altered during the heat treatment. It rather goes back to the times when structure observation was exclusively made by optical inspection of as-processed or etched metallic surfaces. The blurred appearance of many metals after strong plastic deformation led early metallurgists to the assumption that deformed

metals were no longer crystalline. The advent of structure analysis via X-ray diffraction (XRD) by Max von Laue, when applied to cold-worked metals, revealed that deformed materials usually remain crystalline (Laue, 1913). Irrespective of this observation, the term "recrystallization" prevailed.

Also, the use of the term "nucleation" in conjunction with the early stages of recrystallization may be a bit misleading. Originally, it was assumed that the nucleation process by which new recrystallized grains are formed would be based on thermal fluctuations. This model assumption was adopted from classical phase transformation theory. In classical nucleation theory, pertaining to phase transformation, it is assumed that as a result of the permanent thermal motion and rearrangement of the atoms, tiny strain-free clusters, i.e. nuclei, would spontaneously form in the cold-worked matrix. Following the classical energy balance used to explain nucleation phenomena in association with phase transformations, these nuclei would be associated with an energy increase due to the formation of a new grain boundary and an energy reduction due to the formation of a new volume of strain free, hence lower energy material. If such nuclei, assumed to be spherical in shape, were larger than a critical radius then they would be thermodynamically stable and could start to grow and sweep the surrounding deformed matrix.

Later, it was suggested that this classical nucleation theory could not hold for recrystallization phenomena (Sellars, 1978; Humphreys, 1997; Miodownik, 2002; Himmel, 1962; Cahn, 1965, 1966). The main inconsistency with this type of nucleation model is that the stored deformation energy that could be released upon nucleation is very low (about 1–10 M Jm^{-3} (1–10 MPa)) while the interface energy associated with a newly formed high-angle grain boundary is relatively high (about 1 Jm^{-2}). This means that in the context of the classical fluctuation theory nucleation would be impossible.

As will be discussed below in more detail, recrystallization nucleation must instead proceed via the growth of already preexisting subgrains or cells. The discontinuous and competitive coarsening of such subgrains during the nucleation or incubation time can then lead in certain cases to the formation of new mobile high-angle grain boundaries. A higher misorientation of such a gradually forming interface increases the mobility of that boundary and so the rate of growth of the subgrain increases until it finally acts as a nucleus. Since subgrains are typically surrounded by low-angle grain boundaries of usually not more than 1–2° misorientation each, the accumulation of further misorientation during subgrain coarsening requires local orientation gradients to be present in the vicinity of such a growing subgrain that finally prevails as a successful nucleus (Ferry and Humphreys, 1996; Holm et al., 2003; Rollett, 1997; Heidenreich, 1949; Beck, 1949; Cahn, 1950; Humphreys and Chan, 1996; Bailey, 1960; Cotterill and Mould, 1976; Bailey, 1963; Sandström et al., 1978; Varma and Willitis, 1984; Walter and Koch, 1963; Blum et al., 1995; Li, 1962; Doherty and Szpunar, 1984a). The details of these mechanisms will be discussed below.

Likewise, the term grain growth is not very precise as during grain growth most of the crystals actually shrink rather than grow. Only the *average* crystal size increases such as in many other capillary driven competitive ripening processes (e.g. such as for instance known from Ostwald ripening).

23.1.3 Experimental Methods to Study Recovery and Recrystallization

23.1.3.1 Introduction

While integral macroscopic property changes associated with recovery and recrystallization can be efficiently tracked in terms of hardness and electrical resistivity characterization, the associated microstructural changes are more challenging to measure. This applies particularly to recrystallization. This is due to a number of reasons:

Firstly, recrystallization nucleation takes place at very small dimensions, usually at the subgrain scale. Hence, it is difficult to predict where—in a large array of subgrains—nucleation will actually

happen. Recrystallization nucleation is a relatively rare event and strongly dependent on the underlying type of nucleation mechanism (e.g. discontinuous subgrain coarsening; nucleation that shear bands; particle stimulated nucleation (PSN); grain-boundary bulging) (Humphreys and Hatherly, 2004; Humphreys, 1992a). When aiming at the observation of the early stages of nucleation hence adequate microscopy methods in conjunction with the capability to overlook a high field of view are required (Doherty et al., 1997; Cahn, 1965; Doherty and Cahn, 1972). Later stages of subgrain coarsening or cell growth could in principle already be the effect of a grain-growth competition phenomenon subsequent to the actual nucleation stage.

Secondly, recrystallization nucleation often starts in regions that contain microstructural inhomogeneities. These are for instance heavily distorted grain boundaries or heterointerfaces with strain gradients and high lattice curvatures before them; the vicinity of hard second-phase particles; microbands with high local dislocation densities; or shear bands that are characterized by both, locally high stored-dislocation densities and large lattice curvature around them. Probing and understanding nucleation events occurring at these sites requires to first understand the underlying deformation substructures and the specific characteristics that render these sites into suited nucleation sites (Ferry and Humphreys, 1996; Cahn, 1950). This means that recrystallization research is not a "one-mechanism" search but usually requires rather a systemic approach where a variety of possible phenomena and their interactions have to be taken into consideration (Humphreys, 1997; Miodownik, 2002; Holm et al., 2003; Rollett, 1997).

Thirdly, recrystallization can proceed very fast and sweep the deformation substructures inherited from cold working. This means that the microstructural mapping of recrystallization phenomena is often conducted using postmortem and ex situ experimental approaches rather than direct in situ observation.

Fourth, recovery and recrystallization phenomena can strongly depend on many subtle and hard-to-measure details such as material purity, the types of grain boundaries involved, the distribution of the stored energy, interfering ordering and/or phase transformation phenomena, and the complexity of the underlying deformation substructures inherited from preceding cold working. Many of these effects can have a drastic, namely, an exponential influence on recrystallization as they, in part, affect the thermal activation barriers. Thermal activation during recrystallization often follows an Arrhenius dependence, hence the exponential influence. A typical example is the dependence of the grain-boundary mobility and of the grain-boundary energy on the impurity content of the material (Molodov et al., 1984; Ibe and Lücke, 1966, 1972; Ibe et al., 1970; Babcock and Balluffi, 1989; Hashimoto and Baudelet, 1989; Gottstein and Shvindlerman, 1999; Aust and Rutter, 1959, 1960; Hu et al., 1990; Rath and Hu, 1969a; Molodov, 2001; Lücke and Stüwe, 1963; Gottstein et al., 1995, 1997, 1998; Shvindlerman et al., 1995, 1999; Upmanyu et al., 1999; Rollet et al., 2004; Liebman et al., 1956; Christian, 1965; Viswanathan and Bauer, 1973; Furtkamp et al., 1998; Li et al., 1953; Winning et al., 2001, 2002; Winning, 2003; Heinrich and Haider, 1996; Vandermeer and Juul Jensen, 1993; Beck et al., 1950; Molodov et al., in press).

These aspects show that recrystallization phenomena are among the most complex metallurgical topics and therefore require the use of advanced and combined experimental and modeling methods.

23.1.3.2 Indirect Experimental Methods

Indirect methods for analyzing the effects and kinetics of recovery and recrystallization as well as grain-growth phenomena typically probe macroscopic or mesoscopic mechanical, optical, calorimetric, or electromagnetic property changes that are associated with the underlying microstructural evolution during these processes. Examples are changes in resistivity, hardness, strength, or averaged values of the stored deformation energy. Electrical resistivity measurements are characterized by the fact that point

defects and internal interfaces provide a rather high contribution to the resistivity while the dislocation cores and elastic long-range distortions contribute less (Burgers and Louwerse, 1931; Burgers, 1941; Burke and Turnbull, 1952; Smith, 1948; Beck and Hu, 1966; Haessner, 1978; Humphreys and Hatherly, 1995, 2004; Doherty et al., 1997; Doherty, 2005) (**Figure 4**).

A more quantitative approach to determine the changes in internal stresses associated with the annealing of cold work metals is provided by advanced XRD methods. Corresponding experiments can be conducted by using lab-scale XRD devices or the more brilliant high-energy synchrotron XRD methods (Poulsen et al., 2001; Margulies et al., 2001; Leslie et al., 1963a; Schmidt et al., 2004; Larson et al., 2002; Tamura et al., 2003, 2002; Bale et al., 2005; Chung and Ice, 1999; Yang et al., 2003; Chawla et al., 2004).

When exposing polycrystalline metals to a monochromatic XRD setup, the underlying assumption is that each scattering volume of the illuminated material contains a sufficiently large number of crystallites, such that there are always some of the grains that satisfy the Bragg–Brentano diffraction condition for any given orientation of the sample relative to the beam setup. A photon point, line, or areal detector then collects a pattern of diffracted counts versus angle corresponding to a section through the Debye–Scherrer cones. XRD methods typically provide excellent diffraction profiles with little instrumental broadening contribution that is particularly suitable for line profile and crystallographic texture analysis. While the former information (peak broadening) provides information about the elastic distortion of the material the latter information (crystallographic texture) provides information about crystallographic orientation changes. The latter are quite indicative of recrystallization since by definition it involves the motion of high-angle grain boundaries, and hence the orientation changes from deformation textures to recrystallization textures. Data collection in XRD measurement is typically relatively slow due to the low flux density of laboratory-scale monochromatic-beam setups.

Generally, when a material is plastically deformed, the reflections observed in constructive interference Bragg–Brentano of a monochromatic beam detected with XRD can be affected in two ways.

The first possibility is that due to compressive or dilatational stresses the average lattice parameter will systematically become smaller or larger, respectively, reflecting the presence of mean homogeneous strains.

The second possibility is that the breadth and the shape of the peaks can change due to the size of the diffracting elements such as the domain or crystal size or due to an inhomogeneous distribution of the local strains. The latter are also referred to as microstrains. Possible sources of inhomogeneous strain include lattice dislocations, grain-boundary defects, and intracrystalline gradients such as high-dislocation-density walls.

Hence, in conjunction with appropriate peak analysis models that allow the interpretation of XRD peaks on the basis of certain lattice defect distributions XRD methods can be used to provide an average information about the dislocation density of the bulk deformed material at a limited spatial resolution when compared to scanning electron microscope (SEM) or transmission electron microscopy (TEM)-based methods. Also, XRD analysis of defect structures requires the use of a well-justified underlying model that connects a certain dislocation density and distribution with a total displacement gradient field (Mughrabi et al., 1986; Straub et al., 1996).

An interesting advantage of XRD-based methods is that the line broadening can be different for different crystallographic textures. X-ray line broadening data from different such studies have shown that indeed a variation in the stored deformation energy exists. These results were confirmed by TEM, Electron Backscatter Diffraction (EBSD), and Electron Channeling Contrast Imaging (ECCI) measurements. For instance in cold rolled steels it was observed that crystallographic texture components with a {111} axis in normal direction are capable of storing twice as much deformation energy compared to grains that have a {001} axis in normal direction.

The second essential option provided by the use of XRD methods consists in the analysis of crystallographic textures, viz. orientation distributions (Beck and Hu, 1966; Ibe and Lücke, 1966; Poulsen et al., 2001; Chung and Ice, 1999; Bunge, 1969, 1982, 1986, 1987; Wassermann and Grewen, 1962; Bunge and Esling, 1982, 1991; Adams et al., 1993; Duggan et al., 1978; Dillamore et al., 1979; Hölscher et al., 1991; Ushioda et al., 1987; Raabe and Lücke, 1993). While the global orientation distributions do not change much during recovery owing to the very definition of this process that excludes the motion of high-angle grain boundaries, they can indeed change quite dramatically during primary recrystallization (**Figure 5**). This is due to the fact that primary static recrystallization is defined as the formation and motion of high-angle grain boundaries through the deformed material.

An essential advantage of using XRD methods for recrystallization research lies in the nondestructive nature of this approach. Many other methods to probe recrystallizing microstructures require cutting, grinding, or polishing of the samples under inspection. Using XRD beams with high energy, in contrast, allows for the in situ observation of samples during recrystallization without destroying them (Poulsen et al., 2001; Margulies et al., 2001).

Calorimetric methods to probe recovery and recrystallization driving forces and kinetics can be used to analyze enthalpy release rates upon recovery and recrystallization heat treatments (**Figure 6**)

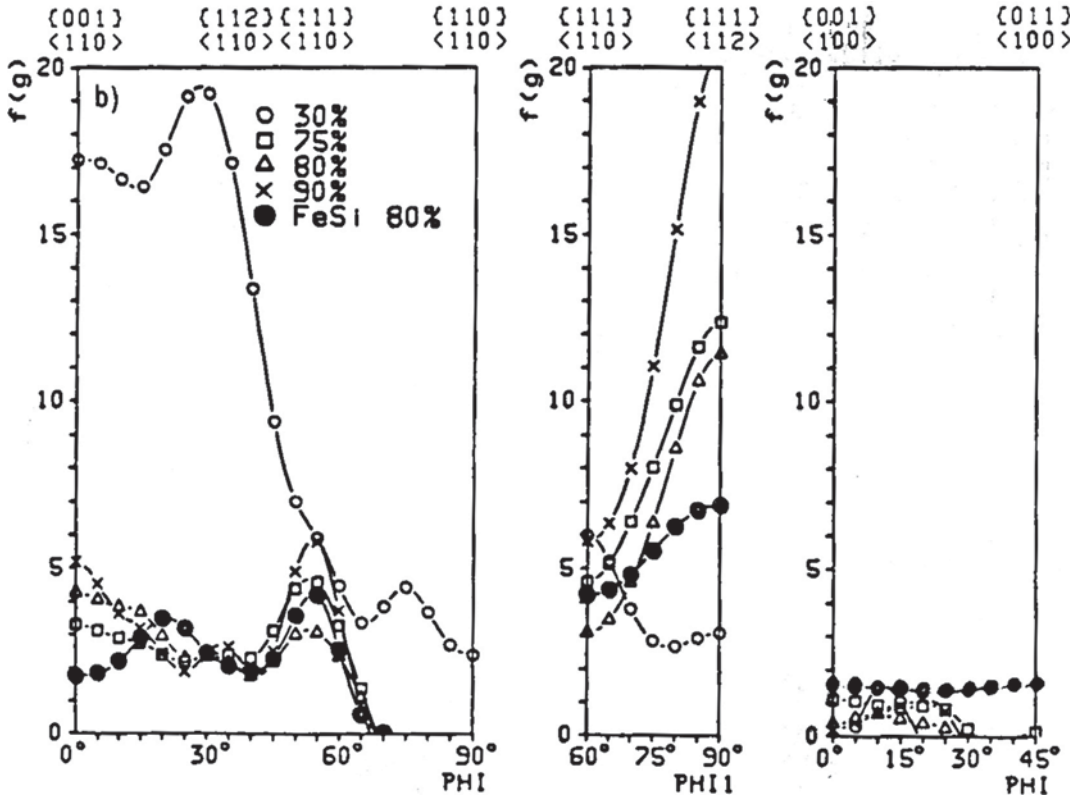

Figure 5 Texture of Fe-16%Cr and Fe-4%Si steels after annealing at 700 °C for different rolling reductions. Weak deformation (30% rolling) does not lead to a texture change indicating that recovery prevails (Hölscher et al., 1991).

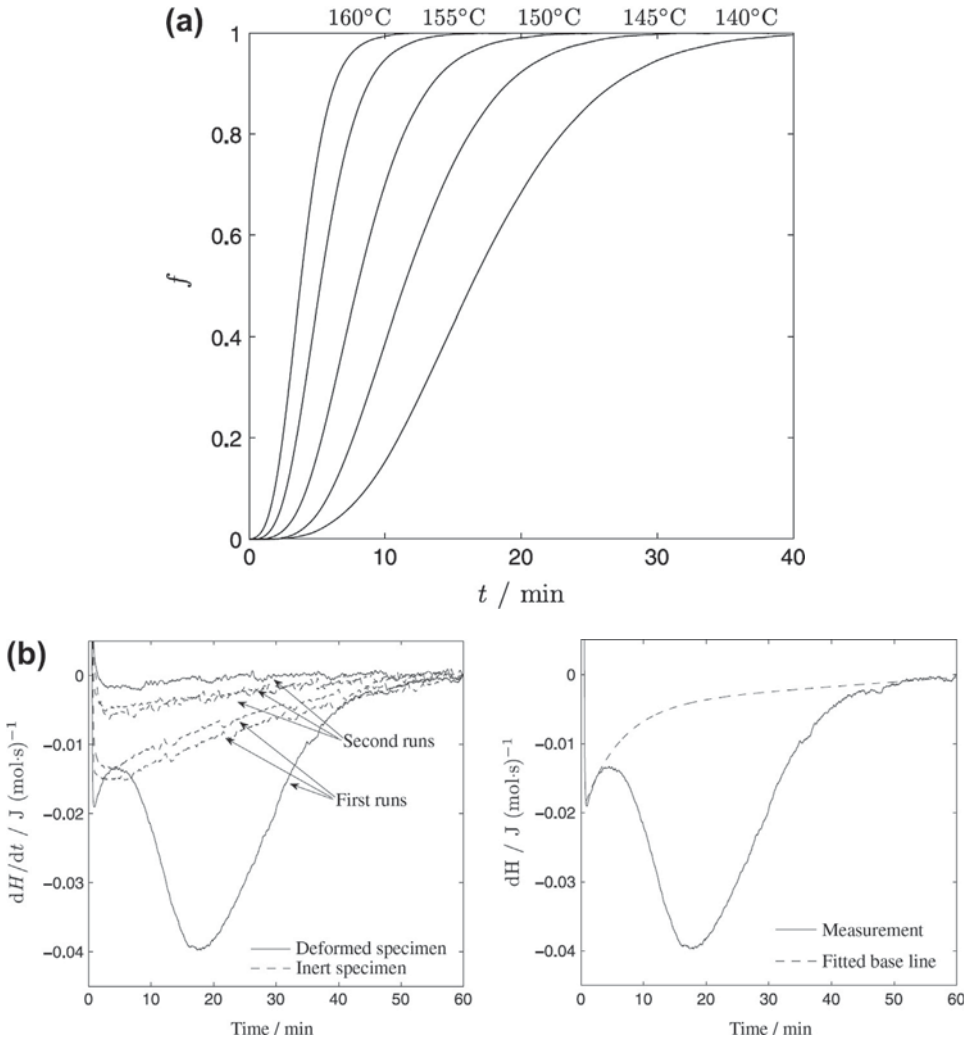

Figure 6 (a) The kinetics of the recrystallization of pure copper as investigated via DSC. The recrystallized fraction, f, determined by isothermal DSC, as a function of time at various temperatures. (b) Using DSC methods in recrystallization analysis: (left) the heat flux signal of a DSC device for the first and second runs of a deformed and an inert copper specimen at 408 K (135 °C). Right: the heat flux of the first run of the same deformed specimen as in the left-hand image together with a fitted base line. (c) Transformed fraction as determined from EBSD measurements for isothermal recrystallization at $T = 413$ K (140 °C) (data points), as a function of time. The error bars indicated for the data points result from choosing different image-quality thresholds in the analysis of the EBSD measurements. The full line represents the recrystallized fraction as determined by DSC for an identically conducted experiment. The DSC curve is shifted by 1 min to shorter times to obtain the best match with the EBSD results (Jägle and Mittemeijer, 2012).

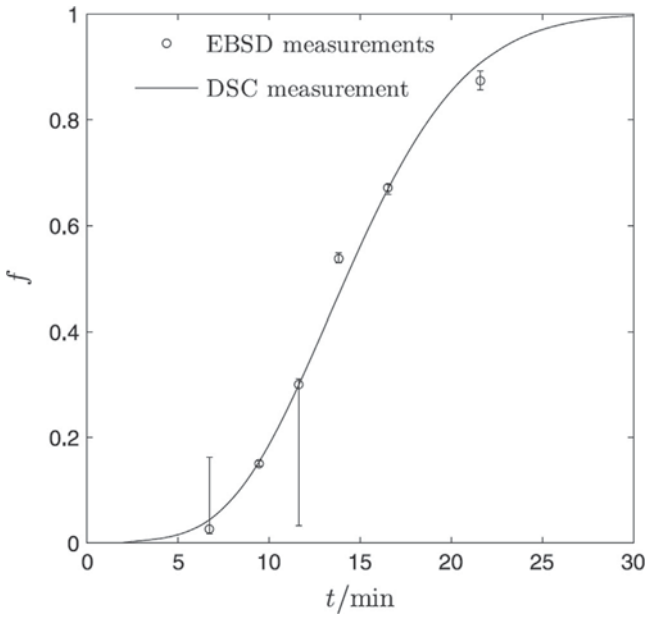

Figure 6 *(Continued).*

(Jägle and Mittemeijer, 2012). Such experiments are usually conducted using a differential scanning calorimetry (DSC) method. In such a setup, when applied to recrystallization phenomena, experiments are typically conducted isothermally (**Figure 6**a). Usually, the deformed samples to be probed have to be stored—like in most recrystallization experiments—in a refrigerator prior to the characterization. This is due to the fact that the activation barriers for initiating recovery and even recrystallization nucleation (for pure metals) can be of similar magnitude as provided by room temperature. Examples are heavily strained lead or high-purity aluminum polycrystals. Then specimens are heated to the probing temperature using the maximum possible heating rate. Owing to the relatively small energy release rates that are characteristic for recrystallization phenomena such DSC methods have to be very well calibrated as they operate close to their resolution limits (**Figure 6b,c**).

It must be underlined though that calorimetry that is conducted on samples during recovery, recrystallization, or grain growth provides an integral value of the energy release rates.

For all calorimetric methods, the global effective activation enthalpy associated with recovery and recrystallization can for isothermal measurements be calculated from a diagram that plots the logarithm of the time that has elapsed between two recrystallization states that are characterized by their respective recrystallized volume fractions and the inverse temperature. Precondition to such a classical analysis of the effective activation barrier is the assumption that the underlying processes are—when occurring simultaneously—described by one single value of the activation energy.

23.1.3.3 Direct Experimental 2D Methods

The most frequently used instruments for tracking recovery and recrystallization phenomena are optical microscopes. They typically allow one to map grain shape changes and also polygonization as well as subgrain coarsening effects when a corresponding sample is subjected to grain-boundary etching.

Polygonization, i.e. the regular alignment of dislocations that can be observed in heat-treated samples after preceding bending, was also made visible by using etch-pit methods.

The primary recrystallized portion of a previously cold-worked portion of material is usually quantified by determining the area fraction of recrystallized versus the remaining unrecrystallized zones. From stereological considerations, the equivalent recrystallized volume fraction can be determined.

In order to reveal crystallographic features, such as the grain-boundary misorientations or the grain orientations, EBSD methods, which are also referred to as orientation microscopy, are frequently used (Adams et al., 1993; Adam et al., 2001; Randle and Engler, 2000; Randle, 1992, 2004).

In EBSD, a stationary primary electron beam of an SEM is diffracted by atomic layers in crystalline materials. These diffracted electrons can be detected when they impinge on a fluorescent screen and generate visible lines. These are referred to as Kikuchi bands or electron backscatter patterns (EBSPs). These patterns are projections of the geometry of the lattice planes in the crystal, and they give direct information about the crystalline structure and crystallographic orientation of the grain from which they originate. When used in conjunction with a database that includes crystallographic structure information for phases of interest and with adequate analysis software for processing the EBSPs and indexing the lines, the data can be used to identify crystallographic textures and phases provided that they have a crystalline structure. EBSD provides information about the local phases, crystal orientations, and local misorientations down to 50 nm resolution—for instance when using an SEM that is equipped with a field emission gun. This renders it a powerful instrument for microstructural characterization in the context of recrystallization (**Figure 7**).

Another, more recently matured technique to track lattice defect ensembles at a wide field of view is ECCI (Gutierrez-Urrutia et al., 2009, 2010; Gutierrez-Urrutia and Raabe, 2011; Eisenlohr et al., 2012). ECCI is an SEM technique that is based on the effect that the backscattered electron intensity is strongly dependent on the orientation of the crystal lattice planes with respect to the incident electron beam due to electron channeling mechanism. Also minor local distortions in the crystal lattice due to dislocations or interfaces cause a modulation of the backscattered electron intensity enabling such linear or planar defects to be mapped. The ECCI method has been used to image dislocation structures in metals deformed during fatigue loading or in the vicinity of cracks, and even stacking faults. For quantifying the change in the dislocation structure during recovery or recrystallization, a special variant of the ECCI method is particularly suited. This approach consists of a combined EBSD and ECCI methods to achieve enhanced contrast by calculating the optimum channeling angle based on the information provided by the EBSD measurement (Gutierrez-Urrutia et al., 2013). In this specific combination ECCI is a powerful, versatile, fast, and experimentally robust method for determining dislocation and interface defect densities and cell-type dislocation arrangements at small preparation time and at a wide field of view (**Figure 8**) (Gutierrez-Urrutia et al., 2009, 2010; Gutierrez-Urrutia and Raabe, 2011).

When higher spatial resolutions are required than offered by conventional SEM, EBSD, or ECCI methods TEM has to be used in recrystallization research (Berger et al., 1988; Wilbrandt, 1980; Wilbrandt and Haasen, 1979, 1980a, 1980b; Weiland and Schwarzer, 1984; Ray et al., 1975a; Hartig and Feller-Kniepmeier, 1985; Klement and Haasen, 1993; Schwarzer and Weiland, 1986; Hu, 1962, 1963; Bailey and Hirsch, 1962; Zaefferer, 2005; Grewen and Huber, 1978). This is a microscopy technique whereby a beam of electrons is transmitted through an ultrathin specimen, interacting with the specimen as it passes through it. An image is formed from the interaction of the electrons transmitted through the specimen; the image is magnified and focused onto an imaging device, such as a fluorescent screen, on a layer of photographic film, or to be detected by a sensor such as a charge-coupled device

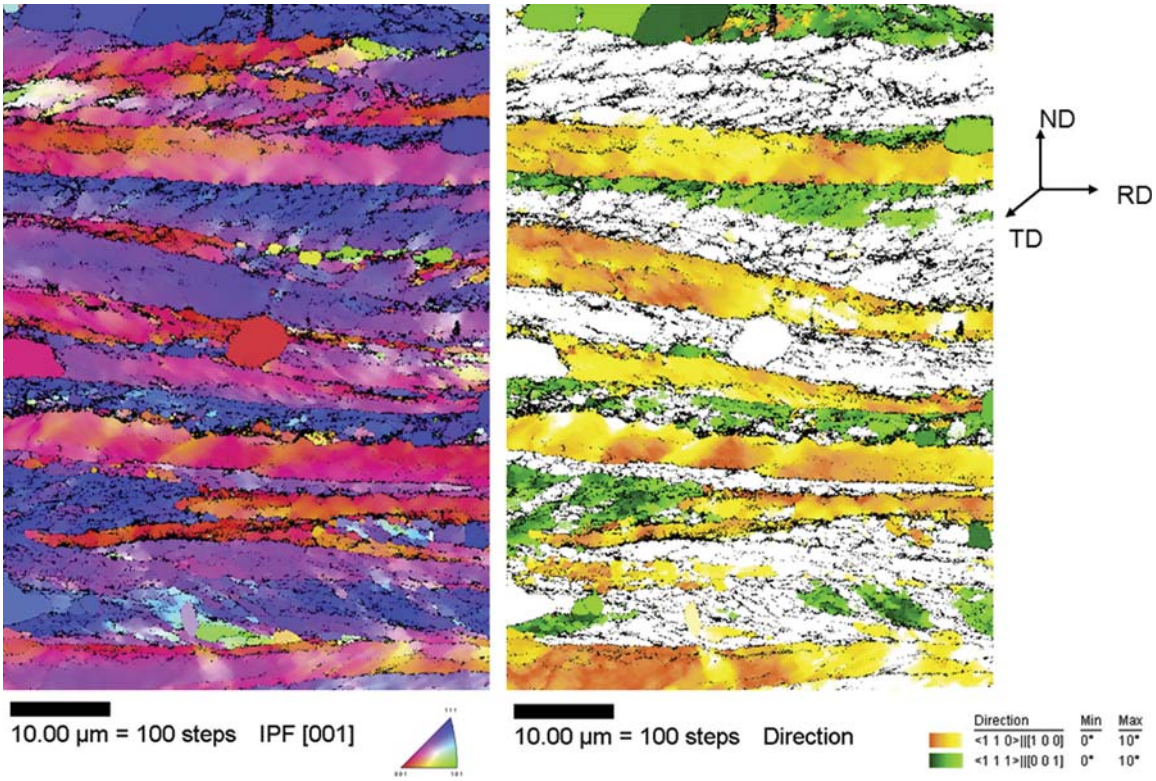

Figure 7 Formation of a new grain during the recrystallization of a 70% cold rolled low-C steel, measured by EBSD.

(CCD) camera. TEMs are capable of imaging microstructures of recrystallizing samples at a significantly higher resolution than light microscopes, owing to the small de Broglie wavelength of the electrons.

23.1.3.4 Tomographic Experimental Methods

By combining conventional EBSD microstructure imaging with sequential serial sectioning of series of subsequent microstructure slices, tomographic microstructure imaging can be performed. This method which is referred to as three-dimensional (3D) EBSD or EBSD tomography is a technique for the 3D high-resolution characterization of crystalline microstructures (Konrad et al., 2006; Zaafarani et al., 2006; Zaefferer et al., 2008). Typically, the technique is based on automated serial sectioning using a focused ion beam (FIB) and characterization of the sections by orientation microscopy based on EBSD in a combined FIB–SEM. These instruments are typically equipped with a field-emission electron gun for obtaining highest EBSD resolutions, a Ga^+ ion emitter unit (FIB), and secondary electron, and backscatter electron detectors. The FIB is usually operated at an accelerating voltage of 30 kV. The EBSD measurements are performed in a range between 15 and 20 kV (**Figure 9**).

On typical two-beam systems (electron beam for EBSD and ion beam for sectioning), the technique reaches a spatial resolution of about $50 \times 50 \times 50\ nm^3$. The maximum observable volume depends on the optical setup and is typically of the order of $50 \times 50 \times 50\ \mu m^3$. The technique provides all the main characterization features of two-dimensional (2D) EBSD-based orientation microscopy and extends

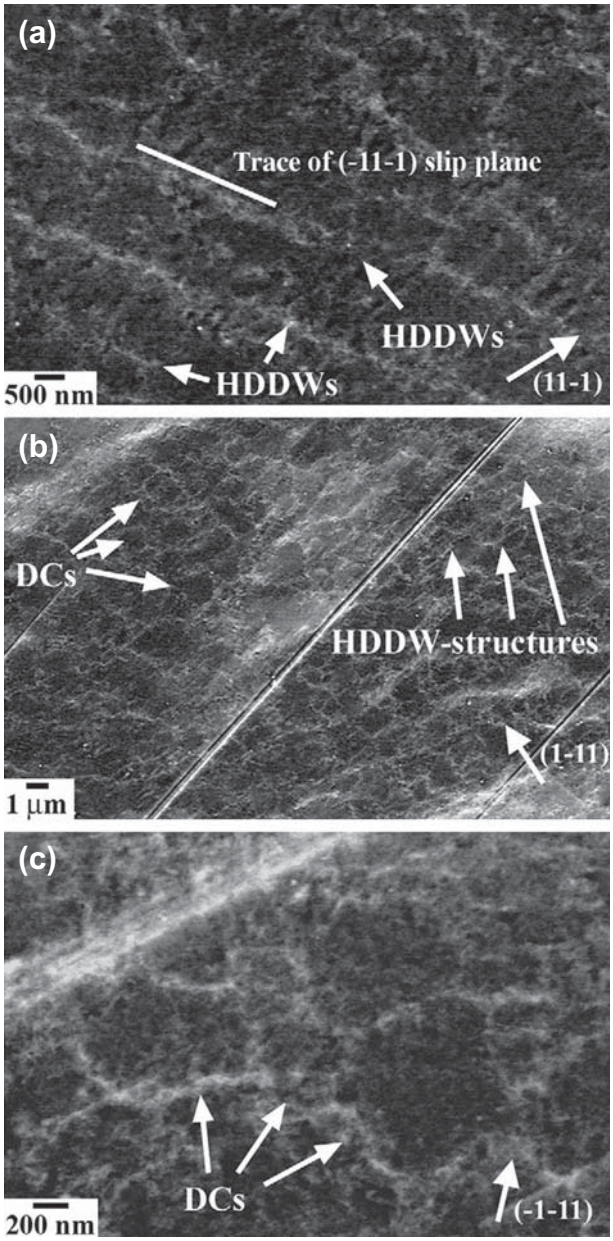

Figure 8 ECCI images of a deformed microstructure at the early stages of the deformation of an Fe-22%Mn-0.6C TWIP steel (wt.%) to a value below 0.1 true strain (ECCI). (a) High density dislocation walls (HDDWs) along the (-1 1 -1) slip plane on a sample tensile deformed to 0.05 true strain (HDDW). The ECCI image was obtained by orienting the grain into Bragg condition using the (1 1 -1)g vector (arrow). (b) DCs and HDDW structures in a sample tensile deformed to 0.1 true strain. The ECCI image was obtained by orienting the grain into Bragg condition using the (1 -1 1)g vector (arrow). (c) Details of the DC structure on a sample tensile deformed to 0.05 true strain. The ECCI image was obtained by orienting the grain into Bragg condition using the (-1 -1 1)g vector (arrow) (Gutierrez-Urrutia et al., 2009, 2010; Gutierrez-Urrutia and Raabe, 2011).

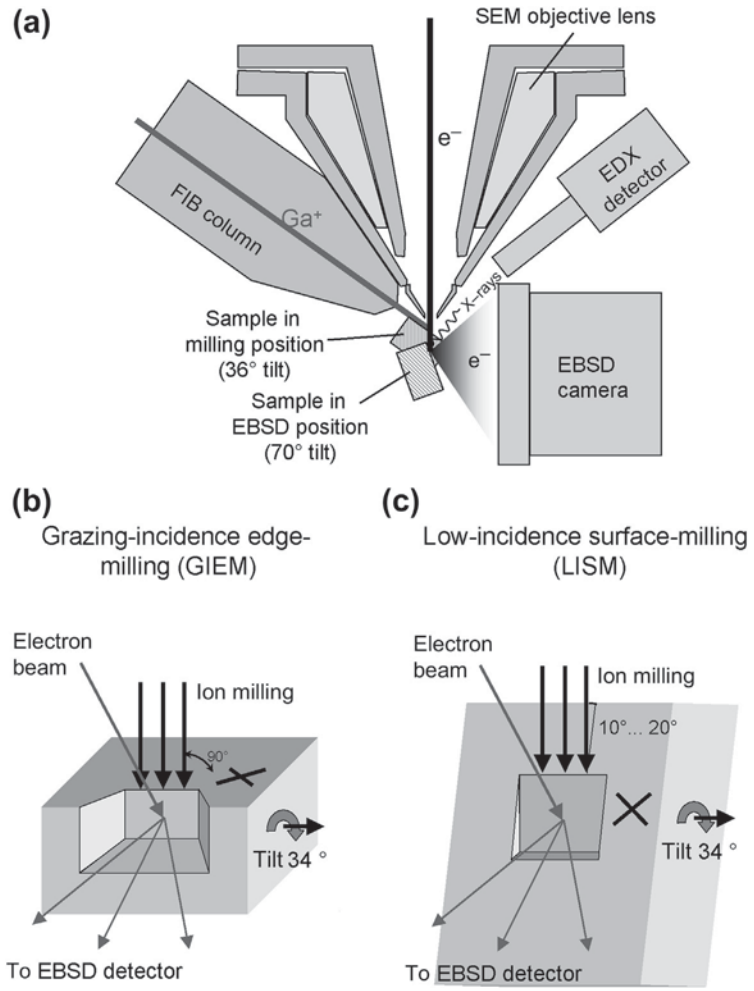

Figure 9 Schematics of the geometry of the 3D EBSD sectioning and mapping procedure. (a) Cross-section through the instrument chamber, showing the sample positions for milling and EBSD analysis in the tilt setup. To change between the two positions, the sample need only be tilted and moved in the y direction. During milling, the EBSD camera is retracted to the chamber wall. Working distance for milling is 8 mm; for EBSD, it is 13 mm. The camera is positioned at a distance of 22 mm from the sample. (b) And (c) Schematics of different variations of the tilt geometry: (b) the graizing incidence edge milling method and (c) the low-incidence surface milling method. For both schemes, the black cross indicates the marker for image alignment that is milled into the sample before the process begins (Konrad et al., 2006; Zaafarani et al., 2006; Zaefferer et al., 2008).

them into the third dimension of space. This enables new parameters of the microstructure to be obtained—for example, the full crystallographic characterization of all interface segments, including the morphology and the crystallographic indices of the interface planes and the crystallographic texture of all phases involved. Of specific interest is the high-resolution mapping of the five-dimensional grain-boundary segment orientation distribution function (**Figure 10**).

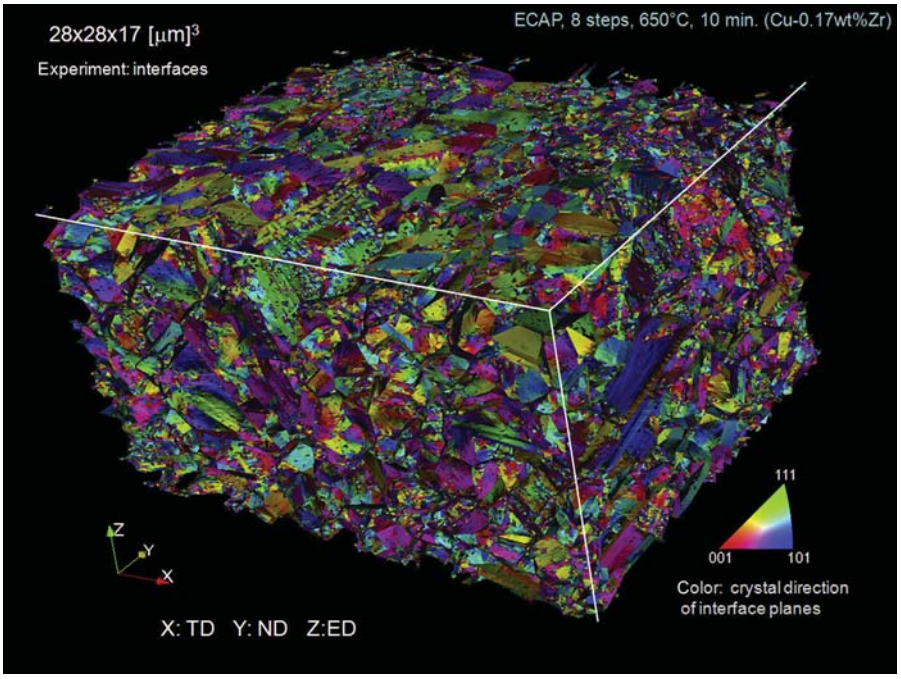

Figure 10 Presentation of the interface distribution (here the normal vectors of the grain boundaries are shown) obtained from a 3D EBSD method. The material is a Cu alloy after eight step Equal Channel Angular Pressing (ECAP) deformation.

An alternative method to track recrystallization in three dimensions consists in using tomographic synchrotron methods. Since such approaches are nondestructive they are particularly suited to study recrystallization as a function of time. Another advantage of synchrotron-based methods is the fact that they allow to probe grain topology and texture evolution also inside recrystallizing and recrystallized bulk materials so that the effects observed are not affected by free surfaces. Such free surface effects are particularly problematic in TEM samples and in EBSD in-situ experiments.

In Bragg-based 3D-XRD microscope setups, a monochromatic high-energy synchrotron beam is focused by using a Laue crystal in order to obtain a small full width at half maximum of the incident probing beam at the focal point. Every volume portion that fulfills the Bragg condition inside the illuminated region of the sample creates a diffraction spot on a detector. Coupling this method with sample rotation and a geometrical 3D path reconstruction setup allows one to map spot shapes and back trace them into the sample to achieve the shape of the grains. Such techniques are successful in achieving reflection from mm-deep grains due to the high energies. By using the high brilliance of third-generation synchrotron sources, microstructures in 4D were studied with a spatial resolution of micrometers and a time resolution of minutes (Poulsen et al., 2001; Margulies et al., 2001; Leslie et al., 1963a; Schmidt et al., 2004; Larson et al., 2002; Tamura et al., 2002, 2003; Bale et al., 2005; Chung and Ice, 1999) (**Figure 11**). **Figure 12** shows an example of some expansion snapshots of a growing grain as observed by XRD tomography (Poulsen et al., 2001).

An alternative to the monochromatic 4D XRD analysis approach involves an experimental procedure using polychromatic microbeam X-radiation (micro-Laue). The micro-Laue setup resolves individual

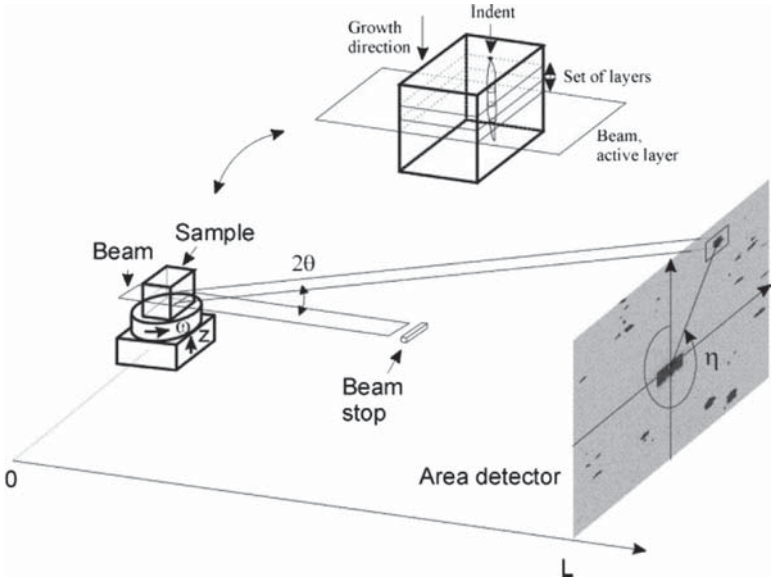

Figure 11 Sketch of an experimental 4D XRD setup (Margulies et al., 2001). Coordinate system (*x*,*y*,*z*) and angles are defined. The *x*-axis is along the beam direction, the *y*-axis is transverse to the beam direction, and the *z*-axis is normal to the beam plane. For the diffraction spot in question, the direction of the diffracted beam is parameterized. All grains within the stripe illuminated by the beam will give rise to diffracted spots during a scan. The inset shows the principle of obtaining a picture of the grain by repeatedly recording an oscillation photograph followed by a vertical translation of the sample stage. L denotes the distance between the sample and the CCD detector (Poulsen et al., 2001; Margulies et al., 2001; Leslie et al., 1963a; Schmidt et al., 2004; Larson et al., 2002; Tamura et al., 2003).

grains in the polycrystalline matrix. Results obtained from a list of grains sorted by crystallographic orientation depict the strain states within and among individual grains. Locating the grain positions in the plane perpendicular to the incident beam is trivial. However, determining the exact location of grains within a 3D space is quite challenging. Determining the depth of the grains within the matrix (along the beam direction) involved a triangulation method tracing individual rays that produce spots on the CCD back to the point of origin. Triangulation was experimentally implemented by simulating a 3D detector capturing multiple diffraction images while increasing the camera to sample distance. Hence, by observing the intersection of rays from multiple spots belonging to the corresponding grain, depth is calculated. Depth resolution is a function of the number of images collected, grain to beam size ratio, and the pixel resolution of the CCD. The 4D XRD method provides grain morphologies, strain behavior of each grain, and interactions of the matrix grains with each other and the centrally located single crystal fiber (Poulsen et al., 2001; Margulies et al., 2001).

23.2 Recovery

23.2.1 Introduction and Basic Phenomena

The early stages of the thermally activated restoration of the inner structure of cold-worked metals proceed at first without notable changes of the grain and phase topology. This stage is referred to as recovery (Vandermeer and Rath, 1990; Stüwe et al., 2002). It comprises a set of thermally activated

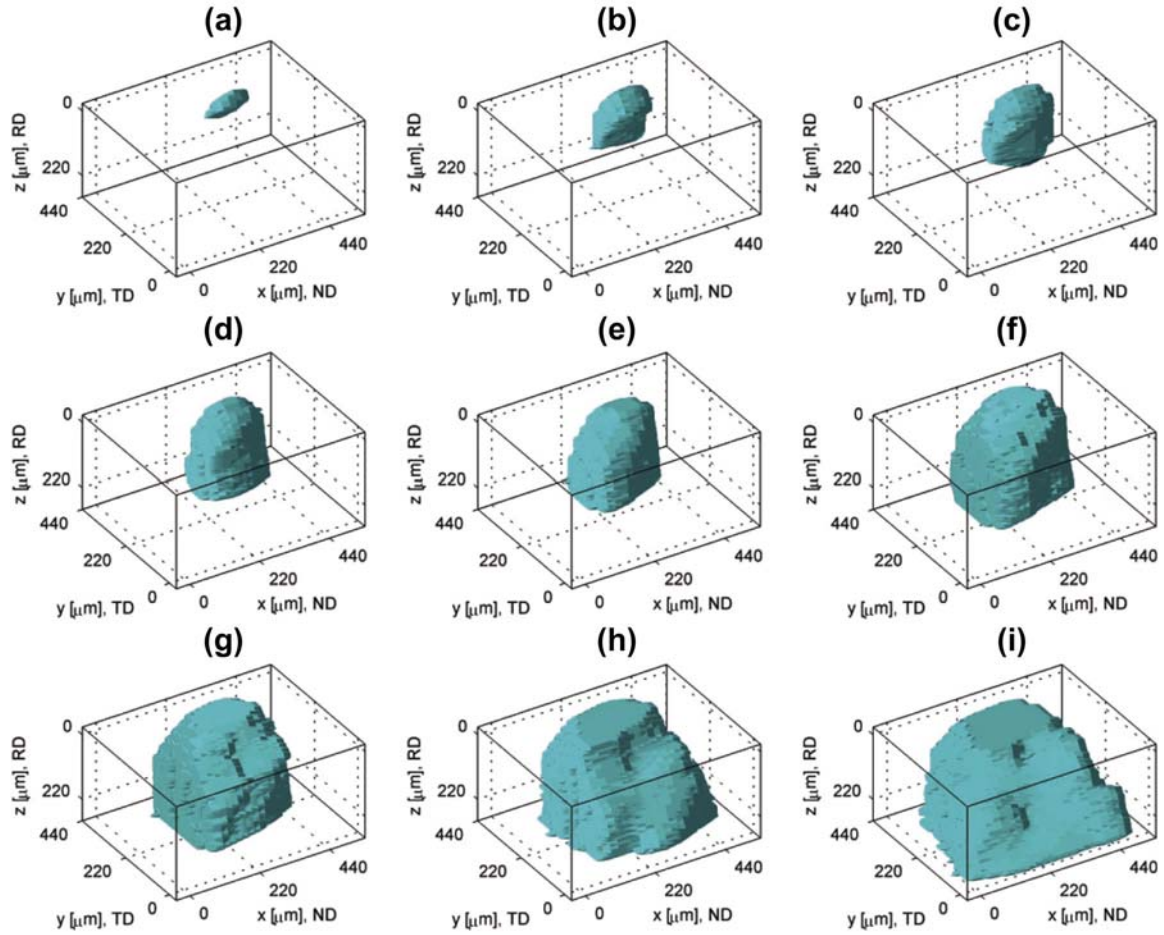

Figure 12 Expansion snapshots of a grain as observed by XRD tomography (Margulies et al., 2001).

gradual softening and microstructural reorganization phenomena in deformed metals to release some of the stored internal energy. The energy relieve is mainly due to point defect motion and dislocation relaxation and reorganization phenomena. When occurring during cold working, it is referred to as dynamic recovery. The properties that are mostly affected by recovery are those that change with the point defect density, such as the electrical resistivity (**Figures 4** and **13**).

Static recovery can be well observed at rather modest temperatures already far below the recrystallization temperature of about 1/3–1/2 of the absolute melting point. The microstructural mechanisms are essentially characterized by the reorganization of the dislocation substructure, driven by the elastic internal stresses that the material has inherited from the preceding plastic deformation and by point defect annihilation (**Figure 14**). The excess point defects that were created during plastic deformation are annihilated either by absorption at grain boundaries or dislocation climbing. This means that recovery proceeds by the annihilation of point defects and the annihilation and rearrangement of dislocations associated with the higher point-defect mobility. The overall dislocation density does not

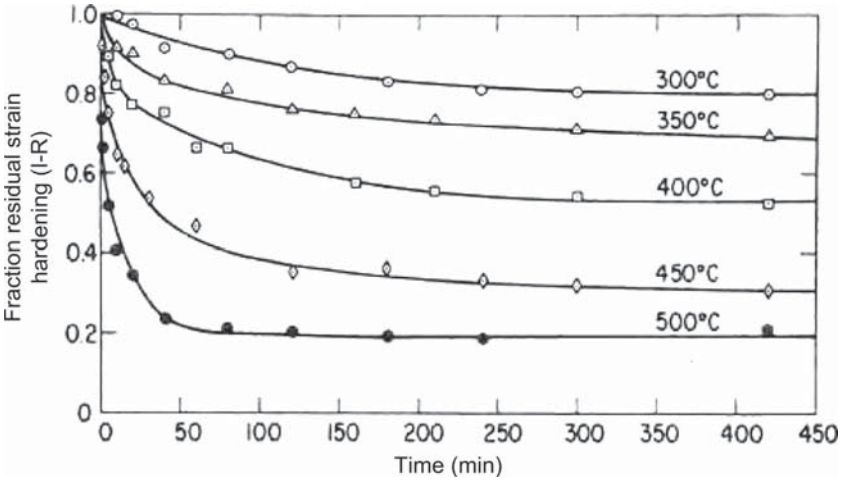

Figure 13 Recovery kinetics of deformed iron expressed in change in the relative flow stress (Leslie et al., 1963c).

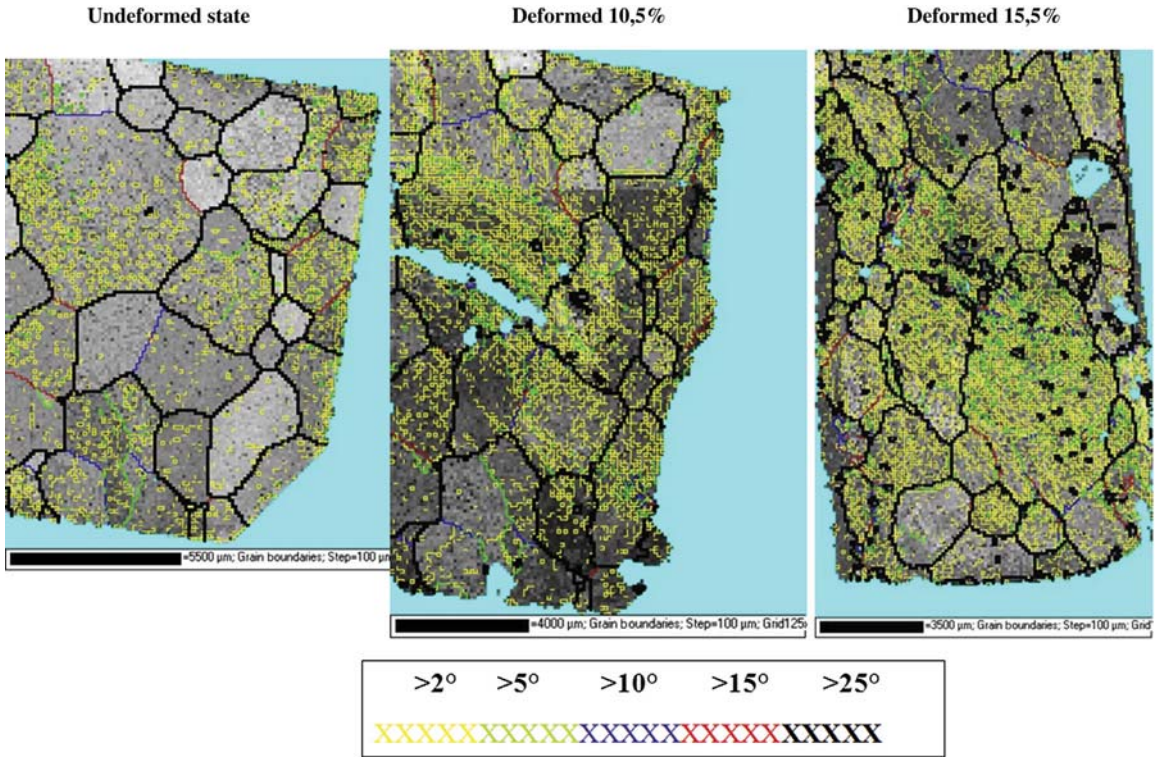

Figure 14 Dislocation substructure evolution during plastic deformation (characterized in terms of EBSD mapping and identification of low-angle grain boundaries) in an Al polycrystal. Images taken subsequently at the same positions.

drop strongly during recovery; however, the internal stresses associated with them, more specific with their configuration, do. The dislocation rearrangement processes lead to the gradual formation of subgrains and subgrain boundaries (e.g. tilt and/or twist low-angle boundaries). This means that recovery starts without incubation or respectively without any nucleation stage but instead starts immediately at temperatures where point defects and dislocations become sufficiently mobile to interact with each other or with other lattice defects (Smith, 1948; Beck and Hu, 1966).

In contrast to recrystallization, recovery does not involve any change in the grain structure of the cold-deformed material—instead, rather the main changes affect the dislocation arrangements inside the deformed grains.

These characteristic recovery phenomena, i.e. the decrease in the dislocation and point defect density and the gradual competitive coarsening of the subgrains, typically leads to the reduction in the internal stress fields and hence to a modest and gradual reduction in hardness (Humphreys and Chan, 1996) (**Figure 4**).

23.2.2 Microstructure Changes during Recovery

23.2.2.1 Elementary Dislocation Mechanisms

The elementary mechanisms that are involved in recovery are the condensation and annihilation of point defects, particularly of quenched-in vacancies, and the gradual relaxation of internal elastic stress fields via cross-slip and reorganization of the dislocations that create these long-range distortions. Even when the density of the dislocations remains nearly the same during recovery, the total elastic energy inherited from cold working can efficiently be reduced just by relaxation of their local arrangement. This is due to the fact that dislocations can reduce their overall lattice distortion when assuming certain low-energy configurations (Vandermeer and Rath, 1990; Stüwe et al., 2002).

As quenched-in point defects can particularly annihilate at dislocations early stages of recovery also include dislocation climb. The reason for observing climb also at modest recovery temperatures, where it does usually not occur, is due to the osmotic pressure that results from a supersaturation of quenched-in point defects.

The second elementary dislocation effect associated with recovery is the cross-slip of dislocations. While dislocation climb is thermally activated owing to the required formation and motion of point defects, cross-slip of dislocations is thermally activated because the dislocation core, when it is spread or even dissociated into partial dislocations in the case of metals with low-stacking fault energy, has to be constricted before the dislocation can cross-slip. This constriction is thermally activated and hence the entire process of cross-slip depends on the stacking fault energy. The thermal activation of the cross-slip increases with the width of the stacking fault (Burgers and Louwerse, 1931; Doherty et al., 1997; Humphreys and Hatherly, 2004; Himmel, 1962).

23.2.2.2 Polygonization and Cell Formation

Structural recovery can be observed when a crystal is first bent in such a way that only one glide system operates, and then is subsequently annealed. The crystal dislocation substructure arising from single slip then breaks up into a number of strain-free subgrains, each preserving the local orientation of the original bent crystal, and separated by plane subboundaries that are normal to the glide vector of the active glide plane. This process is referred to as polygonization, because a continuously curved vector attached to the crystal lattice turns into a portion of a polygon (Beck and Hu, 1966; Haessner, 1978; Humphreys and Hatherly, 1995, 2004; Doherty et al., 1997; Doherty, 2005).

To better understand polygonization, the process must be interpreted in terms of the underlying dislocation distribution and their relaxation steps. When a crystal undergoes plastic deformation under single-slip and bending boundary conditions, then it is possible for all dislocations, both positive and negative, to pass right through the crystal and out at the surface such as in the easy-glide strain regime of a single crystal.

However, for accommodating the imposed curvature a certain density of excess dislocations of the same sign must remain inside the crystal. Such arrays of polarized dislocations are also referred to as geometrically necessary dislocations (GNDs).

The density of these excess dislocations is $1/R\,b$, where R is the mean radius of curvature and b is the magnitude of the Burgers vector. When the bent crystal is subjected to an annealing treatment, these excess dislocations relax into local low-energy configurations such as dislocation walls or tilt boundaries with their interfaces normal to the Burgers vector. When assuming such arrangements, the dislocations mutually compensate their distortion fields and hence reduce the total elastic energy.

This can be understood in terms of the Read–Shockley equation, which describes the elastic energy of an infinite low angle and boundary consisting of straight and infinite edge dislocations. In this low-energy configuration, the compressive field around the core of the dislocations overlaps within the dilatation field of the dislocation above it. This means that dislocations constituting a tilt boundary progressively relieve each other's energy as the tilt angle increases.

The process of polygonization involves individual glide and climb steps of the constituting dislocations. This process requires thermal activation and determines the rate of polygonization. Later stages of polygonization take place by the progressive merging of pairs of adjacent subboundaries. The driving force for this process comes from the progressive reduction of the boundary energy per dislocation in the boundary, as the misorientation of the interface angle increases. This means that the elastic energy associated with two independent low-angle grain boundaries, each characterized by the same misorientation, is higher than that of one single-merged low-angle grain boundary with twice that misorientation.

The rate of low-angle boundary merging is dependent by dislocation climb, since the dislocations in the two merged boundaries will not be uniformly spaced unless some dislocations climb.

In contrast to these well organized polygons that can from during recovery of microstructures resulting from single slip, the distribution of dislocations in a real plastically deformed metal is usually not uniform.

TEM, ECCI, EBSD, and XRD experiments of deformed polycrystals or single crystals subjected to more complex loading situations or strain-path changes that cannot be accommodated by single slip reveal that grains contain more complex subgrains or cells after plastic cold working.

While subgrains are characterized by a local accumulation of dislocations in a tangled in slightly blurred arrangement, cell walls (also referred to as cell boundaries) have a more sharp dislocation arrangement. The interiors of such substructures have a comparatively low-dislocation concentration while the small-angle cell boundaries have a high dislocation density.

Cell formation is characteristic of metals that glide on more than one glide system, so that dislocations with several different Burgers vectors are available to form cell walls. The sharpness of the cell walls formed during plastic deformation varies from metal to metal. There is a clear correlation between stacking-fault energy—and hence the degree of dissociation of dislocations and their ability to climb—and the sharpness of cell walls. Alloys with low stacking-fault energy such as Cu–Zn brass, Fe–Cr–Ni, Fe–Ni, or Fe–Mn austenitic steels have after deformation typically less pronounced, viz. less sharp DC structures. They rather reveal denser dislocation tangles with some regions of low dislocation density and multiple microbands. The values for the stacking fault energy for metals and alloys can vary

substantially. For instance, chemically pure Aluminum (99.999 wt.%) has a very high stacking-fault energy of about 200 mJ/m^2. Commercial purity face-centered cubic-structured metals such as 99.95 wt.% nickel and 99.95 wt.% silver have intermediate stacking-fault energies of about 128 mJ/m^2 and 22 mJ/m^2, respectively. 70/30 copper–zinc alloys (α-brass) have very low stacking-fault energy below 15 mJ/m^2. Highly alloyed Fe–Mn, Fe–Mn–C, and Fe–Ni steels also have low stacking-fault energy in the range between 10 and 40 mJ/m^2 depending on the alloying content. A high aluminum content (2–8 wt.%) that is an attractive pathway to design weight-reduced face-centered cubic steels increases the stacking fault energies for instance of Fe-30 wt.% Mn–C steels from about 20 mJ/m^2 to about 80 mJ/m^2 (Reeh et al., 2012).

These examples of stacking fault energies are an important characteristic and play a significant role in the deformation of metals due to its influence on dislocation mobility and morphology. More specific, the stacking fault energy determines the distance between the partial dislocations and it hence has a direct influence on the ability of dislocations to undergo cross-slip during plastic straining. The lower the stacking fault energy the larger is the separation between the partial dislocations and thus cross-slip and dynamic and static recovery are inhibited.

Copper and silver have recognizable cells with thick tangled boundaries, and nickel and especially aluminum have better defined cells that rapidly sharpen and grow during annealing after deformation (Sandström et al., 1978; Varma and Willitis, 1984; Walter and Koch, 1963; Blum et al., 1995; Li, 1962).

During subsequent recovery, the subgrain boundaries sharpen and turn into well-defined thin-cell walls. These cells progressively grow larger while their interiors become further void of free dislocations. The DCs, both before and after recovery, are normally roughly equiaxed, i.e. their dimensions are nearly the same in all directions, although under some circumstances, depending on crystallographic orientation and crystal size, cells may be elongated and arranged in bands.

The mechanism by which the diffuse cells formed after deformation sharpen and grow is a complex form of polygonization. Since dislocations are present on several glide planes (or, if on a single glide plane, with different glide vectors), the cell walls can as a rule not be simple tilt boundaries. However, where the misorientation across cell walls has been examined, it turns out that they are effectively very similar to tilt boundaries. In zinc, each wall contains at least two families of mixed edge-cum-screw dislocations, but so arranged that the misorienting effects of the screw components cancel and the tilt axis is still parallel to the dislocation lines lying in the wall. There is evidence that cell walls in aluminum have a similar structure. Since a variety of dislocations are available, cell walls have a number of different orientations relative to the crystal axes and can thus completely enclose individual cells.

While the early steps of recovery lead to a gradual sharpening of the substructure walls, later stages of recovery are characterized by their competitive coarsening of existing substructure inside the grain. Kinematically, two extreme scenarios are conceivable in that context. Firstly, when the grain does not contain an overall in-grain net lattice curvature, gradual coarsening of the substructure does not lead to a higher local misorientation associated with each cell wall. Secondly, when the grain is curved, containing GND arrays, gradual subgrain coarsening leads to the accumulation of the content of polarized dislocations (dislocations of the same sign; GNDs) and hence to a higher average misorientation associated with each single-cell wall.

Competitive coarsening of the subgrain structure proceeds through the motion of small-angle subboundaries. The mobility of such very small-angle subboundaries (cell walls) under purely thermal activation (i.e. in the absence of stress) can be vanishingly small. However, as has been shown in the literature, the mobility of such small-angle subboundaries can be drastically increased under the

presence of a small stress (Winning et al., 2001, 2002; Winning, 2003). This is true for pure tilt boundaries, but not for other kinds of small-angle boundaries.

23.2.3 Recovery during Hot Deformation

The individual processes associated with recovery are thermally activated. Therefore, recovery also occurs dynamically already during hot working. In that context, one has to consider the melting point of the alloy under investigation, because most of the activation barriers involved, such as climbing and cross-slip, scale with the absolute melting point (climb rate) and the stacking fault energy (cross-slip rate) of the material. Normalizing the actual deformation temperature, expressed in Kelvin, by the absolute melting point introduces the homologous temperature. This means that rolling pure tungsten at 400 °C can be regarded as a cold-rolling process and the deformation of pure Aluminum at 50 °C must be already regarded as a hot-working process (Haessner, 1978; Humphreys and Hatherly, 1995).

The occurrence of recovery phenomena, such as dislocation cross-slip, dislocation climb as well as substructure sharpening and competitive coarsening during deformation, is referred to as dynamic recovery. Under conditions of rapid deformation, this process is most pronounced in metals with high stacking-fault energy such as aluminum, iron, niobium, or tungsten. Owing to their high stacking-fault energy dislocations in these metals have high nonconservative mobility and a high cross-slip rate that enables dislocation reordering and hence subgrain formation.

It was shown that because of continuous growth of subgrains, or cells during hot working (the subgrain equivalent of normal grain growth), some subboundaries disappear while others grow. The consequence is that the mean subgrain misorientation remains constant at a few degrees, right up to high strains.

23.2.4 Property Changes during Recovery

23.2.4.1 Mechanical Properties

Recovery is characterized particularly by the rearrangement of the dislocation substructure associated with a partial and gradual reduction of the internally stored elastic energy that was inherited from the preceding cold working. This means that the degree and stage of those recovery phenomena that affect the dislocation substructure is to some extend reflected by the mechanical properties of the material that is being probed.

Since the rearrangement of the dislocation structure requires a certain short-range mobility of the dislocations involved, it can be expected that the kinetics of recovery depends to some extend on the stacking fault energy of the material. This is so because the stacking fault energy determines the cross-slip probability of dislocations. Cross-slip is one of the essential recovery steps that can lead to fast dislocation rearrangements, subgrain formation, and hence, to internal stress relaxation. A small value of the stacking fault energy produces a large stacking fault. Dislocation cross-slip requires that the stacking fault is constricted before the actual cross-slip event. This is a thermally activated process and the activation barrier is proportional to the size of the stacking fault.

In metals that have a high value of the stacking fault energy, the dislocation core remains nearly intact so that screw dislocations can undergo cross-slip events without the aid of thermal activation.

This is shown in **Figures 4** and **13** for corresponding mechanical experiments conducted for copper and nickel. It can be observed that no drop in hardness accompanies stress relief or recovery in brass, copper, or nickel. These are all metals or respectively alloys with low or average stacking-fault energy and, owing to the reduced mobility of the underlying dislocations, only little climb and rearrangement

of dislocations can take place, especially in copper–zinc brass and austenitic iron–nickel and iron–manganese steels. In that context, it is worth to mention that already slight dislocation rearrangements can account for a considerable reduction in the stored elastic energy.

From these considerations, it becomes apparent that two types of consequences are conceivable in that context. Firstly, recovery obviously reduces the remaining driving force for primary static recrystallization. Therefore, extended recovery may entail much slower recrystallization kinetics. Secondly, if recovery reduces the internal elastic energy to a very large extent, for instance because the heating rate is very low or in cases where the dislocations a very mobile and hence can rearrange very efficiently, recrystallization can be even entirely suppressed. Such a situation is referred to as "recrystallization in situ" (Burgers, 1941; Humphreys and Hatherly, 1995; Himmel, 1962). Typical materials where very strong recovery can occur, thus competing with primary recrystallization, are pure aluminum, iron, and other high-melting refractory metals with body-centered crystal structure (e.g. tungsten, molybdenum, and niobium). In both materials, the dislocations are very mobile enabling them to undergo easy cross-slip. Correspondingly, softening in these materials during recovery can be very fast so that the driving force that remains for recrystallization becomes very small.

The second important aspect that can shift the competition between recovery and recrystallization toward a higher recovery tendency is a low mobility of high-angle grain boundaries. Since recrystallization is described by the formation and motion of new high-angle grain boundaries, reduced mobility of these internal interfaces gives recovery enough time to also reduce the internal stored energy. This diminishes the driving force for recrystallization and promotes strong recovery.

Under such circumstances as described above, it is conceivable that the whole of the work hardening may be recovered without the occurrence of recrystallization.

For instance, it has been shown that a weakly deformed silicon–iron crystal, iron–chromium polycrystals or pure iron polycrystals and likewise a slightly deformed iron–aluminum polycrystals can recover completely (Hölscher et al., 1991; Raabe and Lücke, 1993, 1992). For iron and iron-based alloys, that can even happen up to high annealing temperatures of 700–800 °C, depending on the heating rate. Slightly deformed aluminum samples can recover almost completely at 400–600 °C while various studies reported that aluminum single or polycrystals will recover about half the work-hardening at 300–400 °C.

The general trend observed in that context is that the larger the preceding deformation was, the smaller the fraction of pure recovery of the work-hardening will be.

Some crystals of hexagonal metals such as zinc or cadmium are exceptions: these can recover completely even after very large tensile strains by easy glide.

The reason for this type of behavior that will be discussed in more detail below lies in the available lattice curvature. The formation of new and mobile high-angle grain boundaries during the nucleation stage of recrystallization requires the occurrence of local zones in the deformation substructure with very high local-lattice curvature, e.g. above 15°. In such substructures, subgrain nuclei can, during competitive subgrain growth, accumulate a sufficiently large curvature to finally form new and highly mobile high-angle grain boundaries. If subgrain growth takes place in an area where no net lattice curvature is available in the deformed substructure, no new high-angle grain boundaries can be formed (Cotterill and Mould, 1976; Bailey, 1963; Sandström et al., 1978; Varma and Willitis, 1984; Walter and Koch, 1963; Blum et al., 1995; Li, 1962; Doherty and Szpunar, 1984a; Raabe et al., 2002a; Raabe and Becker, 2000; Humphreys, 1992a; Bate, 1999).

A number of specific mechanisms determine the relationship between yield stress, dislocation density, and DC structure. While the early stages of recovery show a reduction in yield stress that can be

related to the square root of the dislocation density, the later stages of recovery that are characterized by cell formation and gradual cell coarsening are characterized by an inverse relationship between the flow stress and the cell size. As the interiors of the cells become more and more devoid of dislocations during the later stages of recovery the average cell size (together with the grain size, which is, however, not changed during recovery) determines the strength of the material.

23.2.4.2 Electromagnetic Properties

Plastic deformation slightly increases the electrical resistivity. Various studies have been devoted to the stages by which the electrical resistivity returns to its fully annealed value. This is of interest both because it helps to disentangle the separate contributions made to the resistivity increase by dislocations and by deformation-induced vacancies, and because it helps to elucidate the complex mechanism of the damage caused by neutron irradiation in nuclear reactors; this damage also causes resistivity changes that anneal out in a different manner from those caused by plastic deformation (Beck and Hu, 1966; Haessner, 1978; Humphreys and Hatherly, 1995, 2004; Doherty et al., 1997; Doherty, 2005).

23.2.5 Recovery Textures

The mechanical properties of metals considerably depend on their microstructure and texture, which are a result both of composition and the thermomechanical processing to which they are exposed. While recrystallization is characterized by the formation and motion of new high-angle grain boundaries, recovery preserves the existing grain structure and also the original deformation texture that was created during cold working (Engler et al., 1996; Engler, 1997; Ibe and Lücke, 1966; Bunge, 1969, 1982, 1986, 1987; Wassermann and Grewen, 1962; Bunge and Esling, 1982; Beck and Sperry, 1950; Li, 1961; Dillamore et al., 1967; Hutchinson and Ryde, 1995; Doherty and Szpunar, 1984b; Doherty et al., 1988; Doherty, 1985; Samajdar and Doherty, 1994; Juul-Jensen, 1992, 1995; Juul-Jensen et al., 1988; Dillamore and Katoh, 1974; Raabe and Lücke, 1992; Klinkenberg et al., 1992; Raabe, 1995a; Juntunen et al., 2001; Ray et al., 1975b; Humphreys, 1977a; Ridha and Hutchinson, 1982a; Samajdar et al., 1992; Hjelen et al., 1991; Lee and Duggan, 1993; Doherty et al., 1993a; Duggan et al., 1993; Duggan and Chung, 1994; Samajdar and Doherty, 1995).

This means that the design of adequate recrystallization pathways can be used to create a desired crystallographic texture. Consequently, the proper understanding and use of recrystallization marks a necessary prerequisite for the design of the crystalline anisotropy of a polycrystalline sample (Raabe et al., 2002b; Roters et al., 2010).

In turn, as recovery affects only the in-grain dislocation and cell substructure it can lead to the inheritance of the original cold-working texture to the final texture of the heat-treated material. In this context, two recovery scenarios are conceivable:

One is that all grains undergo recovery instead of recrystallization—for instance when a high stacking-fault energy material is heat treated at low temperatures and after low strains. This would lead to a situation where all original grain shapes and the crystallographic texture remain the same as before the heat treatment and only the in-grain dislocation and cell structure have relaxed as described above (Raabe, 1995b, 1995a) (**Figure 15**).

The second possibility is that some grains undergo recrystallization while others only undergo recovery. Such a phenomenon leads either to the coexistence of recrystallized and recovered grains or to the gradual sweeping of recovered grains by recrystallizing ones—however with reduced driving forces (**Figure 16**).

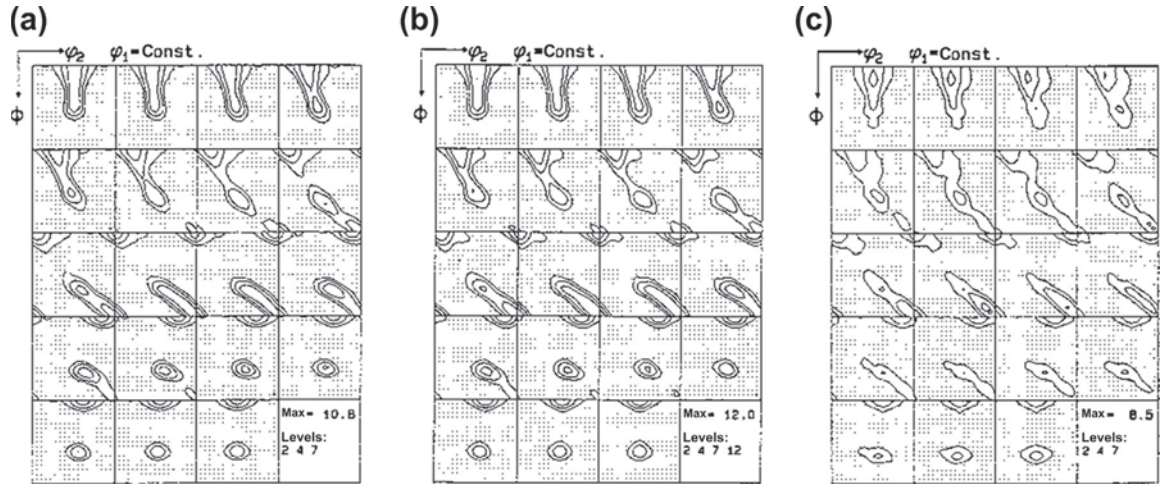

Figure 15 Texture of 90% cold-rolled and 1000 K annealed low-C steel measured by XRD. (a) 5; (b) 6s; (c) 7s (Raabe and Lücke, 1992).

Specifically regarding the second scenario, it is therefore important to understand, for an optimal design of the final microstructure and texture, why at the same heat-treatment temperature and for the same global strain imposed by a machine some grains in the same material recrystallize while others do not and recover instead (Raabe, 1995b, 1995a).

In certain aluminum alloys, this mixed approach involving joint recrystallization and recovery phenomena within the same microstructure is often used for the optimization of the material's anisotropy. In contrast to that, in some ferritic steels, the occurrence of elongated recovered grains within an otherwise-recrystallized microstructure is usually an undesired phenomenon as it leads to inhomogeneous plastic flow and surface roughness during manufacturing. This phenomenon is referred to as "ridging".

For most materials, including alloys with high stacking-fault energy, sufficient initial cold deformation in excess of 70% thickness reduction can be used to suppress strong recovery and the undesired inheritance of crystallographic deformation textures. These effects have been studied in detail on iron and low-carbon steels as well as on aluminum (Wassermann and Grewen, 1962; Bunge, 1982, , 1986, 1987; Bunge and Esling, 1982, 1991; Adams et al., 1993; Duggan et al., 1978; Dillamore et al., 1979; Hölscher et al., 1991; Ushioda et al., 1987; Raabe and Lücke, 1993; Jägle and Mittemeijer, 2012; Adam et al., 2001; Randle and Engler, 2000). It was observed that not only the total deformation or the heat-treatment temperature play an essential role for determining how much of the volume is recovered and how much is recrystallized, but also the orientations of the deformed grains, the grain size, and the accumulated shear strains are central parameters that determine the degree of recovery and the suppression of primary recrystallization after cold working at a microstructural scale.

The strong orientation dependence of recovery can be interpreted in two ways. The first approach is based on the assumption that the driving force is reduced by recovery so that the mechanical instability criterion (sufficient stored elastic energy) required for recrystallization is no longer fulfilled (Himmel, 1962). Recovery and recrystallization reveal different kinetic laws. Whereas in the first case (recovery) the properties change in a near-logarithmic manner, in the latter case (recrystallization) an incubation period followed by a sigmoidal law with a very sudden change in microstructure is commonly observed. It is thus conceivable that if recovery was strong enough to reduce the total driving force, i.e.

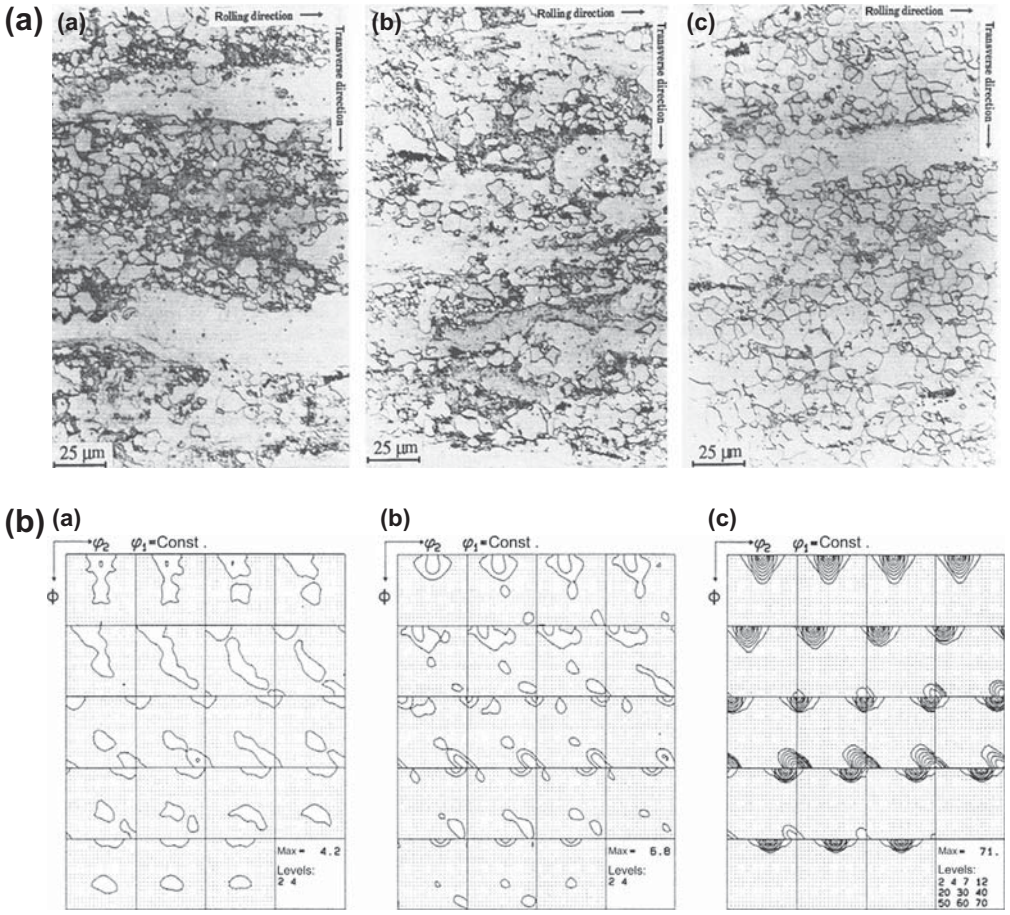

Figure 16 (a) Microstructure of a 90% cold rolled and 1000 K annealed low-C steel in flat sections. (a) 5; (b) 6s; (c) 7s. (b) Corresponding ODFs calculated only from the recovered grains. (a) 5; (b) 6s; (c) 7s (Raabe and Lücke, 1992).

the internal stress associated with the stored dislocations and cell walls, the movement of newly formed large-angle grain boundaries would be very slow or even suppressed. This assumption, however, contradicts three facts. First, the deformation energy stored in different crystals depends on their orientation. This is suggested by experimental results based on corresponding crystal plasticity finite element simulations (Roters et al., 2010) as well as the measurement of internal stresses, stored dislocation densities and cell sizes (Himmel, 1962; Cahn, 1965, 1966; Humphreys and Ferry, 1997; Engler et al., 1996; Bailey, 1960). Second, recovery is not an isolated process but a preprocess to recrystallization during which nuclei are formed. Strong recovery in the conventional sense should therefore provide a large number of nuclei rather than suppress them. Third, in case of a small grain size (polycrystals), it was observed that certain crystals are consumed by growing nuclei that proceed from the former grain boundary and or even from neighboring grains. This experience implies that grains with low stored deformation energy contain a sufficiently large net driving force for recrystallization, viz. a sufficiently high mechanic instability existed in such cases.

The second approach for explaining the suppression of recrystallization is based on the assumption that, albeit a mechanical instability potentially exists, the thermodynamic and kinetic instability criteria are not fulfilled in specific grains. In order to produce new large-angle grain boundaries during nucleation it is essential to provide areas with large local misorientations, quantified by certain densities of GNDs, already within the deformation microstructure. In most metallic alloys recrystallization nucleation then naturally results from discontinuous subgrain growth where some of the subgrains accumulate a sufficiently high misorientation relative to the surrounding microstructure. This accumulation of misorientation increases the mobility of the subgrain boundaries and so the rate of growth of the subgrain increases until it finally acts as a nucleus. Since subgrains are typically surrounded by low-angle boundaries of very low misorientation (usually below 2°), the accumulation of further misorientation during subgrain coarsening requires local orientation gradients inside grains to be present in the deformation microstructure (**Figure 17**). However, such orientation gradients are sometimes not observed within some of the deformed crystals. Such grains can then not provide sufficient kinetic instability. **Figure 18** shows an extreme example of such a joint recrystallized and recovered microstructure. The sample is Fe with large grains, rolled to 90% thickness reduction. The micrograph shows a flat section, i.e. the deformation was practically the same for all areas shown. Upon heat treatment at 1000 K for 120 s some grains recrystallize entirely while others only recover.

23.3 Recrystallization

23.3.1 Introduction

Primary static recrystallization is defined by crystal nucleation and growth into the deformation substructure (**Figure 1**). More specifically, this process proceeds via the formation and motion of new high-angle grain boundaries. In some cases also low-angle grain boundaries can be mobile and, therefore, are able to contribute to the microstructural changes occurring during primary recrystallization. When recrystallization starts the deformation substructure is already in a recovered state because the recrystallization process requires an incubation period and recovery does not.

The level to which the preceding recovery reduces the stored energy from the cold-worked state depends on the stacking fault energy of the material and on the incubation time that has elapsed before the high-angle grain boundaries that have been newly formed during the recrystallization incubation period can sweep the deformation substructure (Stead, 1898; Rosenhain, 1914; Ewing and Rosenhain, 1899, 1900a, 1900b; Alterthum, 1922; Carpenter and Elam, 1920; Czochralski, 1927; Burgers and Louwerse, 1931; Burgers, 1941; Burke and Turnbull, 1952; Smith, 1948; Beck and Hu, 1966; Haessner, 1978; Humphreys and Hatherly, 1995; Doherty et al., 1997; Doherty, 2005).

While materials with a low stacking-fault energy can store a high portion of the internal elastic strains owing to the limited cross-slip and climb capabilities of the dislocations during recovery, alloys and metals and that have a high stacking fault energy such as aluminum and iron can substantially reduce the deformation energy and hence also the remaining driving force for primary recrystallization during the preceding recovery period. In extreme cases recovery can even suppress recrystallization and an elongated and softened grain structure prevails that preserves the crystallographic texture that was formed during cold working. Typically, such behavior is not desired owing to the resulting preserved deformation texture and the topological anisotropy that results from the elongated grain shapes. In some cases, however, partial recrystallization is a microstructural design goal. This applies for instance in cases where a texture that is composed of both recrystallized and deformation orientation components is desired for optimizing the overall crystallographic anisotropy of a polycrystalline product by

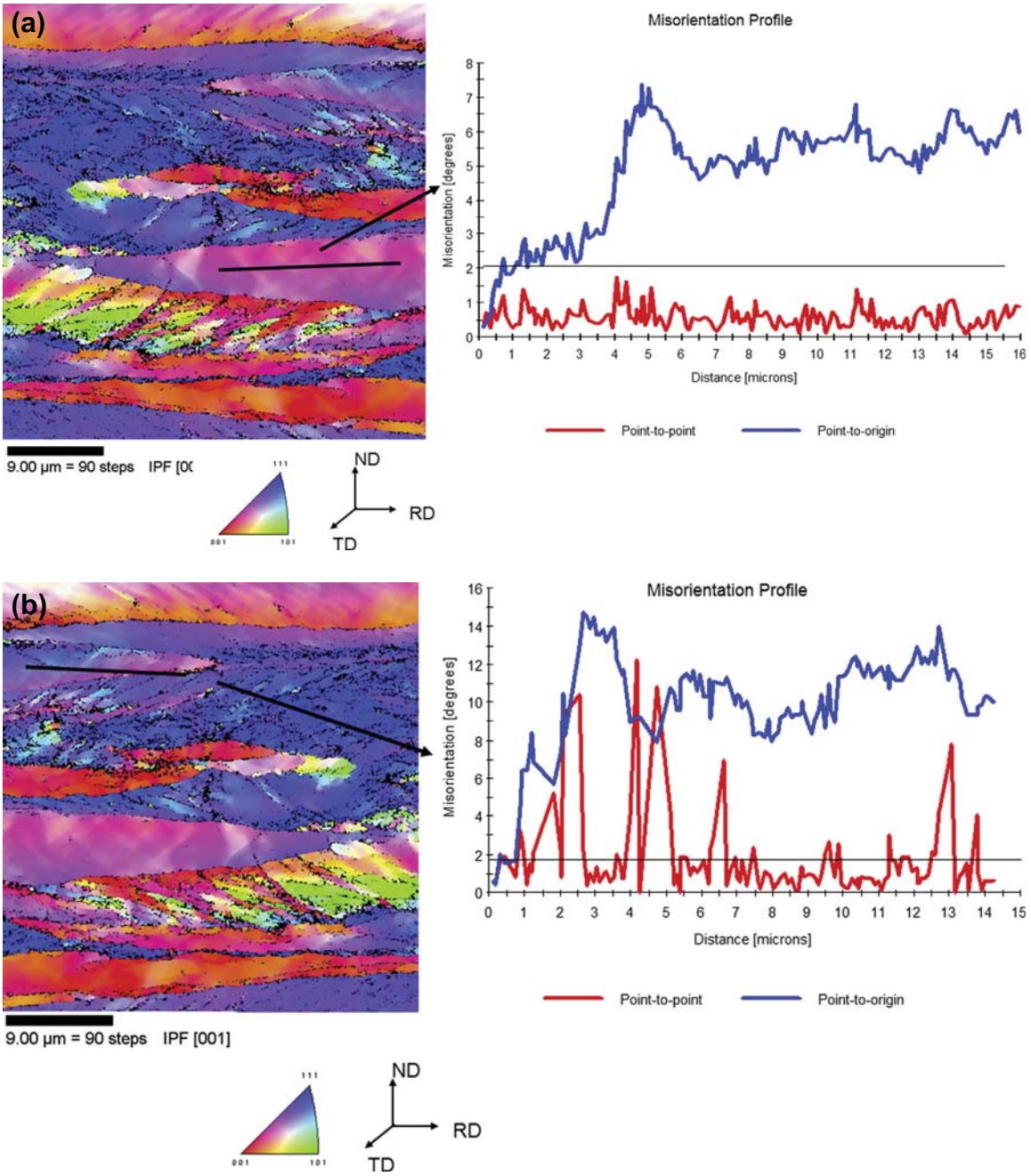

Figure 17 (a) Misorientation profile in a {001} oriented grain in 70% cold rolled low-C steel. (b) Misorientation profile in a {111} oriented grain in 70% cold rolled low-C steel. The misorientation profile reveals much higher jumps and higher overall values (Thomas et al., 2003).

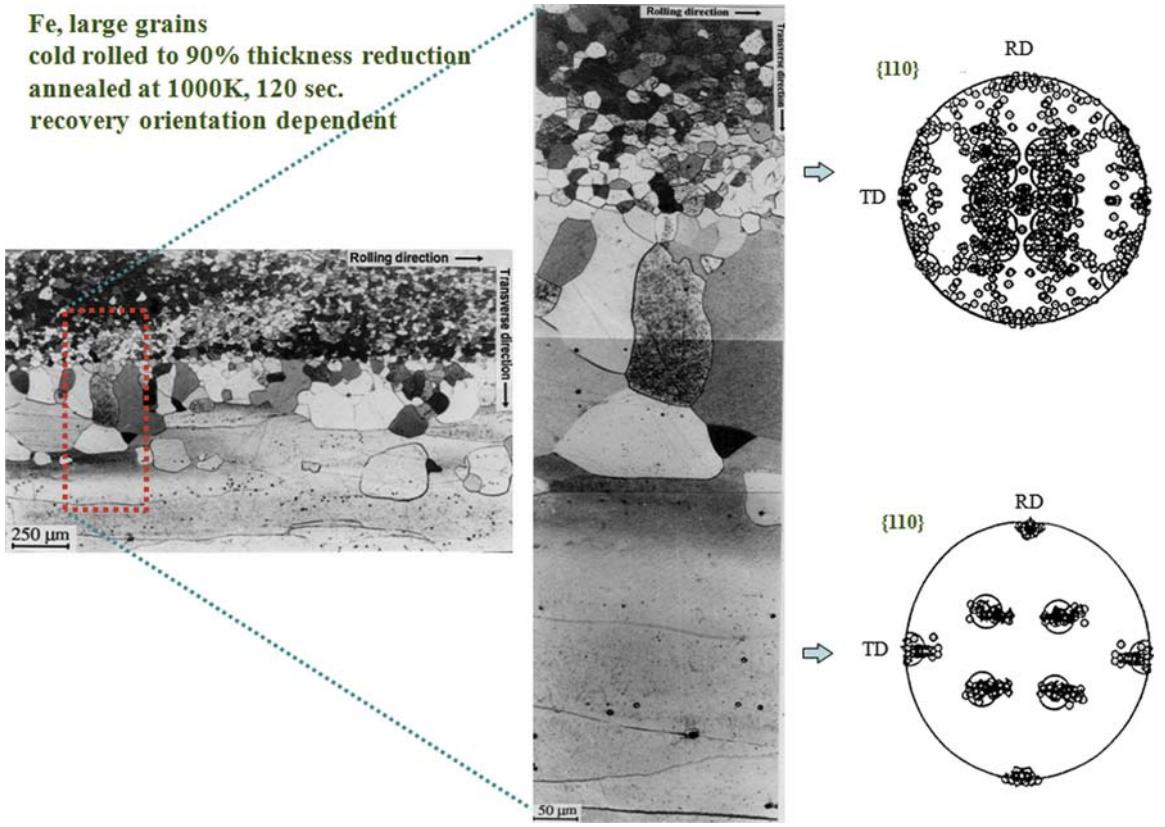

Figure 18 Extreme example of a joint recrystallized and recovered microstructure. The data were taken on a commercial purity iron sample with large grains (mm-sized), rolled to 90% thickness reduction. The micrograph shows a flat section, i.e. the deformation was practically the same for all areas shown. Upon heat treatment at 730 °C for 120 s some grains recrystallize entirely while others only recover (Raabe and Lücke, 1992).

balancing texture components with different individual anisotropy (Bunge, 1986, 1987; Bunge and Esling, 1991; Raabe et al., 2002b; Roters et al., 2010).

Primary static recrystallization, which follows the recovery stage and also competes with it (**Figures 16** and **18**), involves the replacement of the remaining recovered cold-worked structure by new strain-free and approximately equiaxed grains. This means that the analysis of a partially recrystallized grain structure can make use of the quantification of the crystallographic texture, internal elastic distortions, remaining dislocation substructures, grain shapes, and grain size distributions as characteristic microstructural features to differentiate between the as-recovered and the as-recrystallized portions of the material.

Recrystallization starts upon heating the cold-worked sample to temperatures in the range of 0.3–0.5 of the absolute melting point (**Figure 19**) (Burgers and Louwerse, 1931; Burgers, 1941). The temperature regime for recrystallization lies above that required for recovery since the former mechanism goes through a thermally activated nucleation process while the latter process requires only the thermal activation of cross-slip and climb under a state of high point-defect oversaturation and high elastic internal stresses. Although some cases occur such as in the case of heavily wire drawn Cu–Zr two phase

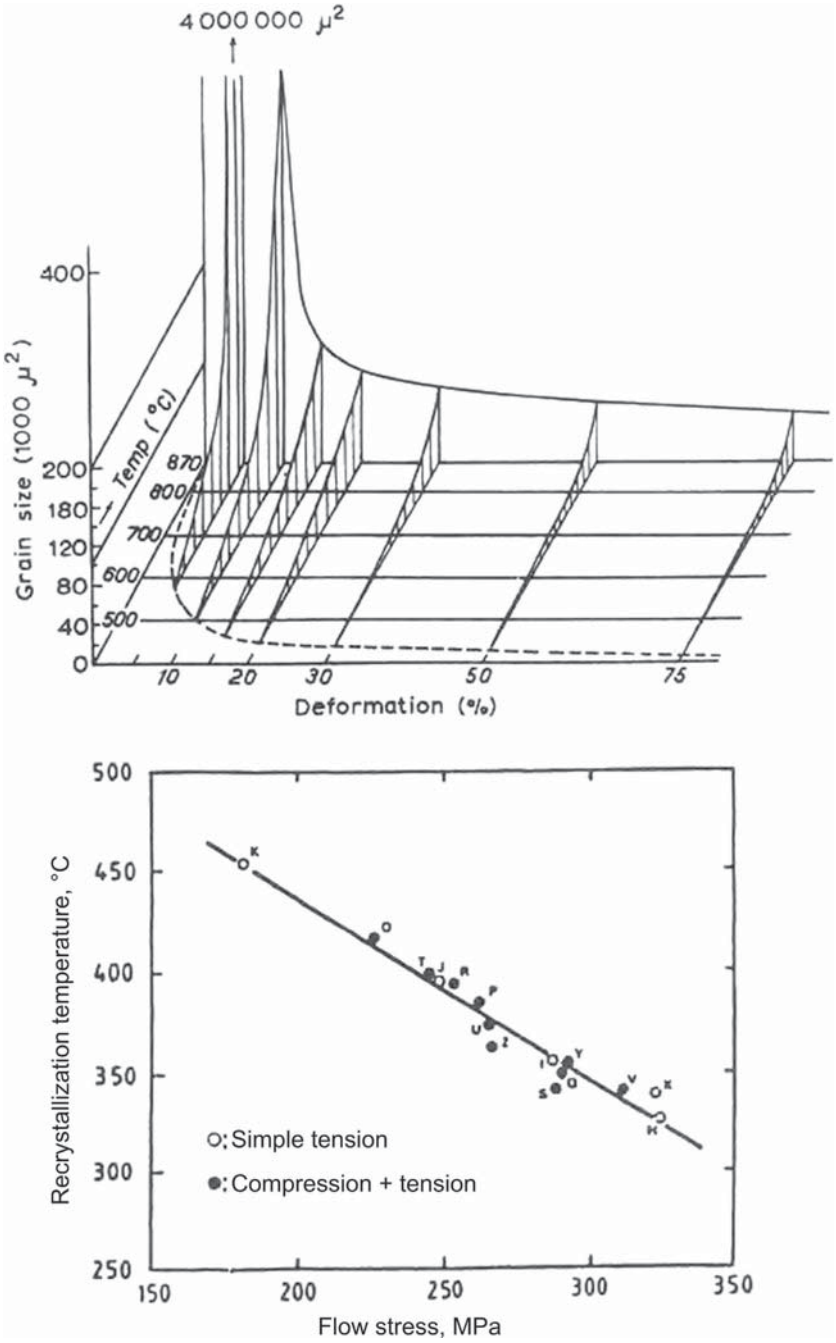

Figure 19 Recrystallization diagram of electrolytically refined iron (Burgers, 1941).

alloys where heavy cold working can even lead to the amorphization of the crystalline structure, there is usually no crystal structure change observed during recrystallization. For engineering estimates, it is often required to provide a simple measure under which circumstances recrystallization starts, namely, the recrystallization temperature. This measure is defined as the temperature at which 50 vol.% of cold-worked material has recrystallized after 1 h. As will be discussed in more detail below regarding the influence of the mobility of the high-angle grain boundaries involved during recrystallization, the actual recrystallization temperature as defined above is strongly dependent on the purity of a material. While high-purity materials can recrystallize already around 0.3 of the absolute melting point, impure materials may not recrystallize before a temperature of 0.5–0.7 of the melting point in Kelvin is reached. The influence of material purity on the recrystallization kinetics is so remarkable because solute atoms change the apparent activation energy of the grain-boundary mobility via an impurity drag mechanism (Lücke and Stüwe, 1963). This means that impurities can have a kinetic influence that acts on an Arrhenius function, namely, on the thermally activated mobility term associated with the motion of a high-angle grain boundary (Molodov, 2001; Lücke and Stüwe, 1963; Gottstein et al., 1995; Shvindlerman et al., 1995, 1999).

Besides this essential role of the interfaces involved a number of other metallurgical parameters are essential for the recrystallization microstructure and kinetics. Here specifically the amount of prior cold working, temperature, time, initial grain size, chemical composition, presence of second phases, crystallographic texture, and the amount of recovery prior to the start of recrystallization play important roles. Also, in a manufacturing environment, the heating rate has to be considered since many commercial heat-treatment cycles work with rather large slabs. This may lead to relatively low effective heating rates entailing substantial inhomogeneities of the recrystallization microstructure and kinetics across the macroscopic dimensions of the material. For instance, large steel coils, when processed in a commercial manufacturing environment, often reveal substantial and through-thickness gradients in the recrystallization microstructure and crystallographic texture (**Figure 20**) (Peranio et al., 2010). For instance, in the field of ferritic steels such inhomogeneities lead to a reduction in the forming properties (Huh et al., 2005; Raabe, 1996, 1997).

From the vast body of experimental data in this field, a small set of elementary empirical recrystallization rules can be filtered:

For recrystallization to start and proceed, typically a minimum amount of preceding plastic cold working is required. For most commercial alloys with a high stacking-fault energy such as body-centered cubic steels and certain aluminum alloys, this value amounts to about 40–50% cold reduction prior to the heat treatment. Cold reduction below a value of 35% is often not sufficient for primary static recrystallization to take place.

Rapid nucleation during the incubation period of recrystallization requires a certain amount of inhomogeneity present in the deformation microstructure. Such inhomogeneous deformation zones can be for instance crystallographically curved areas containing high amounts of GNDs close to the existing grain boundaries (**Figure 21**); shear bands (a crystallographic deformation inhomogeneity that can assume mesoscopic dimensions and penetrate multiple grains under an oblique angle to be dominant deformation axis) (**Figure 22**) (Dorner et al., 2007); microbands (zones of concentrated crystallographic shear, typically inside grains); transition bands (zones of divergent crystal reorientation inside grains, i.e. connected rotation zones in different orientation directions that preserve in part the original orientation in the middle between the branches of the transition band); large precipitates that create sufficient curvature and inhomogeneity in their vicinity during deformation (**Figure 23**); or in-grain areas that have a sufficiently high lattice curvature such as the distorted zones adjacent to grain boundaries. These microstructure features provide not only a high local deformation energy that is

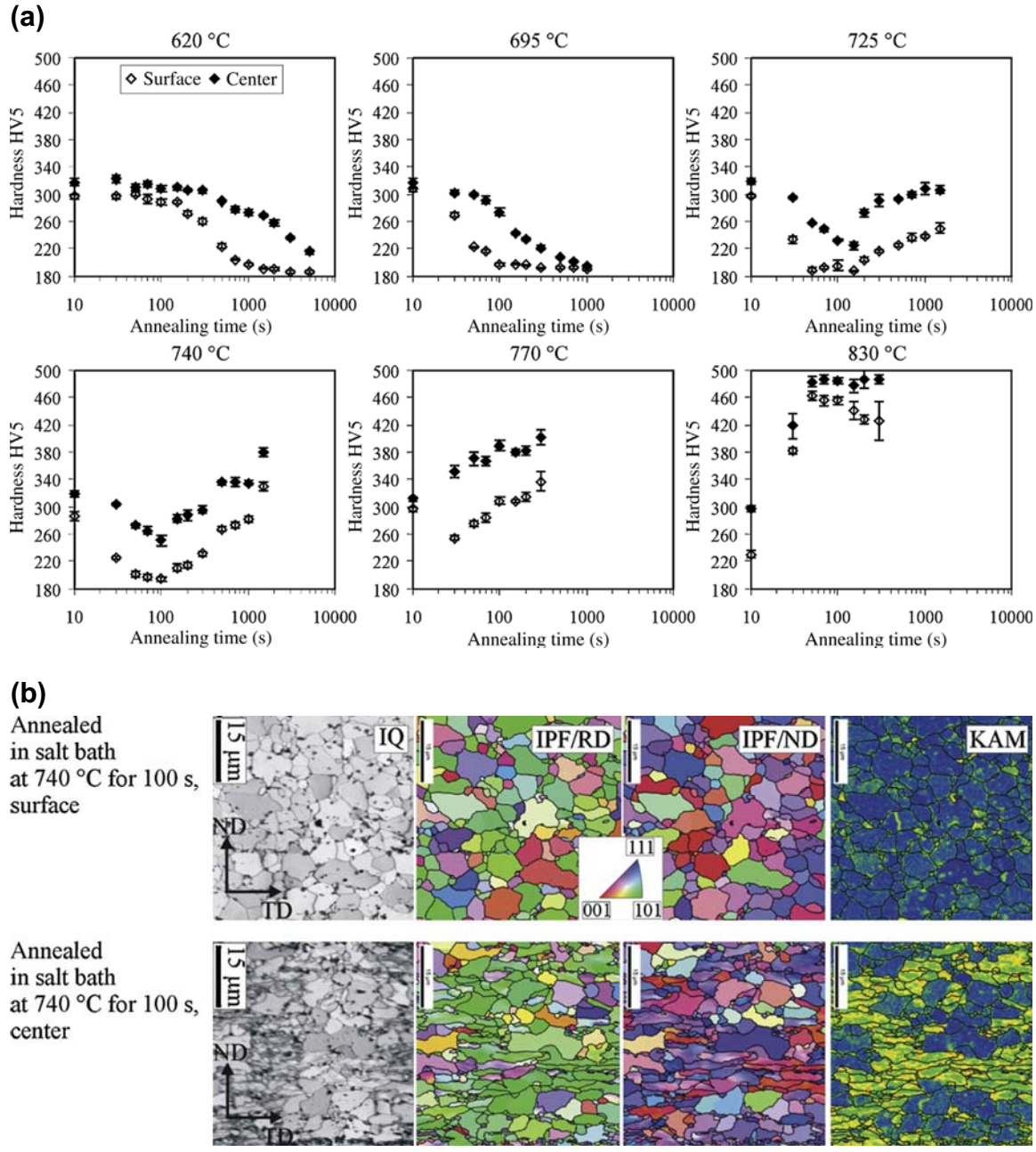

Figure 20 (a) Hardness measurement in dependence of the annealing time measured in the center and at the surface of C-steel sheets. The sheets were annealed in salt bath at ferritic and intercritical annealing temperatures. (b) EBSD microstructure maps: EBSD carried out in the center and at the surface of a transverse section of a sheet annealed in salt bath. The images show the Image Quality map (IQ), the Inverse Pole Figure maps (IPF/RD and IPF/ND), and the Kernel Average Misorientation map (KAM, blue: KAM $= 0°$, red: KAM $= 3°$) obtained at the same specimen area. Grain boundaries with angles larger than $3°$ are indicated by black lines in the IPF and KAM maps (Peranio et al., 2010).

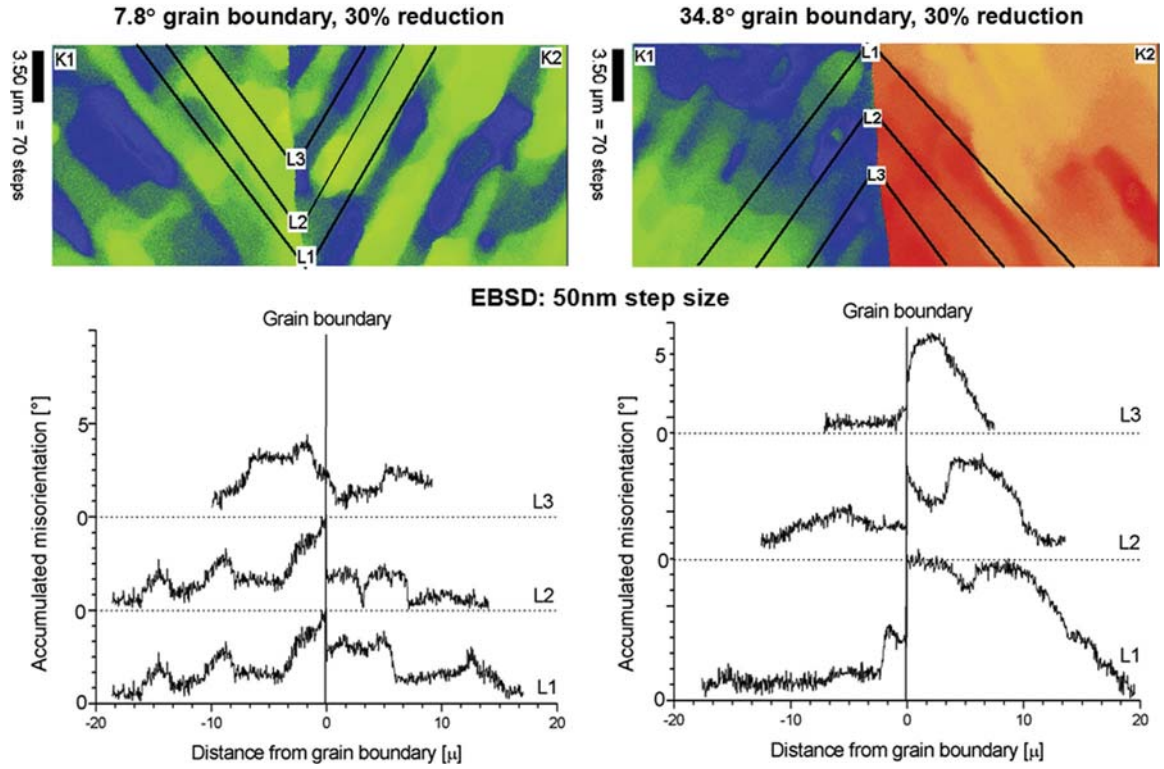

Figure 21 Misorientation before a small-angle grain boundary and before a high-angle grain boundary in Al bicrystals, strained 30%. Different misorientation profiles build up before the two different types of interfaces (Zaefferer et al., 2003).

required as a driving force during nucleation but they specifically promote the accumulation of a large local lattice curvature during discontinuous subgrain coarsening that finally leads to the formation of new high-angle grain boundaries.

Recrystallization phenomena are thermally activated. This means that the rate of the mechanisms that control the formation and motion of the newly formed high-angle grain boundaries depend on the annealing temperature. Usually the temperature dependence follows Arrhenius-type equations, establishing an exponential relationship. The recrystallization temperature of most materials lies between 0.4 and 0.6 of the absolute melting point. In engineering terms, the recrystallization temperature refers to that point where 50 volume % of the material is recrystallized after 1 h. The recrystallization temperature decreases with increasing plastic deformation. The smaller the degree of the preceding cold working is, the higher will be the recrystallization temperature. Also, it was observed that the finer the initial grain size is, the lower will be the recrystallization temperature (Haessner, 1978; Humphreys and Hatherly, 1995). The larger the initial grain size is, the greater is the degree of plastic deformation that is typically required to produce an equivalent recrystallization temperature. An increase in the degree of plastic cold working leads to lower required annealing temperatures and to a reduced grain size after recrystallization. Higher plastic deformation means greater lattice rotations (from dislocation slip or mechanical twinning) inside grains and also to higher stored energies (Raabe et al., 2002a). Therefore, the probability of generating new grains increases with strain. The higher the temperature of cold working, the less

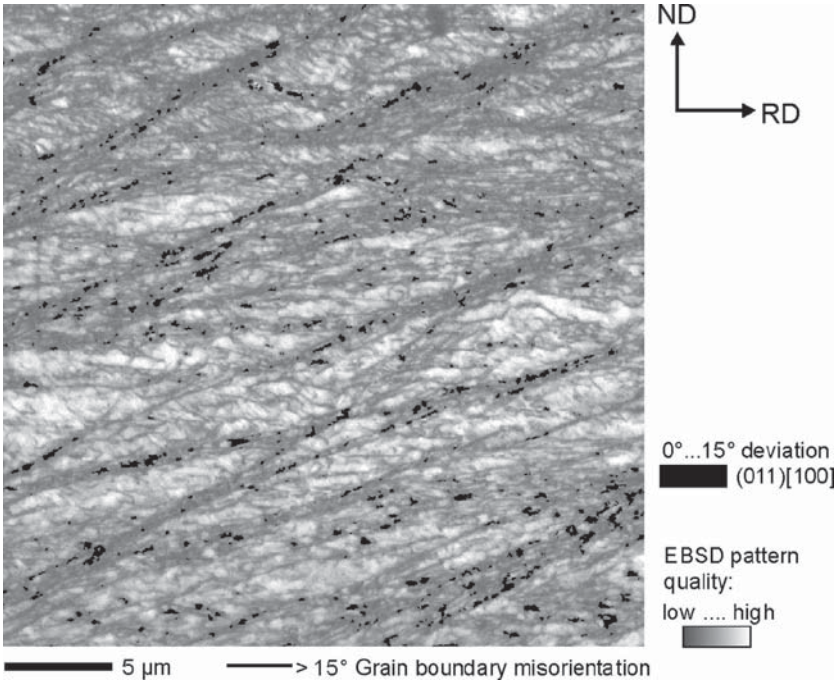

Figure 22 Goss-oriented regions inside of shear bands in a 89% deformed Fe-3 wt.% Si initial single crystal sample. The-diagram shows the EBSD pattern quality map (gray scale) revealing shear bands as regions with low EBSD pattern qualities. The shear bands are inclined by 29–36° to the RD. In addition, Goss-oriented regions are marked in black (Dorner et al., 2007).

is the strain energy stored and thus the recrystallization temperature is correspondingly higher. The overall recrystallization rate increases exponentially with the heat-treatment temperature. Higher recrystallization temperatures usually lead to an increasing probability to form nuclei, hence, to an increased density of nuclei and therefore to a smaller recrystallized grain size. This means that the grain size after recrystallization decreases with increasing prior strain, i.e. the nucleation density increases. In most materials, the grain size after recrystallization decreases as the strain increases.

Crystallographic recrystallization textures are typically profoundly different from those produced during cold deformation. Higher degrees of cold working often lead to more pronounced and sharp recrystallization textures. Prevalence of recovery leads to the inheritance of the cold deformation textures and hence to weaker recrystallization textures. Higher annealing temperatures often lead to more pronounced and sharp recrystallization textures.

During recrystallization, the mechanical properties that were changed during deformation due to strain hardening are restored to their respective values that they had before the cold-working procedure. During this stage of annealing, impurity atoms tend to segregate at grain boundaries, and retard their motion. This mechanism typically may obstruct the processes of nucleation and growth. This so-called solute drag effect can be used to retain the cold-worked strength at higher service temperatures. The presence of second-phase particles causes the retardation of recrystallization. This effect is referred to as particle pinning or Zener pinning. A special situation, where the precipitation of particles can very strongly accelerate (rather than slow down) primary recrystallization, occurs when recrystallization and precipitation of second phases from a supersaturated solid solution occur at the same time. The

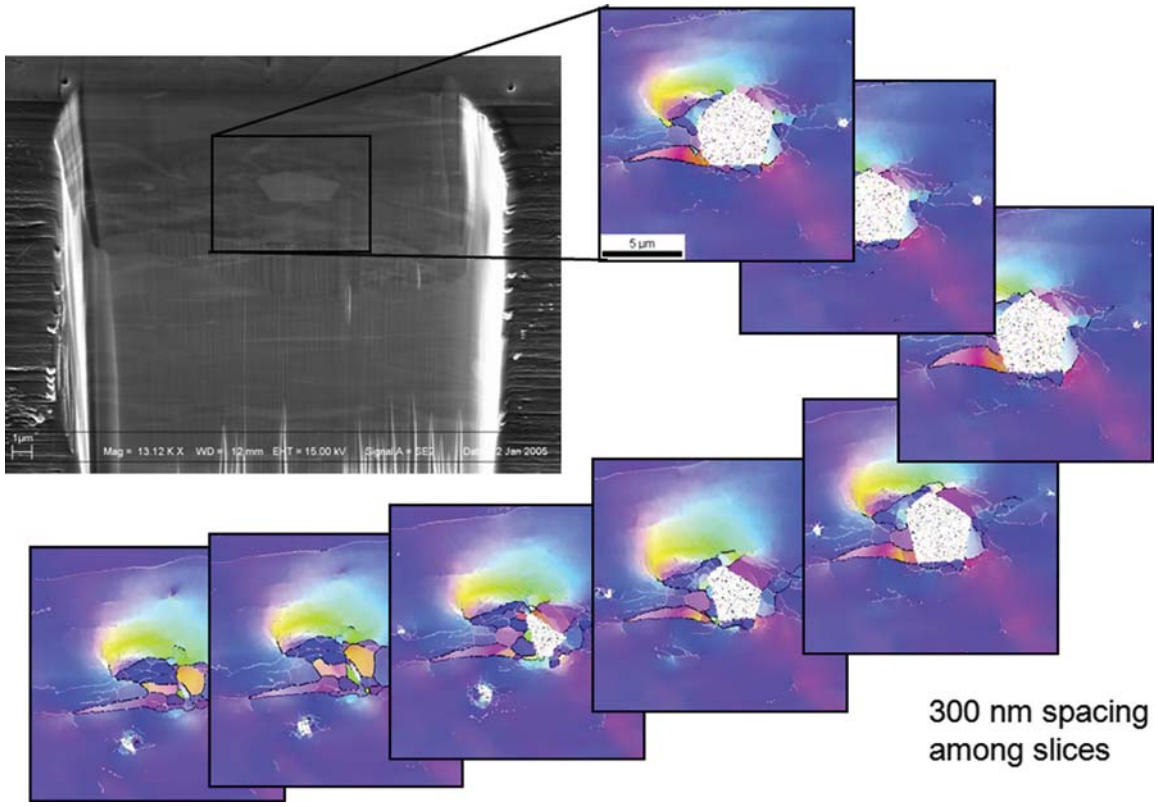

Figure 23 Orientation gradients around a hard Laves particles in a Fe_3Al matrix (Konrad et al., 2006).

acceleration is due to the fact that higher driving forces act when recrystallization (reduction in dislocation density) takes place together with phase transformation or respectively precipitation (release in transformation-free energy). Such situations are referred to as discontinuous precipitation phenomena. They are characterized by the fact that the driving force is not only coming from the stored deformation energy but also from the chemical driving force that is associated with the transformation.

The heating rate can also have a profound impact on the resulting recrystallization microstructure. This is so because a number of thermally activated processes compete during heat treatment. These are for instance dislocation climbing, dislocation cross-slip, motion of low-angle grain boundaries, motion of high and grain boundaries, formation or dissolution of second phases, and segregation. As these different mechanisms show and as will be discussed later in more detail, it is therefore useful to differentiate between chemical driving forces and mechanical driving forces.

23.3.2 Overview of Basic Recrystallization Phenomena

Primary static recrystallization describes the transformation of an as-deformed microstructure above the critical recrystallization temperature and above a critical threshold deformation. In scientific terms, the analysis of recrystallization typically addresses isothermal transformations. In manufacturing, however, recrystallization processes are usually not isothermal.

Primary static recrystallization proceeds by the formation and motion of new high-angle grain boundaries. During recrystallization, no new deformation is imposed. The process follows Johnson–Mehl–Avrami–Kolmogorov (JMAK) sigmoidal kinetics and typically leads to a refinement of the microstructure (Kolmogorov, 1937; Johnson and Mehl, 1939; Avrami, 1939, 1940). Grain structures resulting from primary static recrystallization typically consist of equiaxed crystals. The driving force is provided by the stored deformation energy, i.e. primarily by the long-range elastic stresses associated with the dislocation and subgrain structure that was formed during plastic straining. The driving force can hence be approximated as being proportional to the stored dislocation density, the shear modulus, and the magnitude of the Burgers vector (Aust and Rutter, 1959, 1960; Hu et al., 1990; Rath and Hu, 1969a). The mechanical properties (hardness, yield strength) decay at first slowly during the incipient recovery (incubation or nucleation stage) and then very rapidly, i.e. sigmoidally, when the newly formed grains sweep the deformation microstructure. Final impingement of the growing crystals leads to end of the transformation. The end of primary recrystallization is accompanied by competitive grain coarsening, i.e. grain growth.

Dynamic recrystallization describes the formation and motion of new high-angle grain boundaries during deformation at elevated temperatures (Cotterill and Mould, 1976). Beyond a certain threshold deformation, nucleation occurs and new grains from. These grow only to a certain size since they are continuously further deformed during the ongoing hot working. Kinetics of dynamic recrystallization phenomena are characterized by single peak or multiple peak behavior in the measured strength or hardness. This behavior reflects a locally heterogeneous sequence of strain hardening and subsequent or simultaneous softening by local dynamic recrystallization. In materials with a low or small stacking-fault energy, dynamic recrystallization typically occurs during most commercial hot-rolling and related hot-forming operations.

Grain growth describes the situation where competitive coarsening of the crystals leads to a microstructure where the average grain size slowly increases (Beck and Hu, 1966; Haessner, 1978; Humphreys and Hatherly, 1995; Doherty et al., 1997). The driving force of this phenomenon comes from the reduction in the total grain-boundary area. Like in other processes that undergo gradual structure coarsening under the effect of local interface curvature, such as originally described by the Gibbs–Thompson equation, typically the larger grains grow at the expense of smaller grains.

Secondary recrystallization refers to a specific grain-growth phenomenon where a very small number of grains grow to a dimension that exceeds the average grain size by one order of magnitude or more in terms of the grain diameter. However, secondary recrystallization is a slightly misleading term. When cast into a more appropriate term, it is sometimes also referred to as discontinuous grain coarsening or discontinuous grain growth. It does not describe the sweeping of the deformed microstructure such as encountered during primary static recrystallization but instead it refers to the extensive growth of a few large grains in an otherwise recrystallized grain structure. Hence, it has only a phenomenological similarity to primary static recrystallization because some literature describes the process in terms of a nucleation stage where some of the grains grow first extensively in the incipient stage of secondary recrystallization (pseudonucleation) and a subsequent "growth" stage where these huge crystals sweep the other regularly sized crystals (Rossard, 1963; Sellars and Tegart, 1966; Drube and Stüwe, 1967; Stüwe, 1968; McQueen et al., 1976). This latter growth stage does not require a specific additional driving force but the mere fact that some grains are much larger than others is topologically sufficient that the local curvature provides extensive further growth of these candidates. In physics terms, secondary recrystallization is a grain-growth process where a small number of grains grows extensively and can assume a size that is more than 100 times larger than that of the average size of the grains that surround it. The reason for this behavior can be local back-driving forces, inhomogeneous

microstructures, and inhomogeneities in the grain-boundary properties in terms of energy and mobility. A typical example is the discontinuous grain growth of huge Goss-oriented grains in Fe-3 wt.% Si soft magnetic steels.

Another recrystallization type is referred to as recrystallization in situ (Beck and Hu, 1966; Haessner, 1978). Here again the classical terminology may appear a bit confusing because this phenomenon describes extensive recovery and not a nucleation and growth situation such as encountered in primary static recrystallization. In this situation, the very strong recovery of the as-deformed material proceeds to a level where the remaining driving force for static recrystallization becomes too low and where the subgrain growth has led in part to the formation of high-angle grain boundaries.

23.3.3 The Nucleation Stage of Primary Static Recrystallization

23.3.3.1 Introduction

Many structural transformations in metallic alloys take place via nucleation and growth. This is a heterogeneous two-stage transformation mechanism where those regions that are transformed first during the nucleation stage are separated by atomically sharp interfaces from the remaining untransformed regions that surround these nuclei (Humphreys and Hatherly, 2004; Cahn 1966; Johnson and Mehl, 1939; Shvindlerman and Gottstein, 1999). From a phenomenological viewpoint, recrystallization can also be formally described in terms of this conceptual framework. However, although some similarities indeed exists between conventional phase transformations and recrystallization, it must be emphasized that the latter type of microstructure transformation is a nonthermodynamic equilibrium process because the stored deformation energy (essentially the dislocations) is only in local mechanical equilibrium but not in thermodynamic equilibrium.

The nuclei in static primary recrystallization are defect-free, newly formed crystals that are—at least partially—surrounded by mobile high-angle grain boundaries. Hence, as a recrystallization nucleation, we jointly refer to those mechanisms that lead to the formation of new mobile high-angle grains boundaries or to the overcritical bulging of already existing inherited high-angle grains boundaries.

Although we formally define here two stages in recrystallization, namely, the nucleation stage and the growth stage, both phenomena are characterized by growth, i.e. by the motion of interfaces (Humphreys, 1997). More specific, the main difference between the two processes is that only the first stage, viz. recrystallization nucleation, requires some additional characteristics that determine how, why, where and in which direction the transformation starts.

Although in many cases the deformation substructure is in its function of providing a driving force for the transformation viewed as a homogeneous parameter, recrystallization nucleation cannot be described as a homogeneous phenomenon. In real microstructures, the driving force provided by the preceding cold working is of course not distributed homogeneously. For instance, near-grain boundary regions have in cold-worked metals usually both, higher lattice gradients and higher stored deformation energy compared to the grain interiors. However, the use of a scalar and homogeneous driving force works as a first approximation to understand some elementary kinetics and microstructural properties of recrystallization. Although this simplification works to understand the mechanical driving force acting during primary recrystallization, it does not work when addressing the nucleation stage itself. This means that recrystallization nucleation is principally a consequence of microstructure inhomogeneity. In order to understand nucleation in recrystallization one has to address three main questions: first, where are the highest local driving forces? Second, where does the microstructure reveal a sufficiently large local lattice curvature or already existing misorientations to allow the gradual or spontaneous formation of mobile high-angle grain boundaries that can later

sweep the surrounding deformation substructure with an intrinsic high mobility? Third, where in the microstructure does a sufficiently high gradient exist in the stored energy across a high-angle grain boundary. The first criterion is referred to as thermodynamic instability criterion (existence of a driving force), the second one as kinetic instability criterion (formation of mobile interfaces), and the third on as mechanical instability criterion of recrystallization nucleation (gradient in driving force across interfaces) (Haessner, 1978; Humphreys and Hatherly, 1995, 2004; Doherty et al., 1997; Doherty, 2005).

Classical thermodynamic nucleation criteria developed for isothermal equilibrium phase transformations describe how the newly formed interface (energy loss) that surrounds a new and transformed region (energy gain) and separates it from the as-deformed hence untransformed area leads to a critical nucleation energy barrier that can be overcome by thermal fluctuation if the barrier is not too high.

For homogeneous nucleation, in which the nucleus can start to form in principle at any atomic site in a unit volume, the critical local increase of the free energy (nucleation barrier) must be supplied by thermal activation. In case of heterogeneous nucleation, some of the new interface energy (high-angle grain boundary energy) required can be contributed by an already existing portion of interface. This effect can lead to a notable reduction in the size of the nucleation barrier. This phenomenon is referred to as heterogeneous nucleation. It forms the theoretical basis for the understanding of most nucleation phenomena in materials science.

In recrystallization, however, classical nucleation theory has not proven to be a successful concept. Two specific reasons stand specifically against applying a classical nucleation model to recrystallization: the first one is the very low value of the stored energy associated with plastic deformation. It does usually not exceed several MPa in driving force. The second one is the high interfacial energy of the newly formed high-angle grain boundaries. They are usually of the order of 1 J/m^2 (Molodov, 2001; Lücke and Stüwe, 1963; Gottstein et al., 1995; Shvindlerman et al., 1995, 1999; Upmanyu et al., 1999; Rollet et al., 2004).

Hence, when using these values in homogeneous nucleation theory, an impossibly small density of new grains would be predicted. Even the most effective heterogeneous nucleation sites cannot reduce the barrier to recrystallization nucleation to any significant extent to reach the required nucleation energy.

An alternative theoretical approach how nucleation proceeds in primary static recrystallization was that a new grain does not necessarily develop via nucleation of a totally new crystal with an individual crystallographic orientation that did not exist before in the material but instead a recrystallized grain develops gradually from a recovered region of the existing deformed microstructure, a cell or a subgrain (Humphreys and Chan, 1996; Humphreys, 1992a). The new grain then has an orientation that will be essentially that of the deformed region from which it grew.

This means that according to this commonly accepted view the crystallographic orientations that are formed during the nucleation stage of primary recrystallization already exist in the deformed microstructure. From that we can conclude that in a system where nucleation proceeds exclusively by such a discontinuous subgrain coarsening mechanism all texture components of the recrystallization texture were already hidden at least in some very small portion of the deformation microstructure. This discussion reveals that recrystallization is not characterized by a true nucleation mechanism in the classical thermodynamic sense where new structure units are formed by thermal fluctuation that did not previously exist.

23.3.3.2 Nucleation by Discontinuous Subgrain Coarsening

It was described above that one typical process that can lead to recrystallization nucleation is the discontinuous subgrain-coarsening mechanism. It describes the competitive growth of some DCs at the

expense of others that shrink and finally vanish during the recovery stage. It must be emphasized though that this mechanism can only act as a recrystallization nucleation mechanism in specific cases. For a gradual discontinuous subgrain coarsening to function as recrystallization nucleation mechanism with the result to produce new mobile high-angle grain boundaries that sweep the cold-worked substructure and less recovered cells, it has to occur inhomogeneously in the deformation microstructure. If such competitive subgrain-coarsening phenomenon occurs everywhere in the material, the mechanical instability criterion would be lost and instead recrystallization in situ would take place.

This means that in order to fulfill the instability criteria outlined above, subgrain coarsening must proceed in a heterogeneous fashion where some areas reveal faster subgrain coarsening than others. This may lead first, to a sufficiently high accumulated misorientation to form a new high-angle grain boundary; and second to a directed gradient in driving force between the rapidly and the not-so-rapidly coarsened substructure. This is why the successful nucleation stage is often referred to as discontinuous subgrain coarsening and not just as subgrain coarsening (Haessner, 1978; Humphreys and Hatherly, 2004; Faivre and Doherty, 1979; Humphreys, 1992a; Ferry and Humphreys, 1996). In the classical literature, it is alternatively also called abnormal subgrain growth; however, the term discontinuous subgrain coarsening is more appropriate.

This means that recrystallization nucleation by discontinuous subgrain coarsening is characterized by the rapid growth of a very small minority of the recovered cells that then become the new grains that finally are surrounded by high-angle grain boundaries.

It has often been noted, that only a very small fraction of cells make the transition to a new grain. In a moderately cold-deformed aluminum sample, the subgrains are typically about 1 μm in size while after primary recrystallization a grain size of at least 100 μm is quite common in this material. This ratio suggests a volume increase by a factor of about 10^6. This means that only one subgrain out of a million reaches the transition to become a rapidly growing recrystallization nucleus capable of producing a recrystallized grain.

An essential feature of discontinuous subgrain growth leading to a recrystallization nucleus is the gradual accumulation of sufficient misorientation across the moving interfaces involved in subgrain coarsening. The mobility of grain boundaries, their velocity under a given driving pressure, is typically much lower for subgrain boundaries with a low angle of misorientation than for high-angle grain boundaries. As a result of this mobility difference, only subgrains that are highly misoriented, typically by more than about 15° with respect to at least part of their surrounding substructure, can grow sufficiently rapidly and hence become recrystallizing grains. This observation adds an essential crystallographic aspect to the topology kinetics described above. The requirement for a subgrain boundary to accumulate sufficient misorientation and, hence, achieve higher mobility means that successful nucleation takes place particularly in deformed areas that contain already a high lattice curvature from preceding cold working. Strong lattice curvature typically occurs at shear bands, around second-phase particles (Furu et al., 1993; Hansen and Bay, 1981; Hillert, 1988; Humphreys, 1977a, 1977b, 1979; Leslie et al., 1963b; Siqueira et al., 2011; Humphreys and Kalu, 1987; Humphreys and Ardakani, 1994; Hutchinson, 1989; Hutchinson et al., 1989; Juul Jensen et al., 1991, 1994; Leslie et al., 1963c; Liu et al., 1995; Rath and Hu, 1969b; Ridha and Hutchinson, 1982b; Russel and Ashby, 1970; Miyazaki et al., 2002; Fujita et al., 1996; Inagaki, 1987; Doherty and Martin, 1962–1963; Jones et al., 1979), at grain boundaries, and within instable crystallographic orientations (divergent texture components) (Raabe et al., 2002a).

At modest preceding plastic deformations of the order of 20–40% cold reduction, only few gradient zones are formed, particularly in high-purity metals. In such cases where deformation does not entail high in-grain orientation gradients, i.e. only few regions exist in the lattice with high misorientations

relative to the neighboring substructure, capable nucleation sites do hence not occur frequently. At low reductions (less than 20%) in polycrystalline metals, the only high misorientations are found to occur at prior grain boundaries or at heterointerfaces in cases where a second phase occurs.

In investigations on heavily rolled copper and aluminum-containing particles larger than 1 μm, the density of sites with high local misorientations was shown to increase greatly with strain and, with the strength and size of the heterogeneities. In such cases, heavily strained, and also heavily curved, deformation zones formed around the coarse, second-phase particles (Haessner, 1978; Humphreys and Hatherly, 1995, 2004; Faivre and Doherty, 1979; Engler, 1997; Laue, 1913; Ferry, 2002; Huang et al., 2000).

In more severely strained alloys (e.g. heavy rolling reductions of 80% and more) a very high density, particularly in the normal direction, of high-angle misorientation regions is observed. Typically, the occurrence of a high local misorientation of some cells relative to their vicinity is only a necessary condition for a potential nucleation site to become active. It should be underlined that it is however not a sufficient condition since the vast majority of subgrains at high-angle grain boundaries, and other high misorientation sites, do not become new grains. It has long been recognized in addition to the mobility requirement for a subgrain to grow, a successful subgrain needs to have an energy advantage so that it grows rather than vanishes (Humphreys and Chan, 1996; Humphreys and Ardakani, 1994; Humphreys, 1977b). The usual form of this energy advantage is having a significantly larger subgrain (Humphreys, 1997, 1992a; Miodownik, 2002).

The size advantage may arise from the deformation process if a particular orientation on one side of a high-angle boundary has a larger subgrain size and thus a lower stored energy.

This effect was observed in body-centered cubic metals through the measurement of the mean subgrain size that was smallest in grains having crystallographic {111} oriented planes parallel to the rolling plane, and by measurement of the mean subgrain misorientation that was largest in grains with that orientation (Choi, 2003). In pure iron cold-rolled only to 50%, Inokuti and Doherty, (1977), (1978) found that nucleation occurred by invasion of {111}-oriented grains by neighboring crystals with a larger subgrain size.

This phenomenon was termed "strain-induced boundary migration". It had originally been identified by Beck et al. (1950). In compressed and also in rolled aluminum, cold deformed to only 40–50% reduction, there were no significant subgrain size differences observed in the cold-worked microstructure. However, the required size differences for nucleation for strain-induced boundary migration appeared by the process of subgrain coalescence in one of the grains, that can be considered as the parent grain during this process. The enlarged subgrain then grew into the adjacent grain by migration of the existing high-angle grain boundary between the deformed grains. Detailed analysis of this subgrain coalescence at grain boundaries was identified by Faivre and Doherty, (1979) as requiring the presence, in the parent grain, of an additional high misorientation at a transition band in order that coalescence could take place.

23.3.3.3 Recrystallization Nucleation by Thermal Twinning

The analysis of recrystallization nucleation by the discontinuous competitive coarsening of the subgrain structure has revealed that this mechanism does not lead to other orientations than those already present in the cold-worked microstructure. This means that as a rule no new DCs are spontaneously formed during the nucleation stage.

However, this mechanism does not explain certain recrystallization texture components that manifest a discontinuous deviation from all orientations that were originally present in the cold deformation texture. Such observations apply particularly to metals and alloys with a low stacking-fault

energy such as brass or austenitic stainless steels. Such a more spontaneous change in the crystallographic orientation during recrystallization must be due to an alternative nucleation mechanism, namely, annealing twinning (Berger et al., 1988; Wilbrandt, 1980; Wilbrandt and Haasen, 1980a, 1980b). Indeed, it was observed that twins tend to form first as a thin lamella parallel to the progressing recrystallization front (**Figure 24**) (Berger et al., 1988).

The exact atomistic mechanisms associated with this phenomenon are not entirely understood. One assumption is that a growth defect that leads to fine twins at the recrystallization front while other mechanisms assumed that a dissociation of a moving grain boundary splits off a twin boundary. This mechanism was assumed to occur in order to reduce the overall energy associated with the grain boundary. The phenomenon was observed in a triple point configuration where several grains meet.

As later discussed by Wilbrandt and Haasen (Berger et al., 1988; Wilbrandt, 1980; Wilbrandt and Haasen, 1980a, 1980b) a random twinning sequence using randomly one out of the possible 12 {111}<112> variants available in the face-centered cubic lattice would lead to nearly any orientation

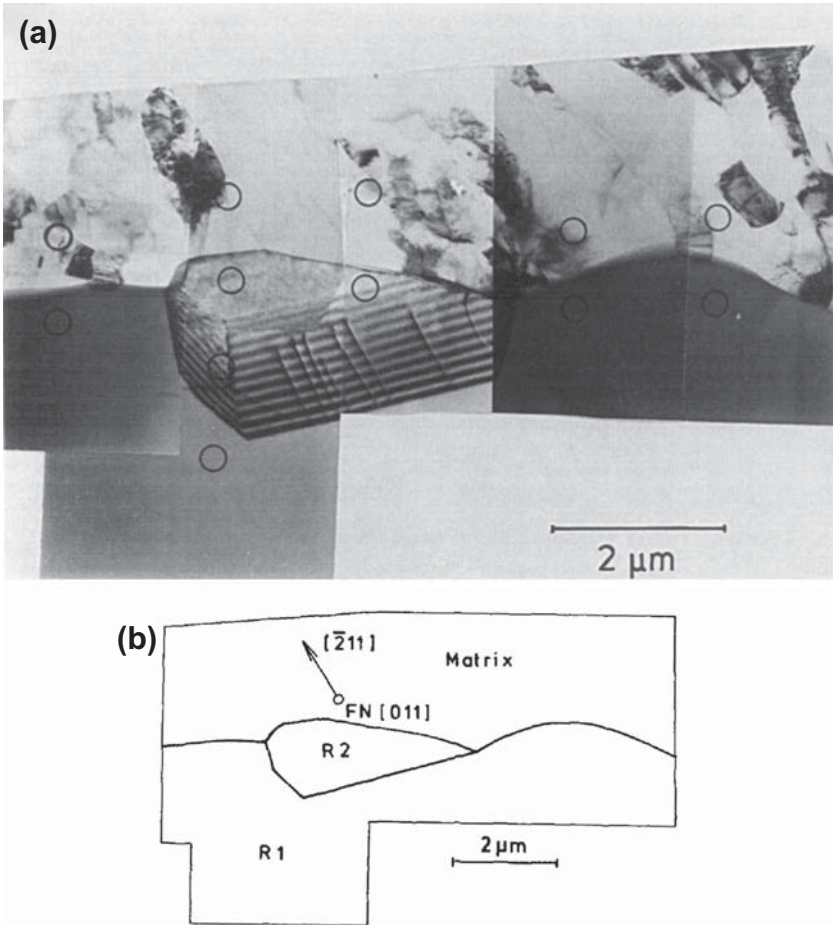

Figure 24 Al specimen annealed at 200 °C and 5 min at 300 °C showing twin formation (Berger et al., 1988).

possible and, hence, to a random crystallographic recrystallization texture. As this complete orientation randomization effect is typically not observed in crystallographic texture measurements (Engler et al., 1996; Ibe and Lücke, 1966; Bunge, 1982, 1986, 1987; Bunge and Esling, 1982, 1991; Adams et al., 1993), it was assumed that there must be a reason for the preference of certain twin sequences. More specific, the authors suggested that either a gain in grain-boundary energy or an advantage in growth kinetics might play the dominant role in thermal twinning. Wilbrandt also observed a number of strong hints regarding the first reason, namely, that the growing grain aims at lowering its grain-boundary energy by twinning until step by step a lower energy of the interface is attained (Berger et al., 1988; Wilbrandt, 1980; Wilbrandt and Haasen, 1980a, 1980b).

In that context, it has to be considered though that thermal twinning would typically lead to the formation of rather immobile boundaries. This applies specifically to the formation of coherent twin boundaries, which are the grain boundaries with the lowest possible mobility (Aust and Rutter, 1959, 1960; Hu et al., 1990). However, special high-angle boundaries, although having low grain-boundary energy, are among the most mobile ones in dilute alloys (Aust and Rutter, 1959, 1960; Hu et al., 1990). One imagines that a compact boundary structure produces low grain-boundary energy but not necessarily high boundary mobility. To move a boundary, atoms have to be transferred from one grain to the other and this is easier if the boundary is not too closely packed and has some free volume (Viswanathan and Bauer, 1973; Furtkamp et al., 1998; Li et al., 1953; Winning et al., 2001, 2002; Winning, 2003; Heinrich and Haider, 1996; Gottstein et al., 1995, 1997, 1998; Vandermeer and Juul Jensen, 1993; Beck et al., 1950; Molodov et al., in press). Thus, there is some competition between frequent formation of low-energy boundaries and the formation of a highly mobile one that covers a large volume of the specimen during its movement. In that sense, a selection mechanism for recrystallized orientations according to their growth rate may have an influence on the resulting recrystallization texture. This discussion underlines the importance the effects of both, energy and mobility of the high-angle grain boundaries, on the annealing texture and microstructure formed in metals during recrystallization in cases where twinning is involved.

23.3.3.4 Recrystallization Nucleation at Prior Grain Boundaries

Recrystallization textures of cold rolled and annealed metals often resemble the crystallographic orientations that are observed for the preferential nucleation of new grains from certain orientations within the deformed substructure (Bunge, 1982, 1986, 1987; Bunge and Esling, 1982, 1991). In that context, specifically the nucleation at a former grain boundary plays an important role. A number of works have shown evidence that the distribution of newly formed crystal orientations at an early stage of recrystallization bears a close resemblance to the final texture.

Additionally, it has to be considered that at a later stage of recrystallization also growth selection phenomena play a role as will be discussed later in a subsequent section.

Hutchinson, (1989) conducted experiments on the role of nucleation at former grain boundaries in iron and low-carbon steels. These studies have shown that new grains with characteristic crystallographic orientations were formed by preferred nucleation at certain original grain boundaries of the as-deformed crystals. In body-centered cubic steels, they observed that in {111}<uvw>-oriented texture components a zone of highly localized deformation exists adjacent to the grain boundary as a result of the constraint imposed by the neighboring crystal and that this heterogeneous structure is favored for the nucleation of new grains on annealing.

The model that had originally been put forward by Inagaki, (1987) describes a possible mechanism by which the local stress state at the boundary may cause a local lattice rotation around the normal direction in certain cases of adjacent {111}//normal oriented grains. According to this approach, such

grains can reveal substantial local grain orientation changes at the grain boundaries between two abutting crystals that belong even to the same texture fiber. Typical texture components that are affected by such a mechanism in body-centered cubic steels are the {111}<112> and {111}<110> texture components (Dillamore et al., 1979; Hölscher et al., 1991; Ushioda et al., 1987; Raabe and Lücke, 1993, 1992; Klinkenberg et al., 1992; Raabe, 1995a; Juntunen et al., 2001; Ray et al., 1975b; Humphreys, 1977a; Ridha and Hutchinson, 1982a). The resulting recrystallization nuclei were found to differ substantially in orientation from the abutting interiors of the grains in which they were formed.

The reasoning behind this model is that the local incompatibility between abutting grains leads to more heavily distorted and more distinctly misoriented regions at the original grain boundaries.

Therefore, these highly distorted near-boundary regions also contain a higher local crystallographic orientation gradient relative to the surrounding deformation matrix and also a higher local stored energy compared to regions that are located inside of the deformed grains. Hence, it is plausible to assume that near-grain boundary regions can more rapidly form new mobile high-angle grain boundaries that then can grow fast owing to the higher local driving force.

In contrast to this model, experiments conducted on pure iron (Inokuti and Doherty, 1977, 1978) showed that after 40% cold reduction via cold-rolling nucleation at grain boundaries occurred primarily by strain-induced migration of the original grain boundary (strain-induced boundary migration). This process regenerated one of the originally existing grain orientations from the deformation texture, and favored those orientation components of low stored-deformation energy. Similar strain-induced boundary migration phenomena were also reported to occur in aluminum.

The mechanism of strain-induced boundary migration has to be clearly differentiated from the grain-boundary nucleation mechanism that has been explained above for body-centered cubic steels: strain-induced boundary migration is characterized by the fact that it does not involve the formation of new mobile high-grain boundaries but only the bulging of existing ones. Hence, strain-induced boundary migration occurs preferably at such former grain boundaries where a high difference in the stored energy occurs across the interface. Humphries could simulate and hence confirm such situations by assuming different substructures on either side of an already existing high-angle grain boundary (Humphreys, 1997). For this purpose, he used a vertex front-tracking model (Humphreys, 1997, 1992b; Miodownik, 2002; Bate, 1999).

23.3.3.5 Recrystallization Nucleation at Shear Bands

Shear bands are mesoscopic band-like deformation inhomogeneities in middle and heavily deformed metallic alloys. They appear under oblique angles relative to the main deformation axis and can penetrate multiple crystals in the deformation structure. They are characterized by a mesoscopic orientation that does not match a distinct crystallographic direction, for instance that of a specific slip or twinning system. Therefore, they are also referred to as noncrystallographic deformation zones (Haessner, 1978; Humphreys and Hatherly, 2004). In cold-rolled materials, they typically form under an angle of approximately 35–40° relative to the rolling direction (RD) (**Figure 22**).

Shear bands are found in many materials. Very frequently, they appear in materials with a low stacking-fault energy (**Figure 25**). However, they also observed in metallic alloys with high stacking-fault energy such as for instance in several aluminum alloys—for instance when these materials contain shearable particles or a high solute content of copper or magnesium.

The underlying micro- and nanostructures of such shear bands typically consist of very small DCs and contain very high dislocation densities. Shear bands often penetrate multiple grains and carry very high local shears. At the transition zones between the shear band interior and the surrounding matrix

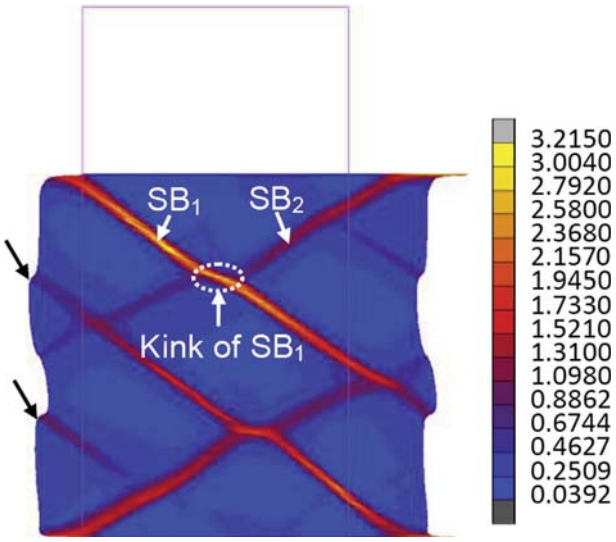

Figure 25 Shear band predicted in copper using a crystal plasticity finite element method. The color code represent the von Mises strain (Jia et al., 2012a,b).

material often very strong lattice curvature and very high densities of GNDs are found. These two properties, namely, the high driving forces and the high local misorientations at the rims of the shear bands are essential prerequisites for nucleation and subsequent growth of new grains. Consequently, such inhomogeneous deformation zones are highly potential sites for nucleation of recrystallization (Engler et al., 1996; Engler, 1997) (**Figures 26** and **27**).

When aiming at the study of the influence of recrystallization nucleation at such shear bands one is confronted with the difficulty that in many alloys nucleation at shear bands competes with nucleation events at other microstructural features. For example in Al-alloys, recrystallization nuclei at shear bands compete with nuclei forming at transition bands, cube-bands, grain boundaries, and second-phase particles (Engler and Vatne, 1998; Engler et al., 1989; Duckham et al., 2002; Korbel et al., 1986; Liu et al., 1989; Doherty and Baumann, 1993).

There is a considerable amount of experimental evidence that shear bands do indeed act as very successful nucleation sites during heat treatment of heavily deformed metallic alloys. Most prominent examples are such with alloys that have small stacking fault energy and high solute element content as for instance brass.

There is further evidence that nucleation at shear bands leads to a randomization of the recrystallization texture. This was first suggested by Ridha and Hutchinson, (1982a), who measured a weak, almost random recrystallization texture in copper for which grain nucleation at shear bands had been observed. This was in contrast to a sharp cube recrystallization texture corresponding to a condition about the occurrence of shear bands of a similar—yet presumably purer—batch of copper. It was suggested that the orientational randomization of the final texture was primarily caused by the nucleation of randomly oriented nuclei at shear bands and, in addition, by the destruction of the sites of cube-oriented nuclei by cutting through the cube transition bands.

More recently, local orientation measurements revealed that new grains formed in a partially recrystallized specimen of 90% cold-rolled polycrystalline Al-1.8 wt.% Cu (Engler and Vatne, 1998).

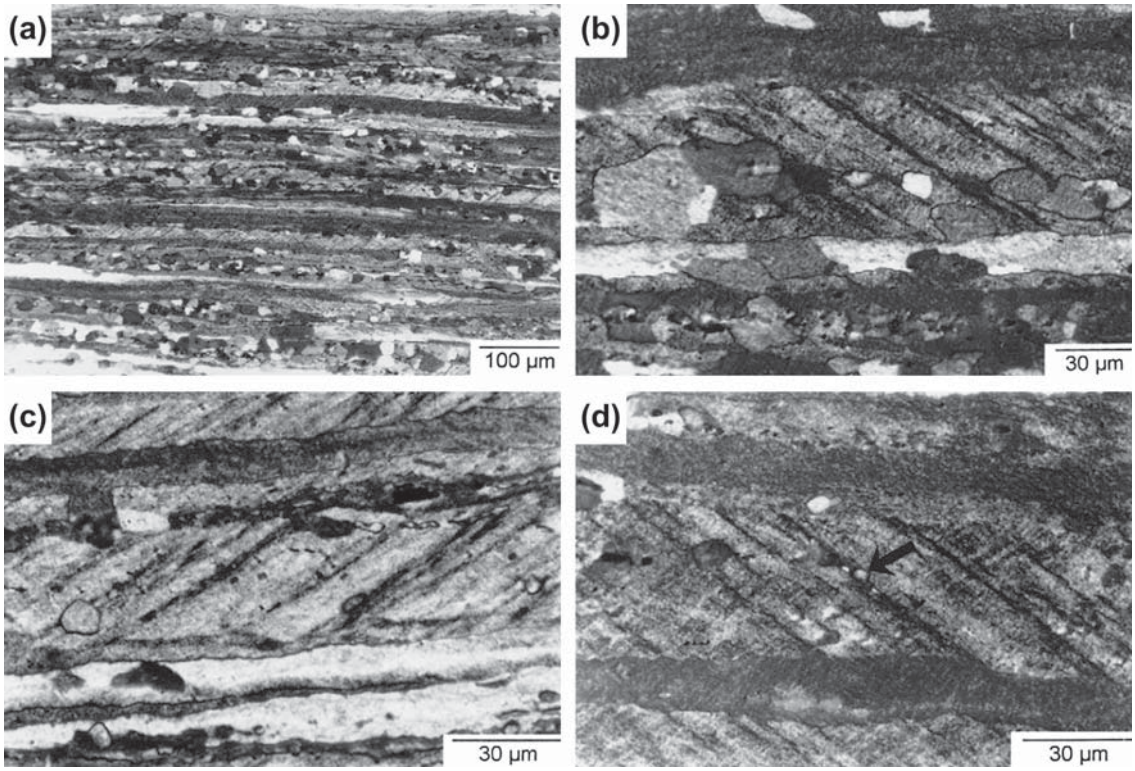

Figure 26 Optical micrographs showing evidence of grain nucleation at shear bands: (a) is a low magnitude view of a partially recrystallized structure; (b) shows grains that appear to have nucleated at shear bands; while (c) and (d) show grains at the beginning stages of nucleation at shear bands (e.g. grain indicated by arrow in (d)) (Duckham et al., 2002).

A distinction was made between grains nucleating at shear bands and grains nucleating at band-like structures parallel to the RD, presumed to be cube bands. The texture corresponding to nucleation at the presumed cube bands demonstrated a cube texture with only minor scatter. The texture corresponding to nucleation at the shear bands was less well-defined with notably less occupation of the exact cube orientation. There also was evidence that there may be preferred nucleation of some orientations at shear bands. Engler and Vatne, (1998) also investigated the influence of shear bands on recrystallization textures in binary Al-1.8 wt.% Cu and Al-3 wt.% Mg alloys by means of bulk and local orientation measurements. These results suggested that a recrystallization texture that is characterized by peaks around the Goss- and Q orientations, accompanied by a reduction in the strength of the cube orientation, provides a strong indication of recrystallization nucleation at shear bands. The Goss and Q orientations were suggested to result from positive and negative rotations around the transverse axis of the sheet associated with the formation of shear bands in copper-$\{112\}\langle 111\rangle$ and S $\{123\}\langle 634\rangle$ oriented grains. The Goss and Q orientations are metastable, in that they possess a low rate of further rotation, and are thus always present for possible nucleation during annealing.

It is the main feature of nucleation events occurring at shear bands that, like for most of the other nucleation mechanisms discussed above, the crystallographic orientation of the successful nucleus, after its competitive growth out of the surrounding subgrain structure, is already present in the

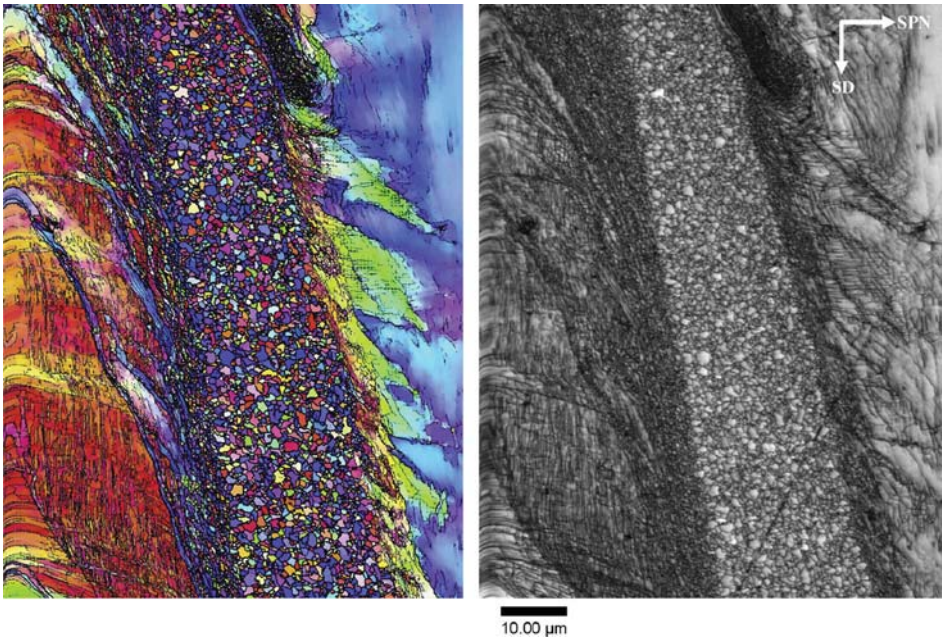

Figure 27 Nucleation at adiabatic shear band in IF steel (Lins et al., 2007).

deformation substructure at that shear band. Therefore, it makes sense to analyze the crystallographic rotations that occur at and in shear bands by simulations. This was recently done in a study using crystal plasticity finite element methods (Jia et al., 2012a, 2012b). It was observed that shear bands do not only lead to characteristic rotation zones, particularly at the transition between the band and the surrounding matrix, but also that this phenomenon is highly orientation-dependent.

More specific, the finite element simulations showed that Copper-oriented crystals, $(1\ 1\ 2)[1\ 1\ \overline{1}]$, and Brass-R oriented crystals, $(1\ 1\ 1)[1\ 1\ \overline{2}]$, had the largest tendency to form shear bands, associated with inhomogeneous texture distribution induced by the shear banding. To also understand the influence of the micromechanical boundary conditions on shear band formation, simulations on copper-oriented single crystals with varying sample geometry and loading conditions were performed. From that, it was found that shear banding can be understood in terms of a mesoscopic-softening mechanism. The predicted local textures and the shear banding patterns agreed well with experimental observations in face-centered cubic crystals with low stacking-fault energy. These observations also explain why in many materials recrystallization nucleation at shear bands does not necessarily lead to entirely random crystallographic textures. Instead, as only certain crystallographic texture components are prone to developing shear bands, for instance during cold rolling, the corresponding spectrum of nucleation orientations should recruit from those lattice rotations that occur in the transition zones between the shear bands and the matrix for these specific crystallographic orientations (**Figure 27**) (Lins et al., 2007).

23.3.3.6 Particle-Stimulated Nucleation

Particles can have two important effects on recrystallization (Haessner, 1978; Beck, 1949). The first one is that large, undeformable particles can generate potential sites for recrystallization nucleation in their

vicinity. The second effect is that small particles exert a retarding force on the migration of subboundaries as well as of high-angle boundaries. This force is referred to as Zener pinning force. Such a pinning force can act twofold as it means that not only the growth of viable nuclei via the motion of high-angle grain boundaries will be retarded, but also the nucleation itself since this includes the migration of low-angle boundaries. In this section, only the effects of large particles on recrystallization nucleation is discussed (**Figure 28**) (Humphreys, 1977a, 1979; Leslie et al., 1963b; Siqueira et al., 2011; Humphreys and Kalu, 1987; Humphreys and Ardakani, 1994; Hutchinson, 1989; Hutchinson et al., 1989; Harun et al., 2006). Particle pinning forces will the discussed in a subsequent section.

The presence of large, hard particles during the plastic deformation of a softer metallic material will induce strong deformation gradients that are associated with both substructure refinement and lattice orientation gradients. PSN is the event by which a recrystallized grain is nucleated in such a deformation zone around a hard inclusion. Many industrial alloys, particularly those of iron and aluminum, often contain micrometer-sized, second-phase particles. This means that PSN most likely is an import nucleation mechanism in many engineering materials, and PSN has been observed in many alloy systems, including those of aluminum, iron, copper, and nickel (Humphreys and Hatherly, 2004) (**Figure 29**) (Siqueira et al., 2011). The work of Humphreys and other authors (Humphreys, 1977a, 1979; Leslie et al., 1963b; Siqueira et al., 2011; Humphreys and Kalu, 1987; Humphreys and Ardakani, 1994; Hutchinson, 1989; Hutchinson et al., 1989) revealed a number of characteristic features of PSN:

Firstly, it was found that recrystallized grains originate at preexisting subgrains within the deformation zone, but not necessarily directly at the particle surface. This observation is plausible since the large lattice curvature that is typically associated with the deformation zone around a hard inclusion (Calcagnotto et al., 2010). This type of microstructure promotes the rapid formation of mobile high-angle grain boundaries during subgrain coarsening inside a curved lattice area. When finally high-angle grain boundaries result from such a competitive coarsening mechanism, these can subsequently sweep the surrounding deformation matrix owing to their high mobility (Gottstein et al., 1995; Shvindlerman et al., 1995; Shvindlerman and Gottstein, 1999). This effect seems to prevail over the availability of an already existing interface (heterogeneous nucleation effect).

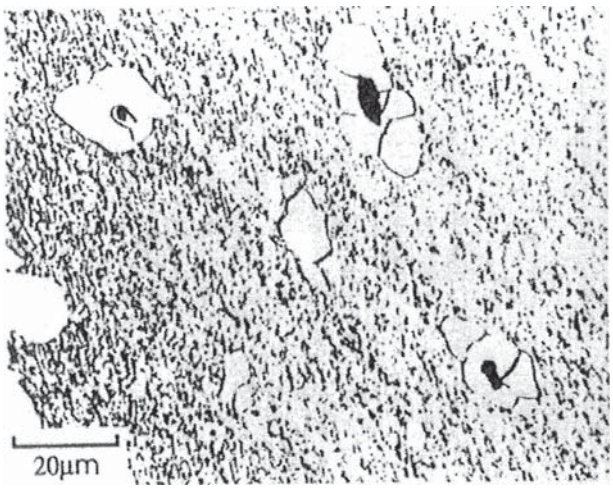

Figure 28 PSN in cold-rolled iron containing hard second-phase particles (Humphreys, 1977a).

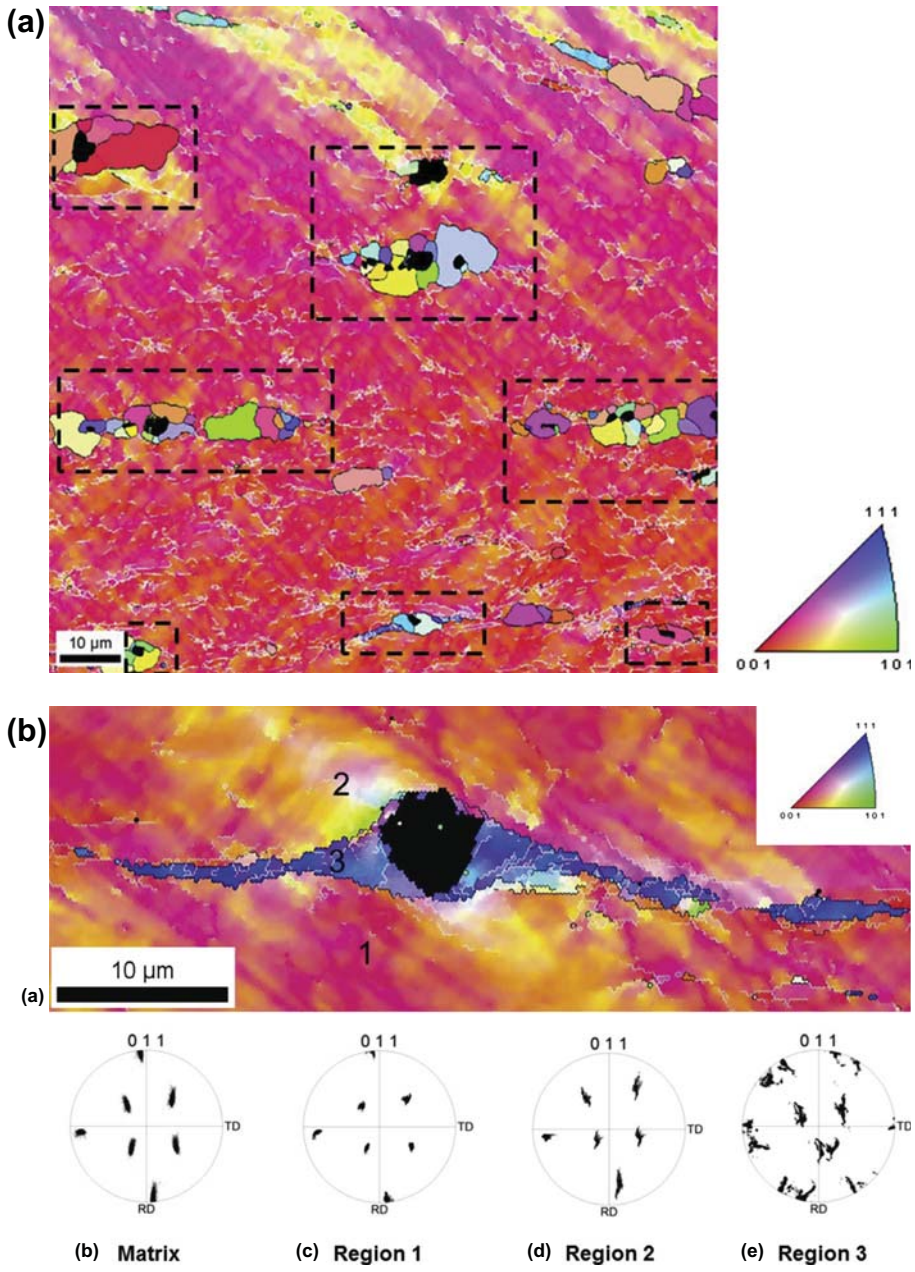

Figure 29 (a) EBSD map showing particle stimulated nucleation in cold rolled coarse-grained ferritic stainless steel. The IPF (inverse pole figure) map shows recrystallized grains (dash square) nucleated preferentially around the particles (black in the map) in a 45° rotated-cube large grain cold rolled and further annealed at 725°C for 15 min (De Siqueira et al., 2013). (b) EBSD results showing details in a 45° rotated-cube large grain: a) IPF map; b) {011} pole figure of the large grain; c–e) {011} pole figures corresponding to the regions 1, 2, and 3, respectively (De Siqueira et al., 2013).

Secondly, it was observed that recrystallization nucleation occurs by rapid subboundary migration. This observation is in line with the statement above, namely, that discontinuous subgrain coarsening in conjunction with a sufficiently high local lattice curvature leads to the rapid formation of mobile new grain boundaries during heat treatment.

Thirdly, it is a typical feature of recrystallization microstructures that are influenced by the PSN mechanism that the further growth of the newly formed grains may stagnate when the deformation zone has been consumed. This result can be understood, since the deformation zone that surrounds a sufficiently large hard particle in an otherwise soft metallic matrix extends only to a certain range into the vicinity of the particle. The material more remote from the interface to the hard particle is often much less deformed and has lower lattice curvature. This means that even if a new high-angle grain boundary was successfully formed in the vicinity of the inclusion, the driving force far away from the particle may no longer be sufficiently high to support further growth of such a newly formed nucleus. This means that microstructures where recrystallization via PSN plays a dominant role may reveal fine recrystallized areas around the particles and more coarse-grained or even recovered zones far away from them. In order to successfully optimize and homogenize the microstructure in such a material, it is hence required that the rigid second phase particles have a sufficiently high density so that the surrounding recrystallized grains can sweep the entire matrix.

Based on these observations, three main criteria for a successful nucleation according to the PSN mechanism can be stated (Humphreys, 1977a, 1979; Leslie et al., 1963b; Siqueira et al., 2011; Humphreys and Kalu, 1987; Humphreys and Ardakani, 1994; Hutchinson, 1989; Hutchinson et al., 1989):

(i) The presence of a deformation zone with sufficiently large lattice rotations. The formation of such a zone will depend on the deformation temperature because the effective recovery reactions in the case of high deformation temperatures will strongly retard the evolution of deformation zones.
(ii) The formation of a nucleus within the rotation zone surrounding the inclusion by competitive subgrain growth involving the motion of angle grain boundaries into a curved lattice region.
(iii) The issue of further grain growth beyond the deformation zone surrounding the hard particle. After the deformation zone is consumed, the potential nucleus must have reached a critical size and acquired a high-angle boundary misorientation (i.e. high mobility) in order to be able to grow into the surrounding matrix. Humphreys has shown that the latter is a restrictive criterion that in most cases determines the efficiency of the PSN mechanism for renewing the entire microstructure (Humphreys, 1977a, 1979; Leslie et al., 1963b; Siqueira et al., 2011; Humphreys and Kalu, 1987; Humphreys and Ardakani, 1994; Hutchinson, 1989; Hutchinson et al., 1989).

Besides these questions on the basic occurrence of new recrystallized grains in the vicinity of hard particles also the resulting orientation distribution of these new crystals is of relevance.

For this purpose Humphreys studied the orientations of PSN grains (Humphreys, 1977a, 1979; Leslie et al., 1963b; Siqueira et al., 2011; Humphreys and Kalu, 1987; Humphreys and Ardakani, 1994). On single crystals of A1–Si alloys deformed in tension, he observed that the orientations of the PSN nuclei are contained within the spread of the existing deformation zone. Annealing of weakly rolled crystals of the same alloys resulted in a sharp recrystallization texture that was rotated from the deformation texture by 30–40° about a crystallographic <112> axis. When assuming single slip, one can show that the orientations of the subgrains inside the deformation zones should, for face-centered cubic metals, rotate around a <112> axis lying in the slip plane and perpendicular to the slip direction. Such <112> rotations were indeed observed in A1–Cu alloys by Russel and Ashby, (1970).

In polycrystalline alloys, the analysis of PSN effects is more complicated (Engler et al., 1996; Engler, 1997; Humphreys, 1992a). Owing to the large number of initial grain orientations and the locally acting stress state—that can in a polycrystal substantially deviate from the global stress state—a more or less random-orientation distribution of the resulting subgrains in the deformation zones was observed. In total, it is therefore commonly observed that microstructures of deformed polycrystalline alloys that are affected by the PSN nucleation mechanism are either weakly textured or even randomly oriented. Both the initial orientations around the particles and also the size and shapes of the particles will have an influence on the orientations within the deformation zones.

The range of the potential crystal orientations resulting from PSN stimulated recrystallization nucleation is therefore enormous.

Some indications of preferred nuclei orientations appearing in the deformation zones of heavily strained materials around a hard inclusion have been reported in recent works by Engler et al. (1996), (1989), Engler (1997), Engler and Vatne (1998). At low levels of deformation (e.g. up to 50% cold-rolling reduction), they reported a randomization of the subgrain orientations within the deformation zones. At higher strains, however, a slight preferred occurrence of rotated cube subgrains appeared in the regions close to the large particles. Nuclei generated at the particles that were studied after a short-time heat treatment also revealed this slight preference of the rotated cube component. Weak recrystallization textures with some preference of a rotated cube texture have been reported in various aluminum alloys where PSN acted as one of the nucleation mechanisms.

A consequence of the general consensus, and success of the PSN mechanism, is that many workers regard PSN as the only possible nucleation mechanism for creating randomly oriented recrystallized grains (**Figure 30**).

23.3.3.7 Suppression of Nucleation through Gradient-Free Deformation

The process of primary recrystallization takes place by the formation and motion of mobile high-angle grain boundaries. The first process is referred to as nucleation.

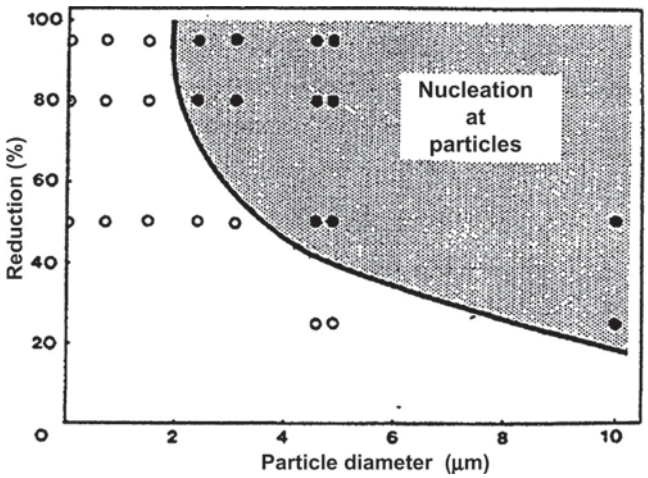

Figure 30 The conditions for particle size and strain for PSN to occur at Si-particles in cold rolled aluminum (Humphreys, 1977a,b).

As was explained above, for the onset of recrystallization a thermodynamic (transformation via nucleation), mechanical (net driving force vector), and kinetic (large-angle grain boundary with high mobility) instability is required. If one of these preconditions is not fulfilled, nonconservative dislocation rearrangement and mutual dislocation annihilation, viz. static recovery instead of recrystallization, can prevail during annealing (Raabe and Lücke, 1992).

Such behavior can be observed in cases of low cold-working prior to annealing. However, it is less well-established that even in case of sufficient initial cold-deformation in excess of 80% cold working, primary recrystallization can be suppressed if the initial nucleation stage is not taking place.

Owing to the mechanisms involved during recrystallization, the crystallographic texture is changed whereas during recovery it remains unchanged. Due to this principle difference, it is obvious that texture investigation is an appropriate diagnostic means of distinguishing between the two mechanisms.

In low-carbon steels, it was observed that samples that have a relatively coarse grain size and that were cold-rolled in a homogeneous form, without introducing substantial internal or external strain gradients, the nucleation stage and hence the entire recrystallization process can be suppressed (Raabe and Lücke, 1992; Raabe, 1995a, 1995b). It was found that certain rolling texture components, i.e. $\{001\}<1\bar{1}0>$ grains of sufficient size, although 90% cold rolled, did not reveal any texture change upon heat treatment at 730 °C for 120 s. EBSD analysis revealed that these grains did not produce recrystallization nuclei. Neighboring grains that had an initially different crystallographic orientation and had undergone exactly the same cold-working procedure were in contrast swept entirely by recrystallization (**Figure 18**).

23.3.4 Role of Grain Boundaries in Recrystallization and Grain Growth

The preceding section was dealing with the formation of new mobile high-angle grain boundaries. This section is concerned with the properties of these interfaces and the great intrinsic influence that they have on the growth of the newly formed grains (Burgers, 1941; Burke and Turnbull, 1952; Smith, 1948; Beck and Hu, 1966; Haessner, 1978; Humphreys and Hatherly, 1995, 2004; Doherty et al., 1997; Doherty, 2005).

Grain boundaries have the essential effect of acting as the main kinetic carrier that enables a growing grain to sweep the surrounding deformation microstructure. This applies specifically to mobile high-angle grain boundaries that are formed during the nucleation process. The relevance of small-angle grain boundaries during the entire recrystallization process lies more in the early stages, namely, in their relevance for the discontinuous subgrain coarsening that was discussed in the preceding section as one of the leading nucleation mechanisms. Hence, the current section concentrates on high-angle grain boundaries and their role in recrystallization and grain growth.

High-angle grain boundaries act threefold on recrystallization:

Firstly, they can move under the influence of a sufficiently high driving force (Winning et al., 2001, 2002; Winning, 2003). However, depending on their crystallographic misorientation and plane orientation their kinetic properties, viz. their mobility, can vary substantially (**Figure 31**) (Winning et al., 2001, 2002; Winning, 2003). Secondly, high-angle grain boundaries have also a relatively high self-energy that is of the order of 1 J/m^2. Therefore, the overall reduction in the total grain-boundary density acts itself as a main driving force, namely for grain growth. Thirdly, both the mobility and the energy of high-angle grain boundaries can vary not only with their geometrical characteristics but also with chemical decoration effects (**Figures 32** and **33**) (Tytko et al., 2012). These features make the migration of grain boundaries the kinetically dominating process of microstructure formation during annealing of cold-worked materials.

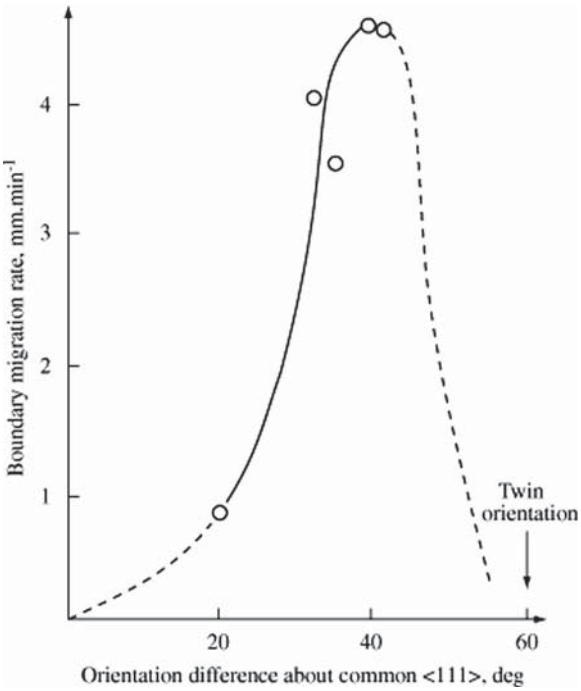

Figure 31 The migration velocity varies considerably with the misorientation angle (difference in orientation between two grains) about the <111> rotation axis, Al (Liebman et al., 1956).

For deriving an expression for the motion of high-angle grain boundaries, it is useful to start with Turnbull's classical rate equation of interface migration: according to Turnbull (Burke and Turnbull, 1952; Sandim et al., 2010) a phenomenological symmetric rate equation, which describes grain-boundary motion in terms of isotropic single-atom diffusion processes perpendicular through a homogeneous planar grain-boundary segment under the influence of free-energy gradients, can be written,

$$\dot{\boldsymbol{x}} = \boldsymbol{n}\upsilon_D\lambda_{gb}c\left\{\exp\left(-\frac{\Delta G + \Delta G_t/2}{k_BT}\right) - \exp\left(-\frac{\Delta G - \Delta G_t/2}{k_BT}\right)\right\}$$

$$= \boldsymbol{n}\upsilon_D\lambda_{gb}\exp\left(-\frac{\Delta H^f - \Delta S^f T}{k_BT}\right)\left\{\exp\left(-\frac{\Delta H^m - T\Delta S^m - \frac{p\Omega}{2}}{k_BT}\right) - \exp\left(-\frac{\Delta H^m - T\Delta S^m + \frac{p\Omega}{2}}{k_BT}\right)\right\}$$

where $\dot{\boldsymbol{x}}$ is the interface velocity (grain-boundary velocity in the current case), υ_D the elementary Debye attack frequency, λ_{gb} the jump width through the interface (which is of the order of a Burgers vector), c the intrinsic concentration of in-plane self-diffusion carrier defects (e.g. grain-boundary vacancies or shuffle sources), $\boldsymbol{n}$ the normal of the grain-boundary segment (when written in vector notation), ΔG the activation energy of motion through in the interface, ΔG_t the Gibbs free enthalpy associated with the transformation (equivalent to the driving force for recrystallization; here written in general form), p the negative gradient in Gibbs free transformation enthalpy across the interface (driving force), Ω the

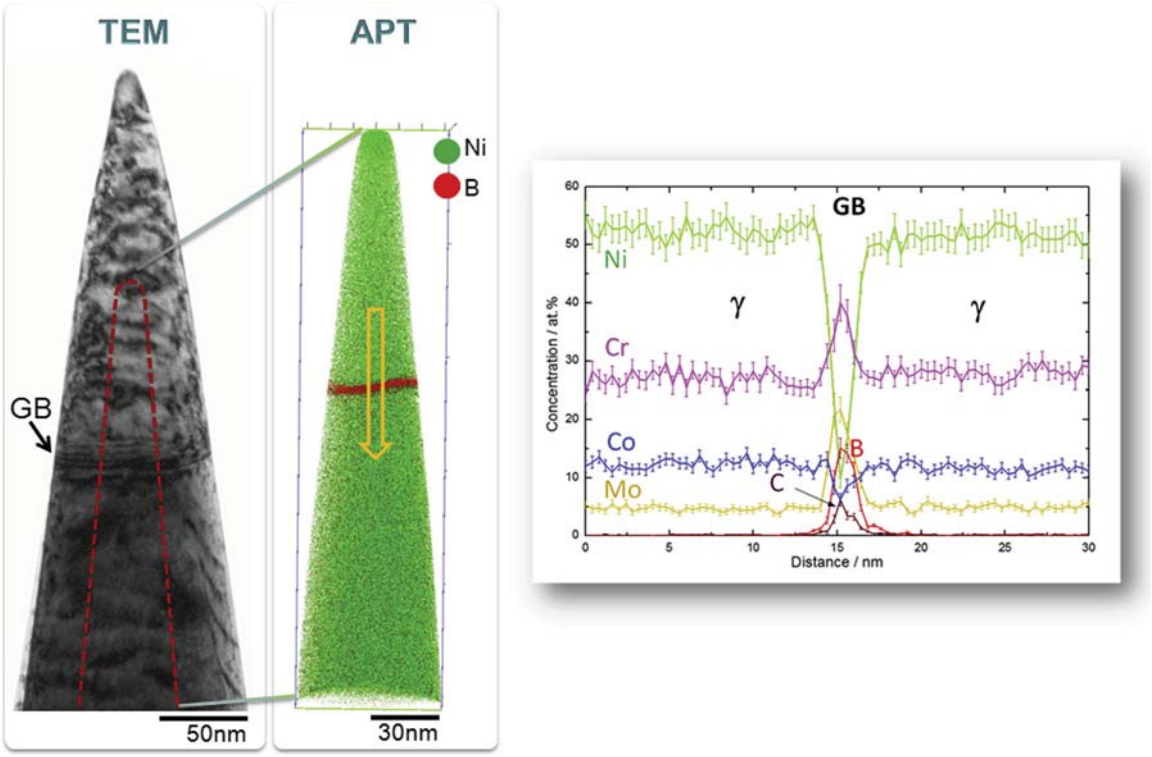

Figure 32 Atom probe characterization of B decoration of a grain boundary in a Ni-alloy (Tytko et al., 2012).

atomic volume, ΔS^f the entropy of formation, ΔH^f the enthalpy of formation, ΔS^m the entropy of motion, ΔH^m the enthalpy of motion, k_B the Boltzmann constant, and T the absolute temperature. The atomic volume is of the order of b^3, where b is the magnitude of the Burgers vector. Bold symbols indicate vector quantities. The Debye frequency is of the order of 10^{13}–10^{14}/s and the jump width of the order of the magnitude of the Burgers vector. Summarizing these terms leads to

$$\dot{\boldsymbol{x}} = \boldsymbol{n} v_D b \exp\left(-\frac{\Delta S^f + \Delta S^m}{k_B}\right) \sinh\left(\frac{p\Omega}{k_B T}\right) \exp\left(-\frac{\Delta H^f + \Delta H^m}{k_B T}\right)$$

$$\approx \boldsymbol{n} v_D b \exp\left(-\frac{\Delta S^f + \Delta S^m}{k_B}\right) \left(\frac{p\Omega}{k_B T}\right) \exp\left(-\frac{\Delta H^f + \Delta H^m}{k_B T}\right)$$

which reproduces the well-known phenomenological Turnbull expression

$$\dot{\boldsymbol{x}} = \boldsymbol{n} m p = \boldsymbol{n} m_0 \exp\left(-\frac{Q_{gb}}{k_B T}\right) p$$

where m is referred to as the mobility of the grain boundary and Q_{gb} the activation energy of boundary motion. The above equations provide a well-known phenomenological kinetic picture, where the

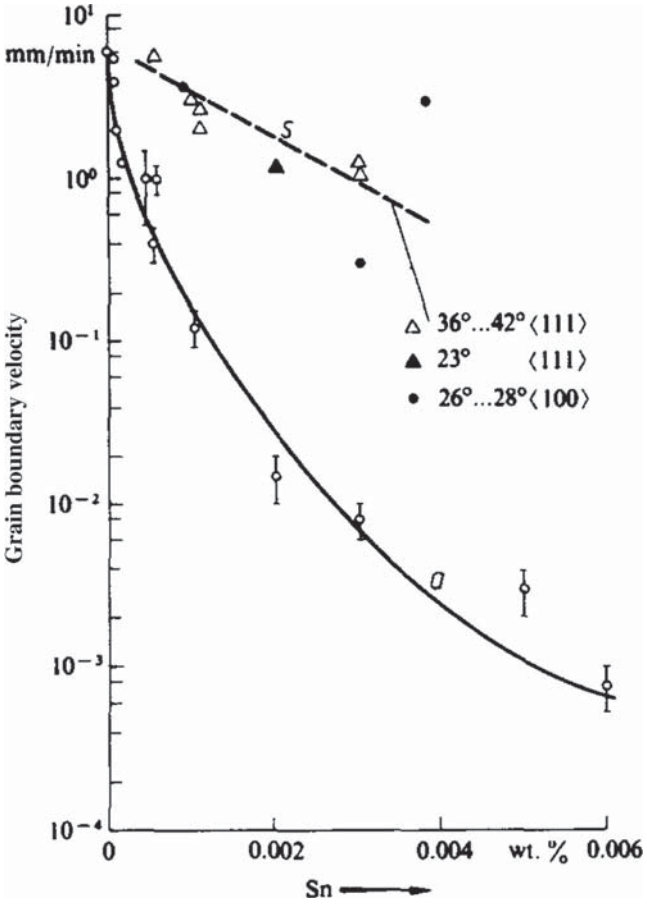

Figure 33 Velocity of special (s) and general (a) GBs in dilute Pb alloys vs. Sn content (Aust and Rutter, 1959).

atomistic processes associated with the grain-boundary motion are statistically described in terms of $m_0 = m_0(\Delta \boldsymbol{g}, \boldsymbol{n})$ and $Q_{gb} = Q_{gb}(\Delta \boldsymbol{g}, \boldsymbol{n})$.

When translating this kinetic picture into a feasible experiment, the challenge obviously lies firstly, in controlling the activation energy in terms of the chemical purity of the moving interface and secondly, in making sure that the driving force remains constant during an experiment. One can also learn from this analysis that retrieving intrinsic grain-boundary characteristics from the polycrystal experiment is a very difficult task.

The most systematic and precise way of measuring the grain-boundary mobility therefore is the use of a bicrystal experiment where the grain boundary between the crystals has a constant and self-reproducing curvature. This leads to a constant capillary driving pressure provided by the grain-boundary surface tension during the motion of the grain boundary. Gottstein et al. (1997) conducted multiple systematic experiments in the basis of this setup (**Figure 34**).

They studied the characteristics of grain-boundary motion by conducting successive high-temperature annealing treatments where the gradual change of the grain-boundary position, which moves according to its constant capillary driving force, is monitored as a function of time. The position-

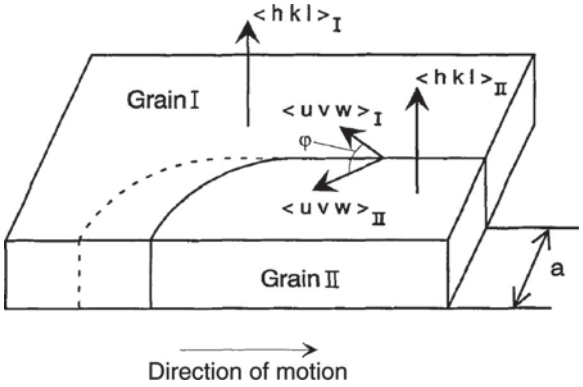

Figure 34 Setup for the measurement of grain-boundary mobility under constant driving force (Gottstein et al., 1997).

sensitive monitoring of the current interface position is conducted in such a way that under an incident X-ray beam one of the crystals is in Bragg-position while the other one is not. The reflected XRD intensity is used as the governing tracking signal. When the grain boundary has moved and the crystal that was originally in Bragg-position is swept by the other grain the reflected X-ray intensity drops. The sample is then automatically readjusted in such a way that the targeted crystal remains in Bragg-position. Hence, when the boundary moves, the specimen is shifted such that the reflected X-ray intensity remains constant during the measurement. The velocity of the moving grain boundary is then equal to the speed of sample movement. As the temperature(s), the grain-boundary velocity, and the driving pressure are known, the parameters of the mobility equation can be extracted from a number of data sets taken for different temperatures.

Several investigations have shown that the grain-boundary mobility depends on the misorientation between the abutting crystals. For instance Aust and Rutter, (1959), (1960) observed that certain low-coincidence grain boundaries move faster than noncoincidence grain boundaries. This result was later confirmed by Shvindlerman and Gottstein (Molodov, 2001; Lücke and Stüwe, 1963; Gottstein et al., 1995; Shvindlerman et al., 1995, Shvindlerman and Gottstein 1999) on Al, Zn, and Sn bicrystals. They observed the smallest enthalpy of activation for tilt boundaries between grains of exact coincidence orientation relationship (**Figure 35**).

On the other hand, numerous growth selection experiments on A1 single crystals, which were conducted by Ibe and Lücke (1966), (1972), Ibe et al. (1970), provided clear evidence that the maximum growth rate misorientation is actually close but yet distinctly different from the exact Σ7 orientation relationship, which occurs at an angle of rotation 38.2°. The angular difference between both results, obtained by very different methods, is comparably small and has been attributed to the large scatter of results in growth selection experiments. However, as already pointed out by Ibe and Lücke (1966), (1972), Ibe et al. (1970), the overwhelming statistics of growth selection experiments substantiate that with progressing growth selection the fastest moving boundaries are observed for a <111> axis of rotation and for an angle of about 40°. Although the difference between growth selection and bicrystal experiments amounts to only 2° the difference is of substantial importance with regard to the interpretation of the misorientation dependence of the grain-boundary mobility. The finding of a high mobility for low Σ coincidence boundaries is commonly interpreted in terms of a decreased tendency to segregation and, therefore, less solute drag in long-range periodic boundary structures, like in CSL (coincidence site lattice) boundaries. This means that grain boundaries that are

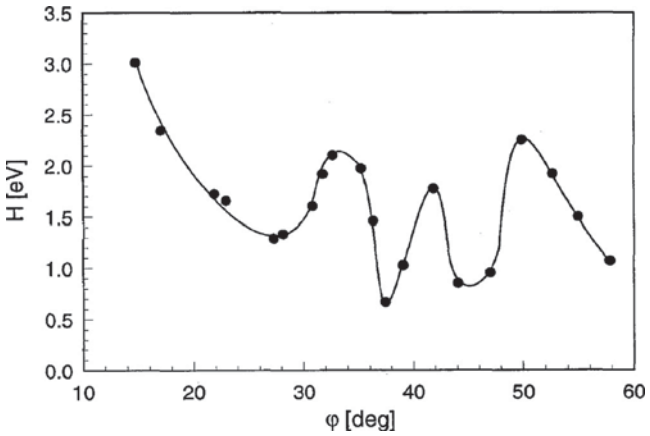

Figure 35 Misorientation dependence of activation enthalpy for grain-boundary motion of <111> tilt grain boundaries in A1 (Gottstein and Shvindlerman, 1999).

intrinsically more densely packed are less prone to be decorated by solute impurities, hence their higher boundary mobility. This however means, that for low CSL-grain boundaries the often observed high mobility is not a property of the grain boundary itself but rather of the orientation dependence of the interaction of solutes and grain boundaries. The finding of a maximum growth rate for off-coincidence (nonspecial) grain boundaries would be at variance with this interpretation.

In order to better understand these rather controversial observations Gottstein and Shvindlerman (Furtkamp et al., 1998; Winning et al., 2001; Gottstein et al., 1995, 1997, 1998) determined the grain boundary mobility of <111> tilt grain boundaries with angles of rotation between 35 and 42° using misorientation intervals of 0.4°. Interestingly, they observed that the activation enthalpy of the grain-boundary mobility reached a maximum for grain boundaries that had 40.5° misorientation. In contrast for the exact Σ7 coincidence misorientation, they observed a minimum of the activation enthalpy of the grain-boundary mobility.

Additionally, the authors observed that the mobility also depends on the preexponential factor of the mobility, which is not constant but again assumes a minimum for the exact Σ7 grain boundary and at maximum for the 40.5° interface. Therefore, they concluded that the temperature dependence of grain-boundary mobility varies with misorientation and that a temperature can be defined, namely, the so-called compensation temperature, where the mobilities of the differently oriented boundaries are the same. This result easily reconciles the seemingly contradictory results of previous bicrystal and growth selection experiments.

23.3.5 Effects of Solute Elements on Recrystallization

Solute atoms can interact twofold with grain boundaries. According to the Gibbs absorption theorem, solute atoms can reduce the self-energy of grain boundaries and hence enhance their thermodynamic stability. Such an effect can for instance be relevant in grain growth phenomena where the primary driving force stems from the grain-boundary energy. More specific, it has been suggested that different types of grain boundaries have different solubility for solute atoms (Gottstein and Shvindlerman, 1999) (**Figure 32**). This means that in grain growth, where many types of grain boundaries are

involved, different types of interfaces can be stabilized differently due to the specific solute content they contain. Also, as discussed in the preceding section, solutes can even modify the intrinsic structure of the grain boundary (Gottstein and Shvindlerman, 1999). This means that at the grain boundary does not only act as a container for solute atoms without changing its own structure but it can rather interact with solutes in a way that a new joint structure can result. Such a situation leads to both, a change in mobility and change in the grain boundary energy.

A second strong effect of solute atoms exists on the mobility of grain boundaries. In this context, it has been observed that also tiny concentrations of impurities within an alloy can have extremely profound effects on the grain-boundary mobility (Stüwe, 1978; Lücke and Detert, 1957).

The equilibrium concentration of impurity atoms on a grain boundary can be greatly enhanced over that in the bulk. Hence, the effects of impurities on grain boundaries are much larger than can be expected based simply on the bulk impurity concentration.

The earliest model of the effects of impurities on grain-boundary motion was suggested by Lücke and Detert (1957). This model assumes a flat interface. The drag force, p_i, that the impurity atoms exert on that flat boundary portion can be written as

$$p_i = nC_0 f$$

where n is the number of impurity atoms per unit area of the boundary, C_0 is the equilibrium concentration (written as atomic fraction) of impurities on the boundary, and f is the force exerted on the boundary by one impurity atom. The concentration of interface impurities is in equilibrium related to the bulk concentration of the same atomic species far away from the boundary, C_∞, i.e. the mean bulk impurity concentration

$$C_0 = C_\infty \exp(-E/k_B T)$$

where $k_B T$ is the thermal energy and E the is the boundary impurity interaction energy.

In steady-state motion, the flat grain-boundary segment moves with a constant velocity v, which is related to the impurity drag force f via the Einstein relation as

$$v = \left(\frac{D}{k_B T}\right) f$$

where D is the diffusion coefficient of the impurity atoms in the abutting bulk matrix. Combining these equations above yields the expression

$$v = \left(\frac{D}{k_B T}\right) \frac{1}{nC_\infty \exp(-E/k_B T)} p.$$

Another model variant of impurity drag was put forward by Cahn (1962). In this approach, the grain boundary is also regarded as a flat interface portion much like in the Lücke–Detert approach outlined above, but in Cahn's model the impurity–boundary interaction energy, E, is a function of their separation distance, i.e. dE/dx. In the moving reference frame that is attached to the mobile grain boundary, the steady-state impurity concentration profile is derived from the diffusion equation according to

$$D\frac{\mathrm{d}C}{\mathrm{d}x} + \frac{DC}{k_B T}\frac{\mathrm{d}E}{\mathrm{d}x} + vC = vC_\infty$$

Cahn (1962) derived a formulation for the steady-state impurity concentration profile and solved it for the case of a triangular-shaped impurity–boundary interaction model. The resulting impurity drag force associated with any type of interaction profile can be calculated according to the integral formulation

$$p = -n \int_{-\infty}^{+\infty} C(x) \frac{\mathrm{d}E}{\mathrm{d}x} \mathrm{d}x$$

Under steady-state conditions, the driving force is equal to

$$p = p_0(v) + p(v, C_\infty)$$

where $p_0(v)$ describes the intrinsic force–velocity relation associated with grain-boundary migration in the material when it does not contain any foreign solute atoms. The resulting relationship between the solute force that acts in the grain boundary and its resulting velocity suggests the existence of two types of regimes. The first type of impurity drag regime is characterized by a monotonic, nonlinear relation. The second impurity drag regime is marked by a situation in which the grain boundary velocity is a multivalued function of the driving force. This can lead to a discontinuous transition in the grain-boundary velocity from the fully impurity-loaded slow configuration to the chemically unloaded fast configuration. This analysis results directly from the Cahn model in conjunction with the incorporation of realistic grain boundary parameters and realistic impurity profile. As outlined above, the analysis assumes that the intrinsic boundary velocity/driving force relation is linear (i.e. connected through the grain boundary mobility) and the impurity–boundary interaction potential is:

$$E(x) \begin{cases} E_0 + \dfrac{E_0}{a} x & -a \le x \le 0 \\ E_0 - \dfrac{E_0}{a} x & 0 \le x \le a \end{cases}$$

For the triangular potential employed, p depends only on the absolute value of E and not on its sign. This means that a repulsive impurity–boundary interaction leads to the same grain-boundary velocity–driving force relationship as for an attractive interaction.

Both, the Lücke and Cahn models consider the case of a dilute, ideal solution. Such an assumption is however commonly not quite appropriate since the impurity concentration on the boundary is often too high to be considered as being dilute.

These basic considerations show that impurity atoms affect grain-boundary mobility via solute drag. Usually, impurity atoms reduce the mobility of grain boundaries, but little is known how much solute drag depends on grain boundary structure, i.e. on misorientation across the boundary. To study this problem, at least for the most relevant grain boundaries in recrystallization, Gottstein and Shvindlerman (1999) investigated the orientation dependence of the grain boundary mobility in pure A1 bicrystals of different chemical purity for <111> tilt boundaries within the angular interval 37–43°. The authors observed that the mobilities of both materials are different for the same type of boundary, but the difference in activation enthalpy is obviously largest for the exact Σ7 grain boundary and smallest for off-coincidence grain boundaries, in particular for the 40.5° <111> boundary. However, the different impurity content has a much deeper consequence, as it also affects the compensation temperature.

These results showed that the change between the ground state and activated state differs for even slightly differently pure material or, in other words, that the segregated impurity atoms also modify the structure of the grain boundary. This would support the frequent observation that the activation enthalpy of the grain-boundary motion can be very high, actually much higher than predicted by impurity drag theory.

23.3.6 Effect of Precipitates on Moving Grain Boundaries

One of the most important mechanisms for alloy design lies in the introduction of second phases. Specifically, many metallic alloys contain a high dispersion of small and second-phase precipitates that can occur in coherent, semicoherent for incoherent form. Such particles can exert a substantial back driving force on the moving grain boundaries (**Figure 36**) (Sandim et al., 2010). These interactions are also referred to as particle-pinning forces or Zener forces (Zener and Smith, 1948).

Grain-boundary-pinning forces arise when second-phase particles occur on the grain boundary. Their presence reduces the grain-boundary area and, hence, the grain-boundary energy. This energy saving, which must be replenished upon unpinning, is referred to as Zener pinning (Zener and Smith, 1948; Rios, 1987; Pimenta et al., 1986; Ashby et al., 1969; Köster, 1974; Martin and Doherty, 1976; Raabe and Hantcherli, 2005; Weygand et al., 1999; Holm et al., 2001; Miodownik et al., 2000). In the following treatment, we consider pinning effects imposed by a stable array of incoherent particles that reside on the grain boundaries of the deformed microstructure. In his first estimate, Zener and Smith, (1948) approximated the magnitude of the pinning force by assuming randomly distributed spherical particles. The boundary was assumed to move as a straight interface through the particle array and to experience a resistive force, F, from each particle. With the grain-boundary energy γ (in units of J/m^2), the force F due to one particle is given by $F = p\,r\,c$, where r is the particle radius. The surface A on which the force is applied amounts to $A = 2pr2/(3f)$, where f is the volume fraction of spherical particles. The Zener pressure then amounts to

$$P_Z = -\frac{3}{2}\,\gamma\frac{f}{r}$$

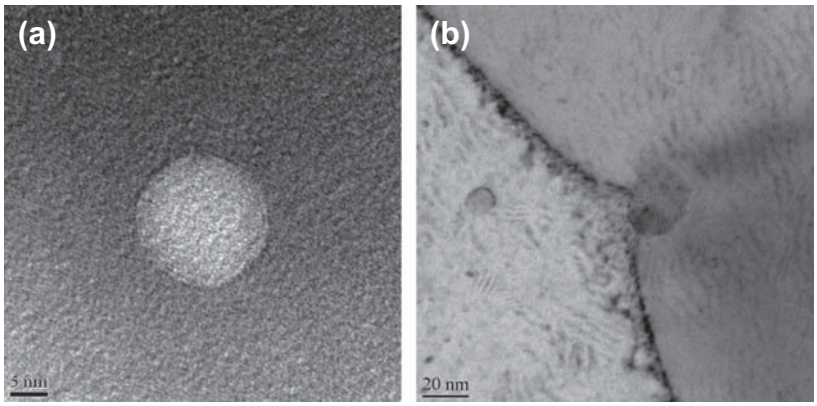

Figure 36 High-resolution transmission electron micrographs of a stainless steels sample deformed to 80% cold reduction and annealed at 800 °C for 48 h showing: (a) individual YCrO3 particle in the ferritic matrix; (b) dragging effect (particle–boundary interaction) during annealing. The RD is parallel to the scale bar (Sandim et al., 2010).

A shortcoming of this approach is that a grain boundary cannot be considered as a rigid interface, but it may have some flexible to bow out between particles when a driving force is applied (Rios, 1987; Pimenta et al., 1986; Ashby et al., 1969; Köster, 1974).

Diverse modifications have been proposed to correct for this flexibility (Rios, 1987; Pimenta et al., 1986; Ashby et al., 1969; Köster, 1974; Martin and Doherty, 1976). They give results that are of the same order of magnitude as the original formulation of Zener. One approach introduces a correction factor that depends on the volume fraction of the particles f:

$$P_{HZ} = -\Phi(f)\frac{3}{4}\gamma\frac{f}{r}$$

When assuming a Friedel-like particle behavior, one obtains the following equation for the drag force,

$$P_{FZ} = -2.6\gamma\frac{f^{0.92}}{r}.$$

When considering a stronger dependence of the corrector factor on the value of f than assumed in the original Friedel model, one obtains a modified expression for the Zener pressure according to

$$P_{FZ} = -0.33\,\gamma\frac{f^{0.87}}{r}; \quad f < 3 \text{ vol.\%}$$

For a reasonable choice of the grain-boundary energy (0.6 J/m^2), the precipitate volume fraction (1 vol.%), and the average particle radius (100 nm) the original Zener pinning force amounts to about 0.1 MPa. When considering the corrections discussed, the pinning force can rise to a maximum value of about 0.5 MPa.

23.3.7 Recrystallization In situ

Dislocation recovery proceeds particularly fast in alloys with high stacking-fault energy (Himmel, 1962; Cahn 1966). In alloys with low stacking-fault energy dislocation recovery is less pronounced (Burgers, 1941; Humphreys and Hatherly, 1995; Himmel, 1962). The reason for the connection of stacking-fault energy and recovery tendency of an alloy lies in the dependence of the cross-slip probability of screw dislocations on the recombination spacing of the underlying Shockley partial dislocations that open the stacking fault between them. In other words, a low stacking-fault energy leads to a wide-stacking fault and hence to a wide spacing among the associated Shockley partial dislocations. For cross-slip the partial dislocations must first recombine under the aid of phonons plus the applied local stress. Therefore, systems with higher stacking-fault energy have smaller stacking faults so that the partial dislocations involved can recombine and cross-slip at lower thermal activation (Mughrabi et al., 1986; Straub et al., 1996; Nes, 1995; Stüwe et al., 2002).

Frequent cross-slip leads to a more rapid reorganization of the stored dislocation arrangements that are formed during cold working and hence to a more rapid reduction in the stored internal energy.

In cases where extensive and rapid recovery leads to such a high reduction in the stored internal energy before the associated recrystallization nucleation leads to the formation of new mobile high-angle grain boundaries, primary recrystallization can be entirely suppressed. Sometimes, this effect occurs only in specific grains so that a mixed microstructure results, containing both recrystallized and

recovered crystals (Figure 18). In such cases, the microstructure inherited from cold working is—at least in part (Figure 16)—transferred into a reorganized, softer microstructure without the motion of high-angle grain boundaries. Such a situation is referred to as recrystallization in situ. Typical materials where very strong recovery and hence recrystallization in situ can occur, competing with primary recrystallization, are pure aluminum and iron as well related alloys with high stacking-fault energy (Bailey, 1963; Sandström et al., 1978; Vandermeer and Rath, 1990; Nes, 1995; Stüwe et al., 2002).

Recrystallization in situ can be exploited also for technological applications: recrystallization phenomena that involve the motion of newly formed high-angle grain boundaries naturally transform the crystallographic texture that is inherited from cold working into a texture that is characterized by specific recrystallization texture components.

When recrystallization in situ takes place, however, the deformation texture is inherited. Thus, in order to design, optimize, and balance a certain annealing texture with specific anisotropy, the corresponding heat treatment can be conducted in a way that some areas of the cold-worked materials undergo primary recrystallization, discontinuously providing specific new texture components, while other texture components of the same microstructure undergo extensive recovery and even recrystallization in situ.

The reasons why in the same microstructure both, primary recrystallization and extensive recovery phenomena (recrystallization in situ) can occur, can be twofold. First, in many commercial products macroscopic gradients of the deformation energy occur within the same sample (Figure 37). Examples

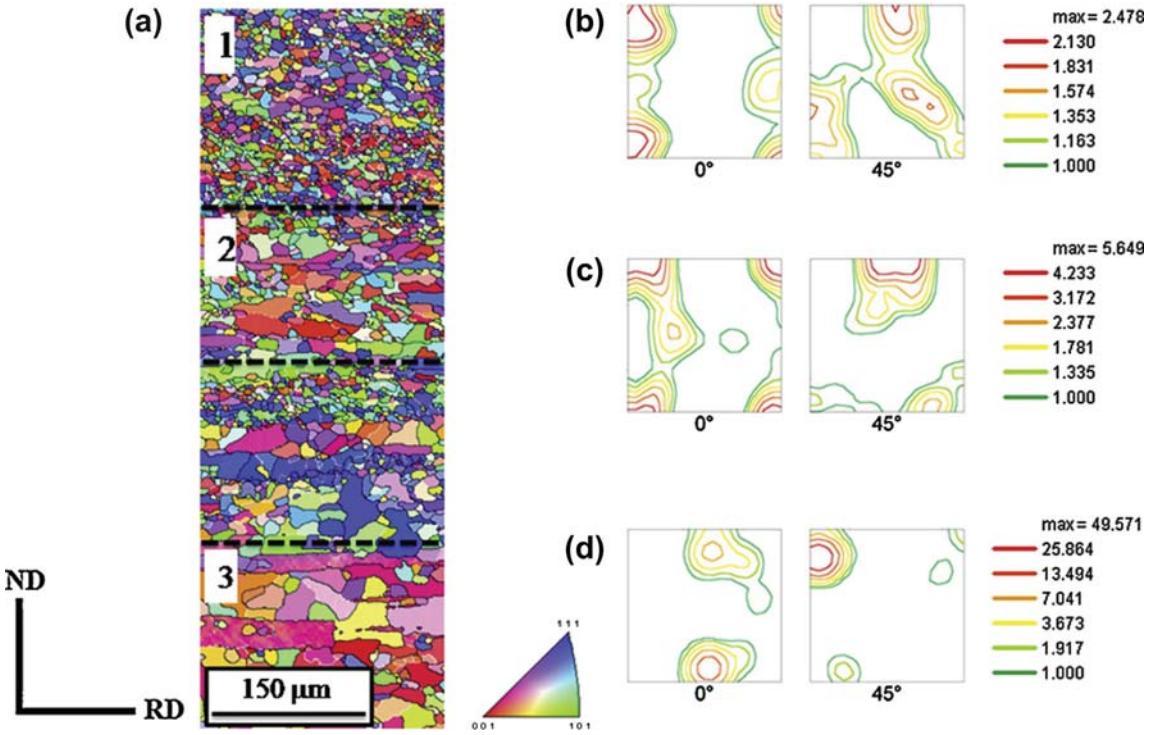

Figure 37 EBSD results showing inhomogeneous recrystallization behavior in a ferritic stainless steel after recrystallization annealing: (a) orientation map; (b–d) ODF (ϕ2-constant sections) corresponding to the specific recrystallized regions marked by 1, 2, and 3, respectively (Siqueira et al., 2011).

are macroscopic-rolling processes where typically higher plastic deformation rates occur close to the surface and subsurface areas of the sheet as compared to the center layers of the same product. A further difference is the applied deformation state: while the center layer during rolling is usually deformed by plane strain state, near-surface areas are subjected to shear deformation. Both types of deformation can lead to different texture components, different local orientation gradients and differences in the accumulated total deformation (Raabe and Becker, 2000; Bate, 1999; Roters et al., 2010). Also, microscopic differences in plastic deformation can occur. Examples are the deformation zones close to large particles and close to internal interfaces.

The second important reason for the inhomogeneity of recrystallization and recovery phenomena in the same sample lies in the dependence of these mechanisms on the host orientation in which they take place (**Figures 16** and **18**). For instance **Figure 16** clearly reveals that with progressing annealing treatment only specific grains in a body-centered cubic low-carbon steel sample are sluggish to undergo primary recrystallization. The orientation distribution function that is shown in **Figure 16**b summarizes only those orientations that did not recrystallize. For longer annealing times, it becomes apparent that only the 45°-rotated cube component, $\{001\}<110>$, prevails as a nonrecrystallized texture component (Raabe and Lücke, 1992).

Also, it must be considered that some crystallographic texture components reveal much higher plastic deformation and higher distortions than other texture components (Raabe et al., 2002a; Raabe and Becker, 2000; Bate, 1999; Roters et al., 2010). This must be explained in more detail: as characterized in terms of classical polycrystal homogenization theory (Taylor–Bishop–Hill theory) the Taylor factor—as a well-known measure of grain scale plasticity—provides information for each orientation how much shear is required (per unit deformation step) to render grain deformation compatible. In the classical Taylor theory, compatible deformation of all crystals is obtained when all grains are subjected to the same externally imposed strain state. In order to comply with this global boundary condition, however, each grain requires a certain amount of shear, distributed on the active slip systems, depending on its specific crystallographic orientation (Raabe, 1998; Raabe et al., 2004b). While some grains can follow the externally prescribed deformation state by activating a relatively small amount of internal shears, other grains require larger internal amounts of shear. Grains of the former type have a small Taylor factor (small amount of shear per unit strain) and grains of the latter type a high Taylor factor (high amount of shear per unit strain). Sometimes, the Taylor factor was therefore chosen as a criterion for high or low nucleation rates during primary recrystallization, respectively. In reality, this situation is more complex. Firstly, the deformation state of a grain is not only a function of the grain orientation but also of its grain neighborhood (Raabe et al., 2001; Kuo et al., 2003; Zaefferer et al., 2003). The interaction of the externally imposed load together with the influence of the neighboring grains adds up to a micromechanical boundary condition that determines the deformation state of a grain. Secondly, the total deformation that goes into a grain does not include any information whether the grain-scale deformation is heterogeneous or homogeneous. For relating the deformation state of a grain to its tendency to undergo either recrystallization or respectively recrystallization in situ, however, both the total deformation and the deformation inhomogeneity matter (**Figure 38**) (Raabe et al., 2002b; Roters et al., 2010).

23.3.8 Strain-Induced Grain-Boundary Migration

The mechanism of strain-induced grain-boundary migration (SIBM) is characterized by the bulging of a portion of an already existing high-angle grain boundary that sweeps the neighboring deformation microstructure and leaves a dislocation-free region behind the migrating boundary (Humphreys, 1997, 1992a; Li et al., 1953; Winning et al., 2001, 2002; Winning, 2003; Heinrich and Haider, 1996).

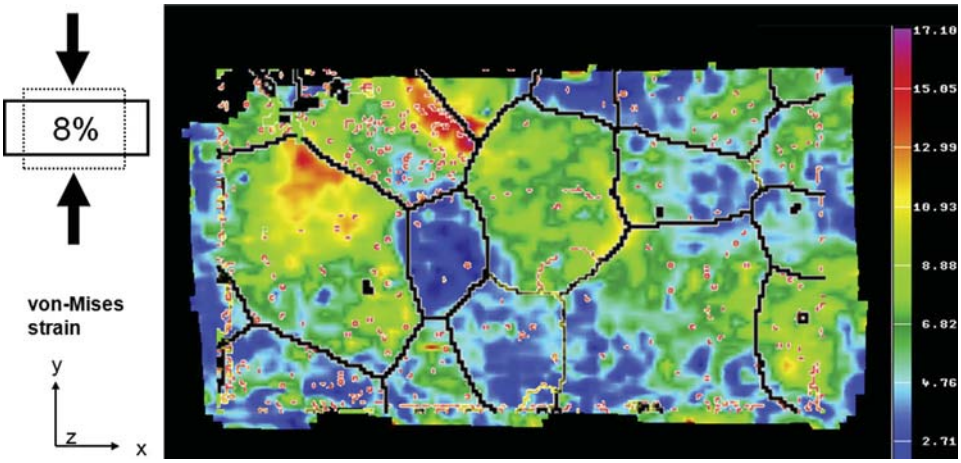

Figure 38 Experimental example of the heterogeneity of plastic deformation at the grain and subgrain scale using an aluminum polycrystal with large columnar grains. The image shows the distribution of the accumulated von Mises equivalent strain in a specimen after 8% plane strain thickness reduction (the deformation is given in % of $\Delta d = \mathrm{d}$, where d is the sample extension along compression direction). The experiment was conducted in a lubricated channel–die setup. The strains were determined using digital image correlation. The high-angle grain boundaries indicated by black lines were taken from EBSD microtexture measurements. The equivalent strains differ across some of the grain boundaries by a factor of 4–5, giving evidence of the enormous orientation-dependent heterogeneity of plasticity even in pure metals (Raabe et al., 2002b; Roters et al., 2010).

It differs from primary static recrystallization as it does not involve the formation of new high-angle grain boundaries (nucleation stage in conventional primary recrystallization) but instead is based on the motion of an already existing internal interface (Humphreys, 1997). SIBM can nonetheless efficiently reduce the internal stored deformation energy.

The driving force for this bulging mechanism stems from the difference in stored dislocation (or DC) energy on opposite sides of the same grain boundary (**Figure 39**). Such situations occur between neighboring texture components of different crystallographic orientation in cases where they reveal

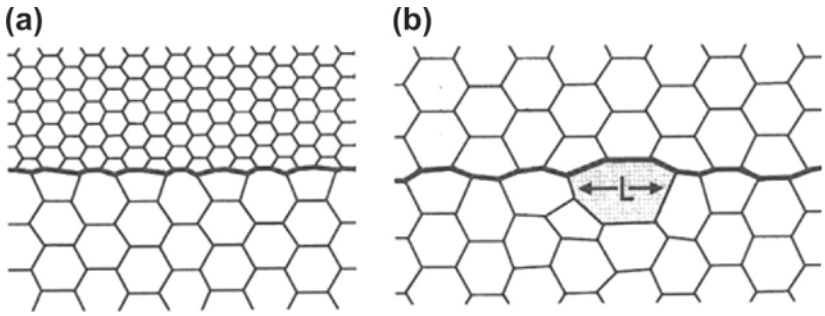

Figure 39 Models for recrystallization by SIBM after Humphreys (Humphreys, 1992a). (a) The conventional model in which SIBM is driven by differences in stored energy, (b) The possibility of SIBM occurring by discontinuous growth of a large subgrain adjacent to a high-angle boundary.

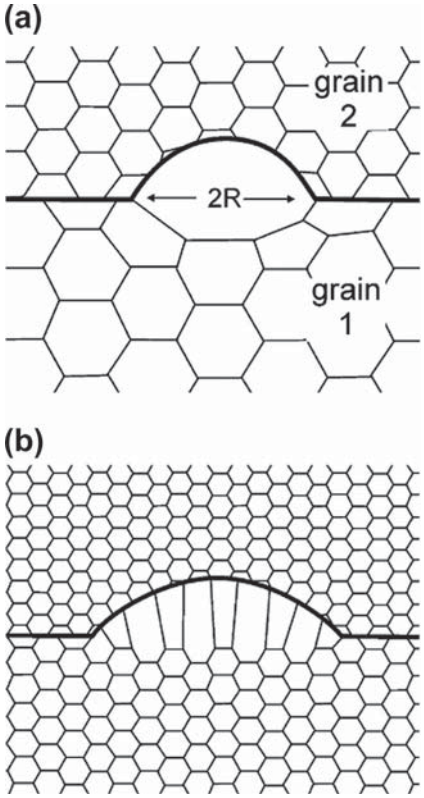

Figure 40 Schematic diagrams of: (a) single subgrain SIBM and (b) multiple subgrain SIBM. After Humphreys (Humphreys, 1992a).

a characteristic difference in the substructure evolution (**Figures 40** and **41**) (Humphreys, 1992a). For instance, in body-centered cubic steels that are deformed by cold rolling, the {001}<110> texture component reveals relatively weak strain hardening while the {111}<112> and {111}<110> texture components are characterized by higher stored dislocation densities and, correspondingly, by smaller DC sizes (**Figures 14** and **42**) (Hölscher et al., 1991; Ushioda et al., 1987; Raabe and Lücke, 1993; Hutchinson and Ryde, 1995; Samajdar and Doherty, 1994).

Consequently, when an existing high-angle grain boundary bulges into a neighboring grain with a lower stored energy and forms a new grain a pronounced global texture change does usually not occur. This means that the recrystallization texture is closely related to the deformation texture.

Strain-induced boundary migration is a frequently occurring recrystallization mechanism at relatively low strains. At deformations below 20–50% rolling reduction, the differences in stored energy among the different texture components are relatively strong (Hurley and Humphreys, 2003) (**Figure 43**). At higher strains, the internal deformation substructure and the gradual deformation texture evolution leads to a more homogeneous distribution of the stored internal deformation energy and the occurrence of conventional discontinuous nucleation phenomena via discontinuous subgrain coarsening as described above.

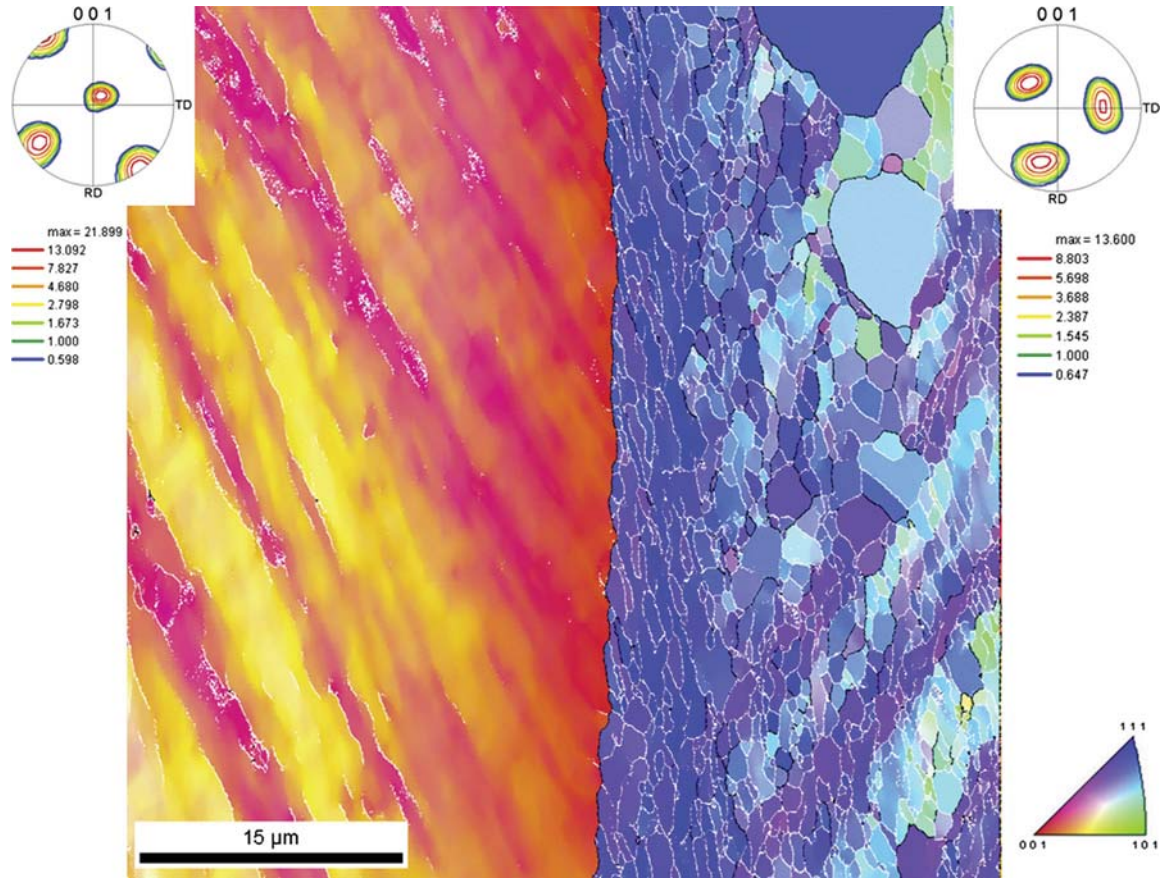

Figure 41 Recovery and recrystallization phenomena in neighboring grains in a 70% cold rolled and annealed (750 °C, 1 min) microalloyed low-C steel.

23.3.9 Recrystallization Textures

Recrystallization processes can lead to characteristic types of orientation changes, viz. to different types of crystallographic textures. One group of phenomena, such as recovery or recrystallization in situ, that are primarily characterized by the continuous rearrangement and relaxation of the internal stored dislocation substructure without involving the motion of high-angle grain boundaries, is naturally not associated with profound transformations of the initial deformation textures. This means that for instance cold-rolling textures remain essentially unchanged when only recovery or recrystallization in situ take place (**Figures 15, 16 and 18**).

This is different for primary recrystallization. As outlined above, the incipient stage of recrystallization is described by the occurrence of different types of nucleation phenomena. As nucleation is described as the formation of new mobile high-angle grain boundaries corresponding recrystallization changes are the consequence, particularly when assuming that the nuclei are randomly distributed and that all grain boundaries have the same velocity when sweeping the deformed microstructure. Typically,

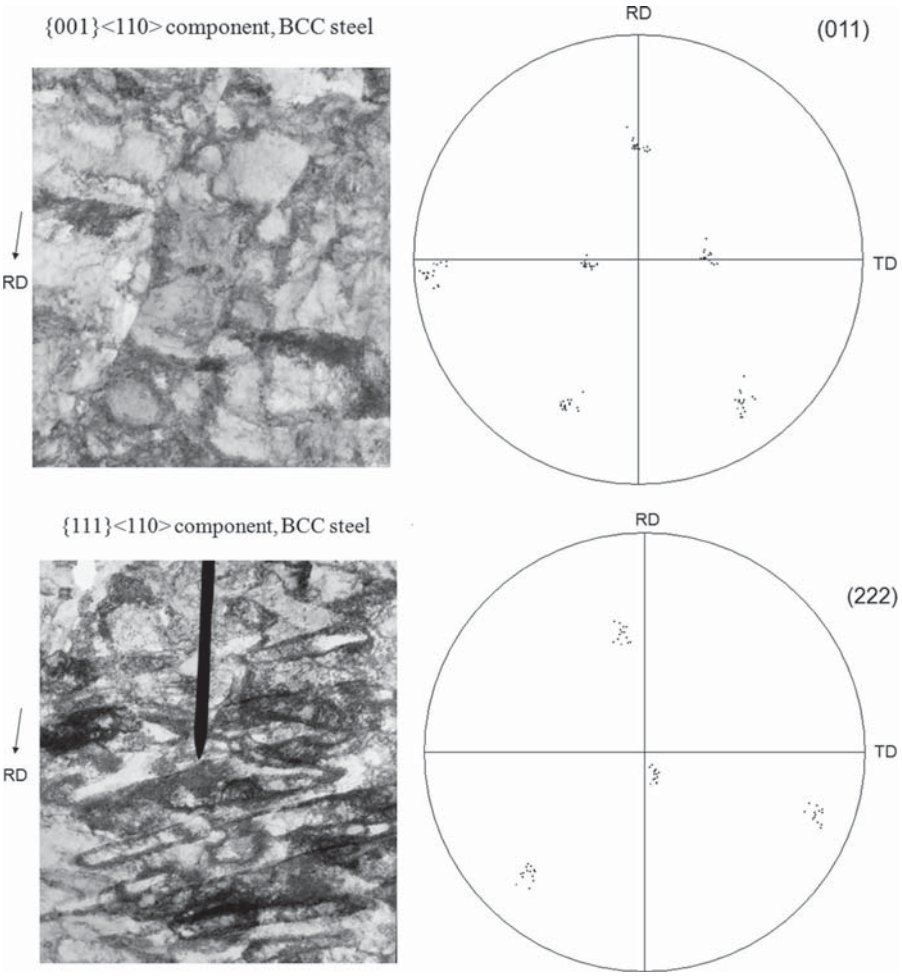

Figure 42 Example of dislocation substructure in 70% cold-rolled low-carbon steel as observed by TEM. The upper image shows DCs with a rather diffuse arrangement in a typical rolling-texture component {001}<110>. The bottom picture shows more sharper and elevated DCs in a texture component {111}<110> (Thomas et al., 2003).

this simplified picture is not correct but instead, usually both, the specific nucleation mechanism and also the growth selection that takes place through the growth competition among the moving grain boundaries together determine the transformation of the deformation texture into the final annealing texture. Corresponding modeling approaches that aim at capturing the multiple possible interactions that arise from these different nucleation phenomena and the different mobilities of the interfaces involved will be discussed in more detail in the next section.

New orientation components that are characteristic for certain nucleation phenomena are in most cases already existent within the deformation microstructure, however, only to a very small volume fraction. For instance, if a hard second phase particle is surrounded by local orientation gradients in the deformed matrix, it is likely that nuclei can form there since these are regions where a high

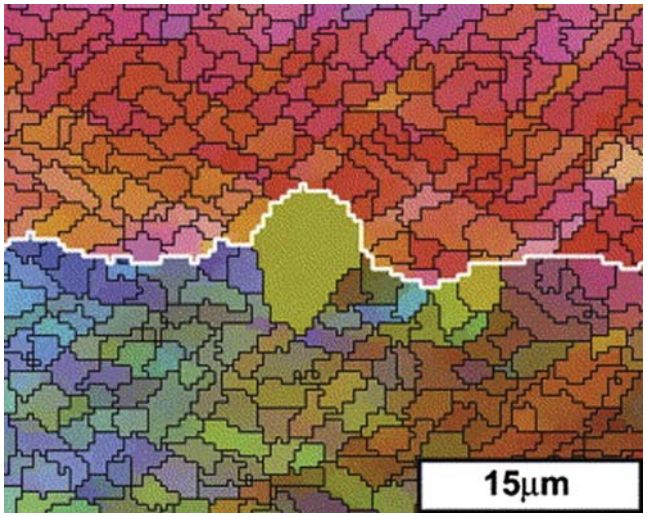

Figure 43 EBSD map (relative Euler contrast), showing an example of single subgrain SIBM during the early stages of annealing in an Al sample rolled to 50%. Bulging of the high angle grain boundary (white line) surrounding the large subgrain in the lower grain may be seen. Subgrain boundaries $>0.5^\circ$ are shown (Hurley and Humphreys, 2003).

misorientation can quickly accumulate to form high-angle grain boundaries. The original volume fraction from which such a nucleus emerges can be so small that it is hardly detectable in a statistical orientation distribution, such as for instance measured by using XRD, of the as-deformed material. In a case where such PSN-determined nuclei growing out of these curved lattice zones represent the dominant nucleation mechanism and where all grain boundaries have the same velocity (as a thought experiment), the final recrystallization texture will be very different from the original deformation texture (**Figures 23, 28 and 29**) (Doherty and Cahn, 1972; Humphreys and Ferry, 1997; Faivre and Doherty, 1979; Bhatia and Cahn, 1978).

A similar situation occurs for recrystallization nucleation at shear bands (Sebald and Gottstein, 2002; Engler et al., 1996; Engler, 1997). In this phenomenon, the nuclei are typically formed at the interface between the shear band interior and the surrounding matrix. This is the zone where the highest stored energy and also the highest lattice curvatures occur. This implies that rapid accumulation of high misorientations through discontinuous subgrain coarsening is possible during the nucleation stage. Hence, such nuclei are often formed rapidly and sweep the surrounding deformation matrix efficiently. The original volume from which they emerge and whose orientation they carry is—like for the PSN case described above—usually so small that it is also hardly visible in the original deformation orientation distribution. Yet, these originally tiny orientation zones are already present as a specific feature of the deformation microstructure and they can prevail in the final recrystallization texture. Typical sites where such mechanisms are assumed to prevail are deformation bands, shear bands, transition bands, PSN, and deformation twins (Berger et al., 1988). In all these cases, the inherited underlying substructures correspond to the most strongly deformed ones with often characteristic orientation deviations from the surrounding matrix orientation. Therefore, these sites have the potential to rapidly create highly mobile boundaries with respect to neighboring grains. This concept is referred to as "oriented nucleation" concept of the formation of recrystallization textures.

Besides these examples that show how nucleation phenomena can affect and initiate orientation changes also mobility differences among different types of grain boundaries can lead to essential and characteristic texture changes during recrystallization. Such mechanisms are referred to as "oriented growth". This concept assumes that nuclei of all orientations are present at the beginning of recrystallization but that the recrystallization texture depends on which orientations grow fastest into the deformed matrix. That the growth rate depends on misorientation has been early established for a long time by single crystal experiments by Liebman et al. (1956) and Aust and Rutter, (1959), (1960) (**Figure 31**). As was outlined above, depending on the purity of the material, certain types of grain boundaries, for instance the near 40°<111> misoriented grain boundary in face-centered cubic metals and alloys, can have a much higher mobility relative to other grain boundaries (Gottstein et al., 1995, 1998; Beck et al., 1950; Molodov et al., in press). This mobility advantage can also lead to specific orientation changes as for a randomly distributed spectrum of nucleation orientations only a few one will grow very fast at the expense of the deformation texture components, namely those that have the fastest orientation relationship to the main deformation texture orientations.

These two examples, describing extreme cases of a texture transformation during recrystallization, are referred to as "oriented nucleation model" and "growth selection model", respectively (Ibe et al., 1970; Ibe and Lücke, 1972; Bunge, 1969, 1982, 1986, 1987; Wassermann and Grewen, 1962; Bunge and Esling, 1982, 1991). They underline that one essential feature of primary recrystallization is the possibility of a complete change of the crystallographic texture from the original deformation texture resulting from heavy cold working to a completely modified recrystallization texture that can either consist of texture components that are due to a characteristic nucleation mechanism or due to the mobility advantage of a certain class of grain boundaries.

For this reason, the analysis of crystallographic textures has always been an important statistical (XRD) and local (EBSD, TEM) analysis vehicle for studying the underlying basic mechanisms of such recrystallization phenomena.

In this context, it is a striking observation that the formation of completely random orientation distributions through cold working and subsequent heat treatment involving recovery and recrystallization is not the rule but a rare exception in metal processing. In other words, the aim of producing polycrystalline alloys with random textures is usually difficult to achieve. Often only the smart mix of different acting mechanisms involving both, recovery and recrystallization or random nucleation phenomena, can help to obtain random textures.

In order to achieve minimum elastic and plastic anisotropy for sheet-metal forming applications such as those encountered in aerospace, food packaging, and automotive manufacturing, the textures of aluminum alloys and steels are often designed to assume minimum plastic anisotropy after recrystallization. **Figure 44** shows an example where an aluminum sheet with a high cube orientation has been produced by rolling and recrystallization. Such a preferred crystallographic recrystallization texture leads to undesired plastic anisotropy of the entire part. In such cases, a random texture is highly desired in the case of aluminum but difficult to produce. What is usually produced in such a case is a successful processing leading to a balanced recrystallization texture with a mixture of the two opposite anisotropies, namely retained and recovered rolling-texture components mixed with recrystallized cube-texture components in aluminum alloys (**Figure 45**) (Zhao et al., 2001, 2004).

In steels with a body-centered cubic structure, typically {111}<uvw>-dominated texture components are desired for sheet forming applications. Two main recrystallization components, namely, the {111}<110> and the {111}<112> orientations typically result from recrystallization annealing of heavily cold-rolled body-centered cubic steels (Bunge, 1986; Duggan et al., 1978; Ushioda et al., 1987;

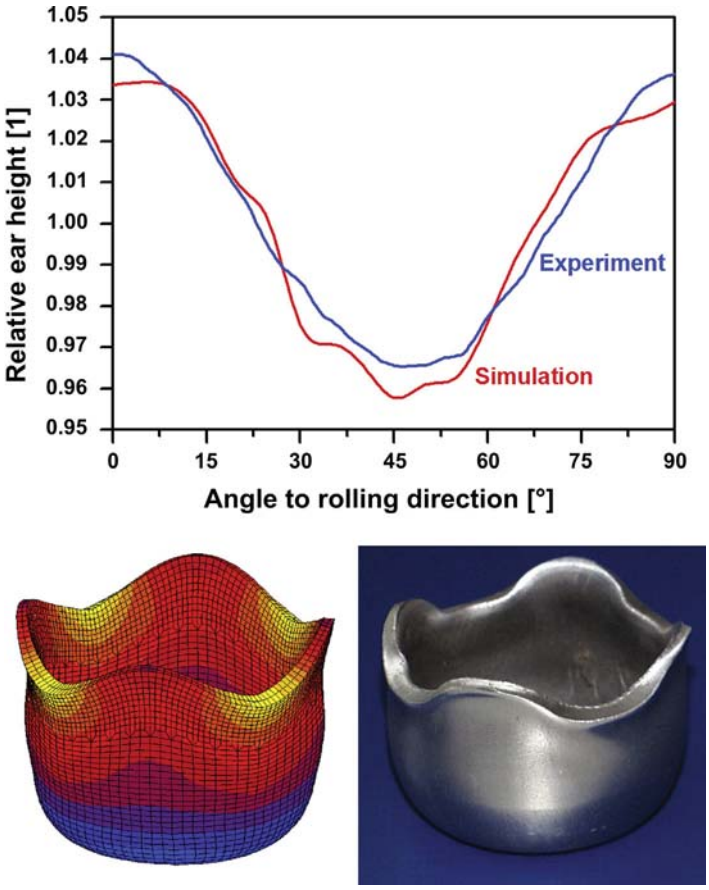

Figure 44 Rolled and recrystallized aluminum sheet with very strong cube texture and the resulting undesired plastic anisotropy. On the bottom left-hand side the corresponding crystal plasticity finite element simulation is shown. It considers the original crystallographic texture of the sheet before cup drawing (Zhao et al., 2004).

Raabe and Lücke, 1992, 1993; Randle, 1992; Klinkenberg et al., 1992; Raabe, 1995a; Juntunen et al., 2001; Ray et al., 1975b; Hutchinson, 1999).

As an example, **Figure 46** shows a fiber representation of the texture transition of cold-rolled tantalum (body-centered cubic structure) polycrystals during heat treatment. Annealing of the samples that were before cold rolled to 90 and 95%, respectively led to a typical recrystallization texture of body-centered cubic metals, namely, to a preferred {111}<uvw> texture (Raabe et al., 1994).

23.4 Driving Forces of Recrystallization and Grain-Growth Phenomena

From a thermodynamic standpoint, most recrystallization and grain-growth phenomena can be formally characterized as nonequilibrium transformations. In either type of process, a driving force acts on a grain-boundary segment. The free-enthalpy change of the system is then associated with the release of stored energy per volume that has been swept by the moving grain boundary (Rosenhain, 1914;

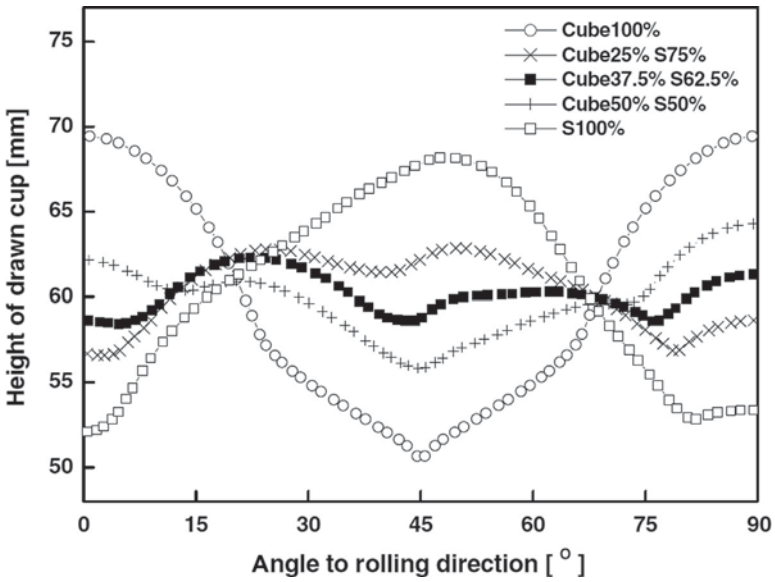

Figure 45 Optimization study by crystal plasticity finite element simulations regarding appropriate mixing of the cube orientation and the S orientation in aluminum alloys. The analysis reveals that appropriate mixing of the two texture components provide a strong reduction of the corresponding earing and thinning behavior (Zhao et al., 2004).

Ewing and Rosenhain, 1899, 1900a, 1900b; Alterthum, 1922; Carpenter and Elam, 1920; Czochralski, 1927; Burgers and Louwerse, 1931; Burgers, 1941; Burke and Turnbull, 1952; Smith, 1948; Beck and Hu, 1966; Haessner, 1978; Humphreys and Hatherly, 1995; Doherty et al., 1997).

In principle, two types of driving forces can be distinguished. The first one is a stored volume energy that acts equally in every portion of the affected grain that is being swept by a moving grain boundary. In such cases, the stored energy can often be simplified and written in scalar form. A most prominent (though simplified) example is the difference in the stored dislocation density across a moving interface. It should be emphasized though that for some experiments, i.e. in the case of differences in elastic or magnetic energy, the tensorial nature of these mechanisms must be taken into consideration. The second class of driving forces is of a configurational, i.e. a topological nature. This means that the driving force and thus also the release in the stored system energy depends on the exact local arrangement of the defects that are removed or rearranged by a moving grain boundary. A typical example is continuous grain growth, i.e. competitive grain coarsening, where the driving force depends on the local curvature and energy of the grain boundary but not on the size of the entire grain. In other words, in continuous grain growth, the local grain boundary portion that moves toward its center of curvature in order to reduce its total length does not "know" the size of the grain that it encompasses. This means that in this case only the local capillary driving force matters. It is however not a constant force that acts equally in each volume portion of the same crystal but it differs everywhere in the crystal and polycrystal depending on the local grain boundary configuration in terms of the curvature and grain-boundary intersection lines and points. During the grain-boundary motion when sweeping a volume dV, the change in the free-enthalpy dG can be written

$$\mathrm{d}G = -p\,\mathrm{d}V.$$

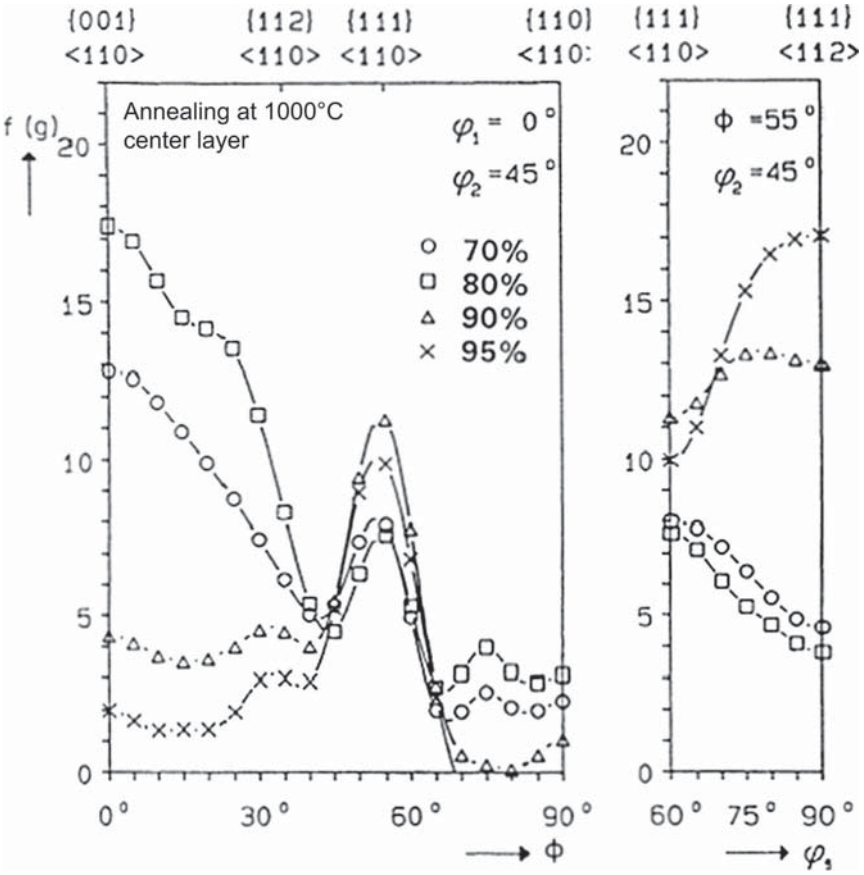

Figure 46 Fiber representation of the texture transition of cold rolled tantalum polycrystals during heat treatment. Annealing of the samples that were before cold rolled to 90 and 95%, respectively, lead to a typical recrystallization texture of BCC metals, namely, to a preferred {111} texture (Raabe et al., 1994).

The symbol p is referred to as driving force. For the case of primary static recrystallization the driving force stems from the stored dislocations and can hence be written

$$p = \rho E_{disl} = \frac{1}{2}\rho G b^2$$

where E_{disl} is the elastic energy of a dislocation per line segment, ρ is the dislocation density, G the shear modulus, and b the magnitude of the Burgers vector. Using typical values for the Burgers vector, the shear modulus and the dislocation density yields a maximum value for the driving force of primary static recrystallization of up to 10 MPa. When aiming at the prediction of recrystallization kinetics, it is recommended to use temperature-corrected values for the shear modulus and for the Burgers vector. Particularly, the magnitude of the shear modulus can be substantially reduced at high temperatures where recrystallization typically takes place.

The driving force for continuous capillary driven grain growth can be written as a Laplace pressure that acts on a curved portion of grain boundary. It reads

$$p = \frac{8\pi r\gamma\, \mathrm{d}R}{4\pi r^2\, \mathrm{d}R} = \frac{2\gamma}{r}$$

where it must be emphasized that r is the local curvature of the affected portion of grain boundary and not the grain size. γ is the grain-boundary energy and dR the local growth increment (Raabe, 2000; Holm and Battaile, 2001; Rollett and Raabe, 2001; Humphreys, 1992b; Maurice and Humphries, 1998; Maurice, 2001; Weygand et al., 2001; Kinderlehrer et al., 2004, 2001; Anderson et al., 1984; Srolovitz et al., 1984; Glazier et al., 1990; Anderson and Rollett, 1990; Tavernier and Szpunar, 1991a, 1991b; Srolovitz et al., 1985, 1986b, 1988; Rollett et al., 1989b, 1989c, 1992; Peczak, 1995; Doherty et al., 1990; Miodownik et al., 1999).

For discontinuous grain coarsening where huge grains sweep much smaller grains the driving force reads

$$p = \frac{3d^2\gamma}{d^2} = \frac{3\gamma}{d}$$

where d is the grain size of the smaller grains that are being swept by much larger grains. This equation shows, since the average grain size d during discontinuous grain coarsening is much smaller than the local grain curvature r in the equation above describing continuous grain coarsening, discontinuous grain growth progresses usually much faster than continuous grain growth (Raabe, 2000; Holm and Battaile, 2001; Rollett and Raabe, 2001; Humphreys, 1992b; Maurice and Humphries, 1998; Maurice, 2001; Weygand et al., 2001; Kinderlehrer et al., 2004, 2001; Anderson et al., 1984; Srolovitz et al., 1984; Glazier et al., 1990; Anderson and Rollett, 1990; Tavernier and Szpunar, 1991a, 1991b; Srolovitz et al., 1985, 1986b, 1988; Rollett et al., 1989b, 1989c, 1992; Peczak, 1995; Doherty et al., 1990; Miodownik et al., 1999).

Using typical values yields a driving force of 0.01–0.05 MPa for discontinuous grain coarsening. A phenomenon that is sometimes referred to as tertiary recrystallization describes the grain-coarsening phenomena where the driving force stems from the difference in surface energy among neighboring crystals:

$$p = \frac{2\Delta\Omega}{h}$$

where $\Delta\Omega$ is the difference in the surface energy among two neighboring grains and h is the radius of curvature of the grain boundary that extends between the two parallel surfaces. Tertiary recrystallization is often observed in thin films. Typical driving forces for tertiary recrystallization are of a similar magnitude as those for grain coarsening, namely, of the order of 0.01–0.05 MPa.

Much higher driving forces can be obtained when recrystallization takes place together with a phase transformation. Such situations are referred to as discontinuous precipitation phenomena. They are characterized by the fact that the driving force for this process is not only coming from the stored deformation energy but additionally from a thermodynamic transformation energy contribution. A well-known example is the joint recrystallization and transformation of a plastically deformed and over saturated solution of Al–Ag that forms AlAg2 precipitates in an otherwise pure-aluminum matrix behind the moving grain boundary. The driving force for such a discontinuous precipitation can be written

$$p = R_g(T_1 - T_0)c_0 \ln c_0$$

where c_0 is the concentration of the over saturated solid solution, corresponding to the maximal solubility at T_0. The temperature T_1 is the chosen heat-treatment temperature that lies below T_0. Discontinuous precipitation phenomena can proceed extremely fast owing to the very high driving forces involved, namely, of the order of 500 MPa.

23.5 Dynamic and Metadynamic Recrystallization

Controlling the microstructure during hot working and heat treatment is of high relevance in the thermomechanical processing of metallic alloys. When crystalline metallic materials are deformed at temperatures above about half of the absolute melting point, the accumulated dislocations can continuously be removed by two different types of mechanisms, namely, by dynamic recovery and by dynamic recrystallization (Haessner, 1978; Humphreys and Hatherly, 1995, 2004; Doherty et al., 1997; Doherty, 2005).

The first type of process, termed dynamic recovery, is a gradually acting mechanism. It occurs in practically all materials in a continuous fashion and leads to the gradual mutual annihilation of dislocations by climbing and cross-slip and to the thermally activated formation of subgrains and subboundaries.

In materials with high stacking-fault energy, such as aluminum, dynamic recovery can continuously remove and balance the strain hardening imposed during the hot working process. Such a pronounced and continuous dynamic recovery process, therefore, leads to an overall steady-state plastic flow when the material is formed above half of its melting temperature.

In contrast to high stacking-fault energy materials, alloys with a moderate to low stacking-fault energy build up considerably higher dislocation densities during hot working when compared to metals that have high stacking-fault energy. Eventually in low stacking-fault energy materials, the accumulated dislocation density becomes sufficiently high to stimulate the nucleation of recrystallization during hot deformation (**Figure 47**) (McQueen et al., 1976; Fritzmeier et al., 1979; Luton and Sellars, 1969; McQueen, 1968; Jonas et al., 1969).

This mechanism is referred to as dynamic recrystallization. It consists in the formation of mobile high-angle boundaries that at least partially surround the nuclei and by the subsequent sweeping of the deformation substructure that was stored during hot working.

The study of dynamic recrystallization phenomena aims at two main directions. Firstly, it is of interest to understand the basic characteristics of high temperature flow curves and secondly, it is of high relevance for the optimization of metallurgical processing to understand the evolution of new grain structures under conditions of dynamic recrystallization. In the latter context specifically, the efficiency of dynamic recrystallization as a mechanism to refine and homogenize the grain size is of high interest.

In a given metallic alloy, the essential characteristics of dynamic recrystallization are determined by three main parameters: these are the initial grain size prior to plastic hot working; the temperature; and the strain rate (**Figure 48**) (Rossard and Blain, 1960; Rossard, 1963; Sakai et al., 1983; Sakai and Jonas, 1984). The initial grain size mainly determines the critical strain of dynamic recrystallization, the peak strain, and the kinetics of the process.

The finer the starting grain size is, the lower are the values for the critical and the peak strains. This effect is due to the fact that dislocations accumulate more rapidly in metallic alloys that have a smaller grain size. A similar effect occurs in those materials that have lower stacking-fault energy. The lower the stacking fault energy, the higher is the strain hardening rate and hence the stored deformation energy.

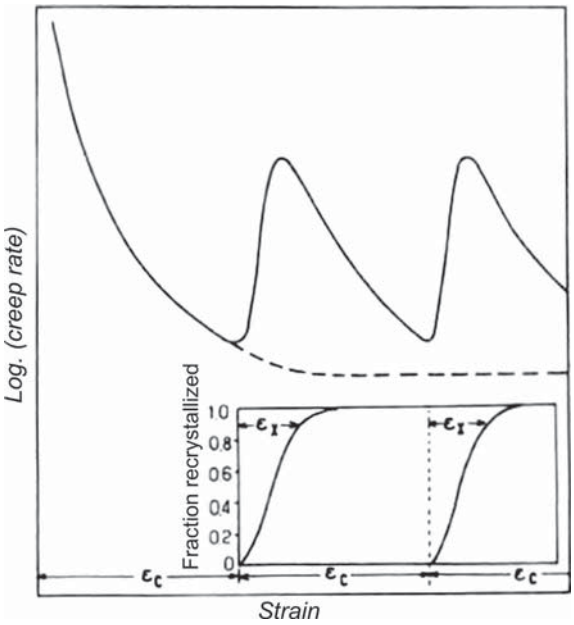

Figure 47 Schematical diagram of dynamic recrystallization (Luton and Sellars, 1969). The term ε_c refers to the critical strain.

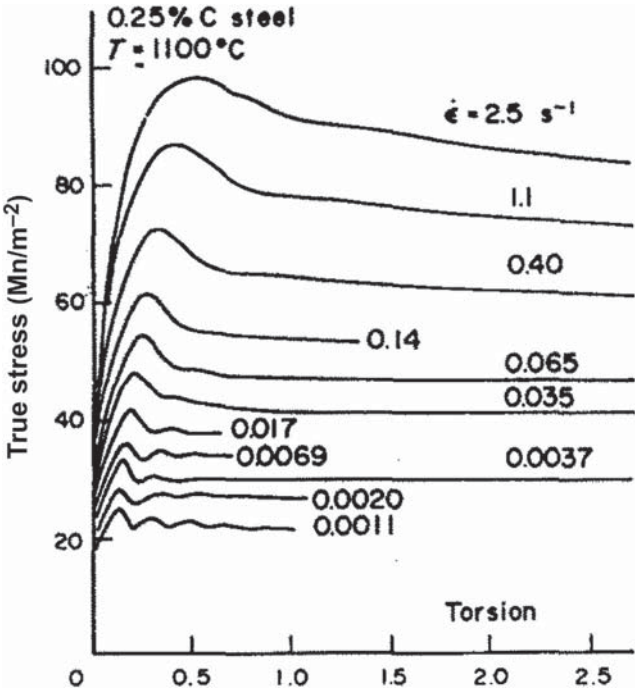

Figure 48 Influence of strain rate on the flow curves derived from hot torsion data at 1100 °C for a C-steel (Sakai and Jonas, 1984).

Peak stresses are also observed to be dependent on the initial grain size, however, the steady-state stress and the final grain size are independent of the initial grain size (McQueen and Jonas, 1975; Sellars, 1978; Sakai et al., 1983; Sakai and Jonas, 1984; Roberts, 1982; Ryan and McQueen, 1990; McQueen et al., 1990; Tsuji et al., 1997).

An important feature is that the flow curves of face-centered cubic metals can show characteristic undulations in the flow stress. This type of phenomenon is referred to as multiple-peak flow behavior (**Figure 49**). It is typical of dynamic recrystallization processes where subsequent waves of incomplete nucleation and growth processes sweep the deformation substructure during ongoing straining (McQueen et al., 1976; Fritzmeier et al., 1979; Luton and Sellars, 1969; McQueen, 1968; Jonas et al., 1969; McQueen and Jonas, 1975; Sellars, 1978).

The analysis and investigation of dynamic recovery processes dates back to the first observation of this phenomenon during the deformation of Pb in 1939 (McQueen et al., 1976; Fritzmeier et al., 1979; Luton and Sellars, 1969; McQueen, 1968; Jonas et al., 1969; McQueen and Jonas, 1975; Sellars, 1978). During the 20 years that followed, most of the observations were made on metals under creep

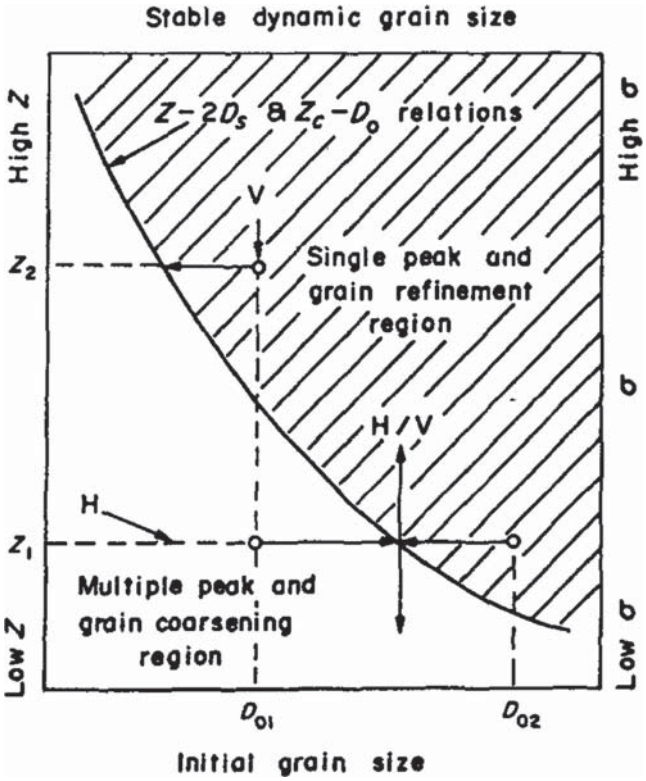

Figure 49 A microstructural mechanism map for distinguishing between the occurrence of two types of dynamic recrystallization. The central curve separates the single (grain refinement) from the multiple peak (grain-coarsening) region. Three distinct types of experiment are represented, namely, the so-called "vertical tests carried out over a range of strain rates and temperatures on material with a fixed initial grain size do: "horizontal" tests (H) carried out at a fixed temperature-compensated strain rate Zl with a series of initial grain sizes; and combined "horizontal/vertical" (H/V) tests involving changes in strain rate or temperature after a period of steady state deformation (Sakai and Jonas, 1984).

conditions. The first detailed investigation of metallic behavior under constant strain rate conditions was published by Rossard and Blain (1960), Rossard (1963).

The classical approach to dynamic recrystallization was primarily concerned with the aim to understand the transition from cyclic (i.e. multiple peak) to single-peak recrystallization (McQueen et al., 1976). As can be seen from **Figure 48**, the flow curves pass through this transition as the strain rate is increased, or the temperature decreased.

In some cases, the transition from multiple-peak to single-peak dynamic recrystallization behavior was characterized in terms of certain critical strain criterion.

It was observed though that this criterion is not valid for the high-temperature deformation regime of face-centered cubic metals in tension and compression.

An alternative criterion for the transition was suggested based on the grain size considerations. The latter indicate that *cyclic* flow curves are associated with grain *coarsening* and that *single peak* flow curves are associated with grain *refinement*.

It was observed that often a single peak behavior was associated with the formation of a necklace or cascade-type multilayer of sets of newly grown grains around the center of a nonrecrystallized larger inner part of a host grain. The growth process and hence also the grain size in this case appears to be deformation limited. By contrast, static primary recrystallization is nearly completely synchronized in fine-grained materials, because the high density of grain nuclei leads to a small spread in the nucleation strain. The grain size under these conditions is determined by impingement, and thus it is nucleation controlled and not growth controlled.

Metadynamic recrystallization is defined as the growth of grain nuclei after the plastic deformation stage with the specific property that these nuclei were already formed during the preceding plastic deformation. It is important to differentiate between static and metadynamic recrystallization, as they proceed at different rates. Also the type of recrystallization has important consequences on the final microstructure and properties of the deformed metals. Once dynamic recrystallization is initiated during deformation, the dynamically recrystallized nuclei continue to grow, even after straining is terminated. The main difference between static recrystallization and metadynamic recrystallization is in the nucleation mechanism of the new grains. Unlike in primary static recrystallization, metadynamic re recrystallization does not require an incubation time for grain nucleation, as dynamically recrystallized nuclei already occur within the deformed microstructure.

23.6 Grain Growth

Practicality all engineering metallic alloys are in a polycrystalline state. This means that each crystal is defined in terms of its crystallographic orientation, its size and local topological environment, and the properties of its grain boundaries (Raabe, 2000; Holm and Battaile, 2001; Rollett and Raabe, 2001; Humphreys, 1992b; Maurice and Humphries, 1998; Maurice, 2001; Weygand et al., 2001; Kinderlehrer et al., 2004, 2001; Anderson et al., 1984; Srolovitz et al., 1984, 1985, 1986b, 1988; Glazier et al., 1990; Anderson and Rollett, 1990; Tavernier and Szpunar, 1991a, 1991b; Rollett et al., 1989b, 1989c, 1992; Peczak, 1995; Doherty et al., 1990; Miodownik et al., 1999).

All such polycrystalline aggregates are subject to capillary-driven competitive grain-coarsening phenomena, provided that the temperature is high enough to overcome the activation barriers. In the metallurgical terminology, these phenomena are often referred to as grain growth.

It is described as a process by which the mean grain size of an aggregate of crystals increases. The driving force for this results from the decrease in free energy that accompanies reduction in

total grain-boundary area. As the crystals become gradually larger, the curvature of the boundaries becomes smaller. This results in a tendency for larger grains to grow at the expense of smaller grains.

It should be emphasized that in many engineering applications grain growth is not desirable, as many mechanically beneficial properties of structural metallic alloys such as strength, strain-hardening, and ductility are improved inversely to the average grain size.

Given a sufficiently high temperature and no factors that impede grain-boundary migration such as second-phase particles or impurities on the grain boundaries, polycrystals will gradually evolve toward a single crystal. In real microstructures this goal is rarely achieved.

In two dimensions, it is in principle possible, provided that all grain boundaries have exactly the same grain-boundary energy and are connected with each other with 120° angles, that the microstructure is free of any grain-boundary curvature so that no capillary-driven grain-coarsening occurs.

It must be emphasized though that such a microstructure is only mechanically stable owing to the local mechanical equilibrium of the grain boundaries when abutting under 120°. In two dimensions such intersections are referred to as stable triple junctions.

From a thermodynamic viewpoint, the driving force of grain coarsening is the overall reduction in the total grain-boundary area per volume. Hence, even a microstructure that is under local mechanical equilibrium is not necessarily also in thermodynamic equilibrium.

In most cases, however, even in quasi 2D situations as sometimes encountered in thin-film grain structures, microstructures are not free of local curvatures of the grain boundaries involved. In three dimensions, curvature-free and at the same time compatible grain topologies are not possible in full mechanical equilibrium (Raabe, 2000; Holm and Battaile, 2001; Rollett and Raabe, 2001; Humphreys, 1992b; Maurice and Humphries, 1998; Maurice, 2001; Weygand et al., 2001; Kinderlehrer et al., 2004, 2001; Anderson et al., 1984; Srolovitz et al., 1984, 1985, 1986b, 1988; Glazier et al., 1990; Anderson and Rollett, 1990; Tavernier and Szpunar, 1991a, 1991b; Rollett et al., 1989b, 1989c, 1992; Peczak, 1995; Doherty et al., 1990; Miodownik et al., 1999). This means, that in three dimensions, all polycrystalline microstructures must necessarily contain some local grain-boundary curvature.

A classical kinetic approach to describe such a gradual coarsening phenomenon was suggested by Burke and Turnbull.

In this derivation, the velocity of a portion of grain boundary is related to the pressure gradient across it as described above in terms of the phenomenological Turnbull rate expression for grain-boundary motion as was derived above

$$\dot{\boldsymbol{x}} = \boldsymbol{n}mp = \boldsymbol{n}m_0 \exp\left(-\frac{Q_{gb}}{k_B T}\right)p$$

where m is the mobility, $\boldsymbol{n}$ the normal vector of the interface, p the driving force, and Q_{gb} the activation energy of grain-boundary motion. Rewriting the growth rate $\dot{\boldsymbol{x}}$ in terms of a scaling relation for the time-evolution of the average grain size D according to

$$\dot{\boldsymbol{x}} = \boldsymbol{n}\frac{\mathrm{d}D}{\mathrm{d}t} = \boldsymbol{n}mp$$

The driving force p can be written

$$p = K\frac{\gamma}{D}$$

where K is a scaling constant, γ the grain-boundary energy, and D the average grain size. Integrating the resulting expression

$$n\frac{\mathrm{d}D}{\mathrm{d}t} = nK\frac{\gamma}{D}$$

with respect to time, we obtain that the average area of the grain evolves with time as

$$\langle D\rangle^2 - D_0^2 = K\gamma t$$

This shows that grains grow at a rate that is essentially proportional to the square root of time when considering that the initial grain size D_0 is much larger than the current average grain size $\langle D\rangle$.

It has to be emphasized at this point that in this derivation we have only considered the reduction in grain-boundary energy for the driving pressure. Possible additional sources that might enter into the total energy reduction are that the grain boundary might be separating grains consisting of different phases, or one grain may have a higher dislocation density than another. If neither of these effects apply, the pressure can arise simply as a product of the curvature of the grain boundary. This pressure acts toward the center of curvature.

It is interesting to note in that context that it is actually in a real microstructure not the average grain size that acts as a driving force for grain coarsening but it is the *local* curvature of the interface that matters. In other words, any local grain-boundary curvature aims at reducing the total grain-boundary area per volume by moving toward the center of the curvature radius. This elementary process of grain coarsening is explicitly guided by the local curvature and the grain does not "know" if actual grain size.

The actual connection between grain size and local curvature comes simply through the principle that for a large grains have either very low curvatures, and hence, slow growth rates of their grain boundaries, or the curvature of their grain-boundary facets point outward, toward the surrounding smaller grains.

As mentioned above, a neutral, curvature-free microstructure, irrespective of the actual grain size, occurs when all grains in a 2D grain structure have the same hexagonal grain shape and mechanically stable intersecting *triple junctions of* 120°. A triple junction is the point at which three grain boundaries meet. This local mechanical equilibrium among three intersecting grain boundaries in two dimensions does only apply when all interfaces have the same grain-boundary energy.

Mullins, (1956) pointed out the random grain structures are, however, inherently unstable. In 2D, grain boundaries that are associated with microstructures that are characterized by certain size distribution actually have to "curve" so that they can intersect at triple junctions under preservation of the local mechanical equilibrium. In two dimensions, this means that grains with less than six sides have centers of curvature lying inside their boundaries. Conversely, grains with more than six sides have centers of curvature lying outside their boundaries. This gives rise to the driving pleasure derived above, being proportional to both the grain-boundary energy and the local grain-boundary curvature. The resulting velocity of boundary migration is always directed toward the centers of the interface curvature.

For 2D grain structures, this observation was cast into the so-called N-6 rule. This rule states that an N-sided grain evolves under 2D grain growth according to

$$\frac{\mathrm{d}D(N)}{\mathrm{d}t} = m\gamma\frac{\pi}{3}(N-6)$$

where $D(N)$ is the 2D grain size as a function of its number of grain-boundary facets N and γ is the grain-boundary energy. The latter parameter is here assumed to be identical for all interfaces. This

so-called Mullins-von Neumann rule (Mullins, 1956; von Neumann, 1952) shows that actually the number of grain-boundary sides determines the crystal growth and not the grain size itself. Topologically, it should be noted, though, that larger grains are very unlikely to contain a small number of boundary facets, and so the two formulations are approximately equivalent.

Although in three dimensions this problem is more complicated, the main kinetic and energetic characteristics of grain growth remain in principle unchanged, namely: (i) grain boundaries migrate toward their centers of their curvature; (ii) small grains have usually larger curvature values associated with their grain-boundary facets and hence reveal higher grain-boundary velocities so that these become smaller at the expense of larger grains; and (iii) the average grain size increases with time.

However, one main difference in the grain growth exists between two dimensions and three dimensions. In three dimensions, no grain topology exists (as in 2D), which satisfies both, zero curvature grain-boundary facets and local mechanical equilibrium at the grain-boundary interaction lines and points. The application of 3D surface evolver simulations has recently shown that in average grain shrinkage occurs for grain shapes that have a smaller number of facet areas than 14. Grains that have a larger number of grain facets will in average become larger during grain growth. The minimal-area tessellating grain shape in three dimensions is the 14-sided tetrakaidecahedra, a shape whose surface is made up of six hexagons and eight squares (**Figure 50**) (Krill and Chen, 2002).

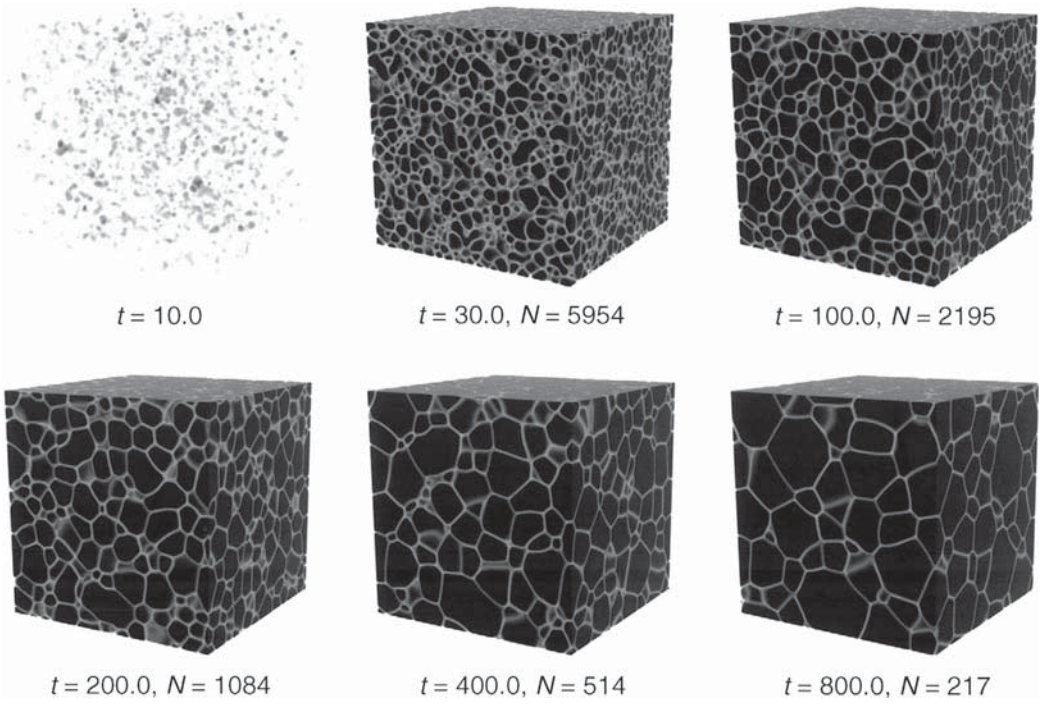

Figure 50 Phase-field simulation of microstructural evolution performed on a 180·180·180 simple-cubic grid, visualized by mapping the interfaces. The elapsed time t and the number of grains N are specified under each image. The microstructure at $t = 10.0$ illustrates the homogeneous nucleation of crystallites from the supercooled liquid initial state (Krill and Chen, 2002).

23.7 Secondary Recrystallization: Discontinuous Grain Coarsening

In some cases during grain coarsening, a sudden and every rapid growth of a small number of grains can occur. The final dimensions of such rapidly growing grains can be of the order of multiple centimeters (**Figure 51**) (Dorner et al., 2006).

Since this process has a phenomenological similarity to a nucleation and growth mechanism involving only a few crystals, it is sometimes also referred to as secondary recrystallization. A more specific terminology refers to it as a discontinuous grain coarsening or to abnormal grain growth. The latter two terms are considered to be more adequate as no sweeping of cold-worked microstructures is involved during such discontinuous grain growth. The other crystals undergo continued grain growth.

A number of general features can be identified that characterize discontinuous grain coarsening:

During the nucleation stage of secondary recrystallization, only a small number of grains start to grow to very large dimensions. These few large grains are, however, not freshly nucleated in any way but they are particular crystals that already existed in the preceding microstructure. It is observed that the early stages of growth of these abnormally large grains are slow. This indicates that at the beginning of secondary recrystallization a certain incubation period occurs.

When those grains that show an extraordinary high growth rate exceed the average grain-size diameter by a factor of 4–5, they will prevail in the resulting microstructure and show further discontinuous growth even if the surrounding continuously coarsening grains are not impeded by impurities or particles. This means that a grain diameter advantage of a factor 4–5 is topologically sufficient to promote abnormal grain growth.

The crystallographic orientations of the abnormally growing grains typically deviate substantially from those that surround them, at least during the early stages of secondary recrystallization.

A common feature to all discontinuous grain coarsening phenomena, at least in their incipient stages, is the fact that normal uniform grain growth is selectively inhibited. This means that for secondary recrystallization to take place normal grain growth must be very slow so that large secondary grains can effectively grow at the expense of the surrounding crystals.

Figure 51 Typical size of Goss grain after abnormal grain growth (Dorner et al., 2006).

Such inhibition typically occurs by the presence of second dispersed phase particles, by impurities that decorate certain grain boundaries, by specific energetic, structural or kinetic grain-boundary characteristics, by an inherited topological advantage of certain grains, or by crystallographic texture effects. In some materials also the inhomogeneity of dissolving precipitates on grain boundaries seems to play a role for promoting secondary recrystallization. Microstructures resulting from discontinuous grain growth are often characterized by strong crystallographic textures.

Typically textures resulting from secondary recrystallization are different from those obtained after primary recrystallization and normal grain growth. Also it is observed that a well-defined minimum annealing temperature must be exceeded for initiating discontinuous grain coarsening. The largest grains are normally produced just above this temperature; at higher annealing temperatures smaller secondary grains result.

As outlined above, the driving forces for discontinuous grain coarsening result from the reduction in the total grain-boundary area per volume. Different to the driving force of continuous grain growth, which results from the local grain-boundary curvature, the driving force of secondary recrystallization, once the huge grains have started to grow abnormally, arises from reducing the grain-boundary energy in units of the small grains that surround the huge grains.

Owing to the fact that a number of interacting phenomena, such as described above, can give rise to abnormal grain growth, computer simulations under different intern boundary conditions can help to clarify which mechanism is decisive to produce a certain discontinuous grain growth phenomenon (Humphreys and Hatherly, 2004).

From such simulations, it was concluded that an inhomogeneous distribution of the grain-boundary energy alone is usually not sufficient to explain abnormal grain growth. In most cases, it was observed that a second mechanism has to assist promoting abnormal grain growth, such as certain grain boundaries with a much higher mobility compared to others (Anderson et al., 1984; Srolovitz et al., 1984, 1986b, 1988; Glazier et al., 1990; Anderson and Rollett, 1990; Tavernier and Szpunar, 1991a, 1991b; Rollett et al., 1989b).

Such a situation occurs naturally when discontinuous grain coarsening occurs in a strongly textured polycrystal, where only a few grains assume a different grain orientation relative to their grain neighborhood. Such a microstructure implies that most of the normally growing grains have small-angle grain boundaries between them while the abnormally growing ones might have high-angle grain boundaries around them. This means that normally growing grains, that undergo continuous grain coarsening, are surrounded by interfaces that have both low energy and low mobility. If a few grains with a high misorientation (hence surrounded by high-angle grain boundaries) are embedded in such a grain structure, they should have a growth advantage in terms of the higher grain-boundary energy and higher grain-boundary mobility.

Another effect that has been discussed as relevant in secondary recrystallization is the fact that the Zener force is proportional to the grain-boundary energy. Since the grain-boundary energy is a function of five crystallographic parameters, namely, the three misorientation angles and the interface plane normal inclination, the Zener force can act selectively, depending on the grain boundaries involved—more specific that grains that are surrounded by interfaces with a low grain-boundary energy are exposed to a small particle drag force. By way of contrast, grains with a high grain-boundary energy will experience a higher Zener drag force (Holm et al., 2001; Miodownik et al., 2000). Similar effects apply to impurity drag, where the solubility and the interaction force with the solutes is different for different types of grain boundaries. Hence, certain grain boundaries might have an advantage over others for instance in a situation where their solute content is below that of others.

Commercially highly important examples where abnormal grain growth plays an essential role for a product are the formation of secondary recrystallized grains with a strong Goss texture (110)[001] (i.e. the (110) plane is oriented parallel to the sheet surface and the [001] direction is oriented parallel to the RD) in silicon–iron electrical steels and the formation of cube oriented textures in nickel alloys that are used as substrates for growing ceramic superconductors.

One of these examples, namely, the Goss texture in soft magnetic FeSi alloys, is discussed in a bit more detail in the following:

The strong Goss texture, (110)(001), that develops in commercially produced Fe-3% Si soft magnetic steels is due to a secondary recrystallization process (Goss, 1935; Ruder, 1935; Burwell, 1940). The preferred abnormal growth of Goss-oriented grains is characterized by the presence of an inhibitor phase in the material. As inhibitor phase one refers to a second solid phase that is finely dispersed in the primary matrix and interacts with the grain boundaries. The nature of the interaction between these inhibitor particles and the FeSi grain boundaries is not exactly understood. It is assumed that they interact either through conventional Zener drag or via Zener drag plus solid solution when the particles start to dissolve in the intercritical-annealing regime. As intercritical annealing, we refer here to a heat treatment where partial phase transformation occurs (Goss, 1935; Ruder, 1935; Burwell, 1940).

In that context, it must be considered that the magnitude of the back driving forces associated with both Zener drag and impurity drag depends on the crystallographic character, energy, and misorientation of the grain boundary. In FeSi electrical steels, these small precipitates are usually nitrides and sulfides. It was observed that at an early stage (the "nucleation stage" of abnormal grain growth) of the secondary recrystallization process some fraction of the inhibitor phase starts to dissolve so that locally the back driving forces cease to pin the grain boundaries. This stage is characterized by a sudden size increase of very few Goss-oriented grains which—once they reach a size advantage of several grain diameters relative to their neighbor crystals—rapidly consume the entire polycrystalline matrix (**Figure 52**).

In an approach to understand this complex phenomenon different models were considered (Hu et al., 2008). One line of argumentation was concentrated on a possible initial size advantage of Goss grains in the microstructure after primary recrystallization. The rationale behind this assumption was that the largest driving force for grain growth occurs for the biggest grains in the matrix. It was hence discussed

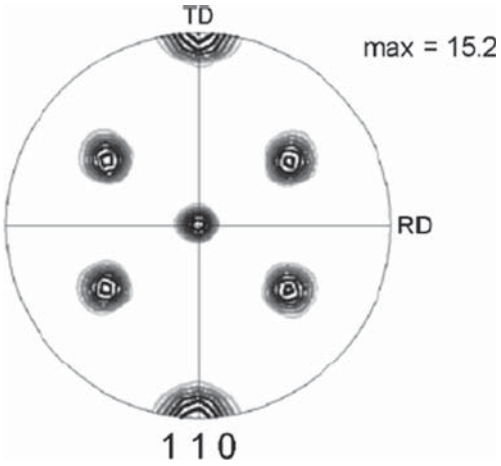

Figure 52 Goss texture of Fe-3 wt.% Si steel after abnormal grain growth (Dorner et al., 2006).

whether a faster growth of Goss-oriented nuclei during primary recrystallization might lead to a certain number of these grains with a larger initial size in the matrix prior to the onset of abnormal grain growth. However, by using large-scale EBSD measurements, it was found that Goss-oriented grains have the same average grain size as crystals with other crystallographic orientations that do not grow abnormally.

Hence, the argument of an initial size advantage of Goss-oriented grains did not seem plausible.

Another line of the discussion suggested the possibility that Goss grain might have a smaller grain neighborhood in the as-recrystallized state since they are during primary recrystallization formed in shear bands where the nucleation rate is high and hence many smaller grains are formed. It was discussed that this configuration might lead to a growth rate advantage during the early stages of grain growth (Burwell, 1940; Hillert, 1965; May and Turnbull, 1958; Shimizu and Harase, 1989; Lin et al., 1996; Hayakawa and Szpunar, 1997; Rajmohan et al., 1999; Morawiec, 2000; Chen et al., 2002). Another hypothesis assumed a preferential coalescence mechanism in clusters of Goss-oriented grains because of their very low relative misorientation (Matsuo, 1989; Inokuti et al., 1981). At last a selective process due to a special orientation relationship between Goss and matrix grains has been claimed to act as the main cause of the secondary recrystallization (Shimizu and Harase, 1989; Lin et al., 1996; Hayakawa and Szpunar, 1997; Rajmohan et al., 1999; Morawiec, 2000; Chen et al., 2002).

23.8 Phenomenological Kinetics of Recrystallization

Owing to their nature as nucleation and growth mechanisms, recrystallization phenomena can be kinetically described by a JMAK approach, which is characterized by a sigmoidal shape when plotting the transformed volume fraction as a function of time (**Figures 6a** and **53**). The topological model

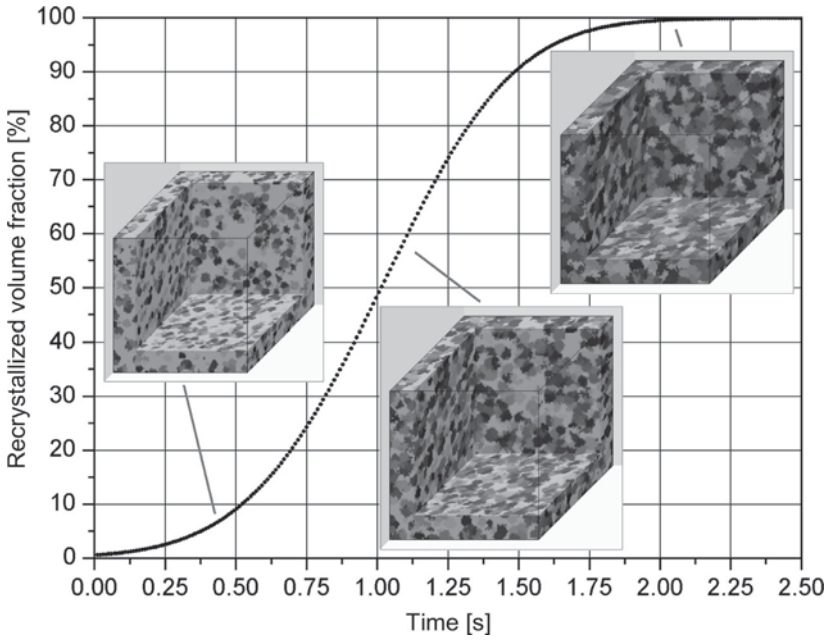

Figure 53 Sigmoidal recrystallization curve predicted by a cellular automaton model that includes inhomogeneity of the crystallographic texture and of the grain-boundary mobility (Raabe, 1999, 2002).

behind the Avrami kinetic formulation is the most common formulation for describing isothermal discontinuous transformation kinetics that are based on nucleation and growth into a homogeneous matrix (Kolmogorov, 1937; Johnson and Mehl, 1939; Avrami, 1939, 1940).

When applied to primary static isothermal recrystallization kinetics it describes the volume fraction that is transformed from the cold worked to the recrystallized state.

In the 1940s, various authors independently developed a similar kinetic formulation that is sometimes therefore referred to as the JMAK equation (Kolmogorov, 1937; Johnson and Mehl, 1939; Avrami, 1939, 1940).

More specific, the original Avrami model assumed site-saturated nucleation (all nuclei exist at $t = 0$s and no new nuclei are formed). statistically distributed nucleation (both in real and orientation space), and isotropic growth at a constant growth rate.

About the growth rate and the statistical nucleus distribution Kolmogorov, Johnson and Mehl made the same assumptions; however, they used not a site-saturated but alternatively also a time-dependent nucleation rate (continuous nucleation).

Interestingly, the theory was initially developed for low molecular-weight materials such as metals. Later, it was extended to the crystallization of high molecular-weight polymers (Raabe, 2004; Raabe et al., 2004a; Godara et al., 2006; Jia and Raabe, 2006).

Avrami based his approach on the topological consideration that a phase is nucleated by small nuclei that already exist in the preceding host phase in which the transformation spontaneously takes place and whose effective number is n_0 per unit volume. The number of nuclei per unit region at time t decreases from n_0 in two ways: (i) some of them become active growth nuclei in consequence of free energy fluctuations and with probability of occurrence p per unit time and (ii) some of them get swallowed by growing grains of the new phase. The number of growth nuclei can increase linearly with time (continuous nucleation) or the large majority of the growth nuclei can be formed near the beginning of the transformation (instantaneous nucleation or site-saturated nucleation). Further, the authors made the assumption that when one grain impinges upon another growth ceases. This means that now grain growth occurs.

According to the results of JMAK analysis, the dependence of the recrystallized volume fraction X on time can be written

$$X(t) = 1 - \exp(-k_0\, t^q)$$

where k_0 is a constant and q is the Avrami kinetic exponent. When using the underlying metallurgical quantities for site-saturated nucleation conditions we can write this equation as

$$X(t) = 1 - \exp\left(-\, n_0 \frac{4}{3}\pi v^3 t^3\right)$$

where v is the constant growth rate and n_0 is the effective number of nuclei per unit volume. The recrystallization time t_R is

$$t_R(n_0) = \left(n_0 \frac{4}{3}\pi\right)^{-1/3} \frac{1}{v}$$

and the grain size after recrystallization amounts to

$$d = 2vt_R = 2\left(\frac{1}{n_0}\frac{3}{4\pi}\right)^{1/3}$$

For the corresponding case of continuous nucleation the same equations read

$$X(t) = 1 - \exp\left(-\dot{n}\frac{1}{3}\pi v^3 t^4\right)$$

with the recrystallization time

$$t_R(\dot{n}) = \left(\dot{n}\frac{1}{3}\pi v^3\right)^{-1/4}$$

and the grain size after recrystallization amounts to

$$d = 2vt_R = 2\left(\frac{v}{\dot{n}}\frac{3}{\pi}\right)^{1/4}$$

For extracting the kinetic coefficient from of discrete simulations, one can rewrite this expression in the following form

$$\ln(-\ln(1 - X(t))) = \ln k_0 + q\ln(t).$$

From the analysis above, we learn that the kinetic coefficient for the site-saturated nucleation conditions amounts to 3 and that for continuous nucleation to 4 (Haessner, 1978; Humphreys and Hatherly, 1995).

Sometimes, kinetic coefficients far outside of the here presented regime of 3–4 are discussed in the literature (Sellars and Tegart, 1966; Humphreys, 1997; Himmel, 1962; Cahn, 1965, 1950; Ibe and Lücke, 1966; Hu et al., 1990; Rath and Hu, 1969a). However, such analysis should usually be treated with care since kinetic coefficients that substantially deviate from this regime are probably influenced by recovery and grain-growth phenomena. Then, however, the corresponding kinetic laws for recovery or grain growth rather than the conventional sigmoidal Avrami kinetics alone should be used for analyzing corresponding datasets. Alternatively, full-field numerical models must be used, which consider the various mechanisms in the same simulation run (Humphreys, 1997, 1992a; Miodownik, 2002; Raabe and Becker, 2000; Raabe, 2000; Holm and Battaile, 2001; Rollett and Raabe, 2001; Humphreys, 1992b; Maurice and Humphries, 1998; Maurice, 2001; Weygand et al., 2001; Kinderlehrer et al., 2004, 2001; Anderson et al., 1984; Srolovitz et al., 1984; Glazier et al., 1990; Anderson and Rollett, 1990; Tavernier and Szpunar, 1991a, 1991b; Srolovitz et al., 1985, 1986b, 1988; Rollett et al., 1989b, 1989c; 1992; Peczak, 1995; Doherty et al., 1990; Miodownik et al., 1999; Raabe, 1998).

Another main result can be retrieved from the statistical analysis presented here: as pointed out before, however, real recrystallization phenomena are characterized by more complex and spatially not statistically distributed nucleation mechanisms, by a nonhomogeneous deformation substructure (hence an inhomogeneous driving force), and by a nonconstant growth rate of the grain boundaries involved. Understanding this high degree of inherent inhomogeneity of recrystallization phenomena naturally advocates the use of more complex and spatially and/or orientationally discrete simulation methods involving also the preceding deformation history of the material (Raabe and Becker, 2000; Bate, 1999; Roters et al., 2010; Raabe, 1998, 2007; Zambaldi et al., 2007; Radhakrishnan et al., 2000, 1998; Hurley and Humphreys, 2003; Hallberg, 2011; Carel et al., 1996; Nagai et al., 1990; Bernacki et al., 2007, 2008, 2009; Merriman et al., 1994; Zhao et al., 1996; Bernacki and Coupez, 2011; Logé et al., 2008; Janssens et al., 2007). Such simulation approaches will be presented in the next sections.

23.9 Modeling Recrystallization and Grain-Growth Phenomena

23.9.1 Introduction

The use of models for describing recrystallization phenomena with the aim of predicting crystallographic texture, kinetics, microstructure, and mechanical properties in the context of materials processing is a challenging task (Raabe, 1998, 2007; Zambaldi et al., 2007; Radhakrishnan et al., 2000, 1998; Hurley and Humphreys, 2003; Hallberg, 2011; Carel et al., 1996; Nagai et al., 1990; Bernacki et al., 2009; Merriman et al., 1994; Zhao et al., 1996; Bernacki et al., 2007, 2008; Bernacki and Coupez, 2011; Logé et al., 2008; Janssens et al., 2007; Crumbach et al., 2004; Rollett et al., 1989a; Raabe et al., 2004b). This judgment is motivated by the common observation that substantial changes in recrystallization phenomena can be stimulated by rather small modifications in the metallurgical state (e.g. chemical purity, thermodynamic state, crystallographic texture, microstructure inhomogeneity, and microstructure inheritance from preceding process steps) or in the external boundary conditions (time, temperature fields, strain fields, and joint thermal and mechanical constraints) (McQueen and Jonas, 1975; Miodownik, 2002; Ferry, 2002). This sensitivity of recrystallization is due to the fact that most of the metallurgical mechanisms involved during texture formation in the course of recrystallization such as grain nucleation, grain-boundary mobility, or impurity drag effects are thermally activated. Typically, these mechanisms follow Arrhenius functions the arguments of which can strongly depend on some of the parameters listed above and interact with each other in a nonlinear fashion. Similarly, the microstructural state of the deformed material from which recrystallization proceeds is often not well known or not so well reproduced in models. The requirement to establish a better connection between the inherited deformation microstructure and the onset of recrystallization has been reflected in a number of investigations that aimed at using for instance crystal plasticity finite element simulation results as starting configurations for recrystallization simulations (Raabe and Becker, 2000; Bate, 1999; Roters et al., 2010; Zambaldi et al., 2007; Radhakrishnan et al., 2000; Bernacki et al., 2007; Bernacki and Coupez, 2011). Although various types of homogenization models of crystal deformation are nowadays capable of providing information about the average behavior of the material in the course of a thermomechanical process, it are often the details and inhomogeneities, i.e. the singularities in the deformed structure that strongly affect recrystallization. This means that even a good knowledge of average plasticity parameters does not generally solve the open questions pending in the field of recrystallization modeling (Raabe and Becker, 2000; Bate, 1999).

Moreover, in commercial metal-manufacturing processes typically encountered in physical metallurgy many of the influencing factors, be they of a metallurgical or of a processing nature, are usually neither exactly known nor sufficiently well defined to apply models that require a high degree of precision with regard to the input parameters.

These remarks underline that the selection of an appropriate recrystallization multiscale model for the prediction of crystallographic texture, microstructure, and properties for a given process must follow a clear concept as to what exactly is expected from such a model and what *cannot* be predicted by it in view of the points made above (Rollett, 1997). This applies in particular to cases where a model for the simulation of recrystallization textures is to be used in conjunction with real manufacturing processes.

The main challenge of using multiscale process models for recrystallization, therefore, lies in selecting the right model for a well-defined task, i.e. it must be agreed that microstructural property is to be simulated and what kind of properties should be subsequently calculated from these microstructure data. From that, it is obvious that no model exists that could satisfy all questions that may arise in the context of recrystallization textures (Humphreys, 1992a; Rollett, 1997; Mahin, 1980; Saetre, 1986). Also one has to clearly separate between the aim of predicting recrystallization textures and microstructures (Miodownik, 2002;

Sebald and Gottstein, 2002; Humphreys, 1992a; Raabe and Becker, 2000) on the one hand and the materials properties (functional or mechanical) on the other. While the first task may by pursued by formulating an appropriate recrystallization model within the limits addressed above, the second challenge falls into the wide realm of microstructure–property theory. This means that one should generally separate between the prediction of the microstructure and the prediction of some property from that particular microstructure. Typically through-process modelers are interested in the final materials properties in the first place rather than in the details of the microstructure of a recrystallized material. The modern attitude toward this discrepancy is the commonly accepted understanding that a decent description of materials properties requires the use of internal (i.e. of microstructurally motivated) parameters that can be coupled to suited microstructure–property laws. A typical example along that philosophy would be the grain-size prediction via a recrystallization model and the subsequent application of the Hall–Petch law for the estimation of the yield strength (Janssens et al., 2007; Crumbach et al., 2004).

This section addresses exclusively the first question, more precisely, only models for primary static recrystallization will be tackled placing particular attention on the prediction of microstructure and crystallographic texture.

23.9.2 Statistical Models for Predicting Recrystallization Textures

The analytical formulation of physically based statistical models with a simple mathematical structure and yet at the same time equipped with a solid metallurgical basis for fast applications in the area of process simulation remains an important challenge in materials science (Janssens et al., 2007; Crumbach et al., 2004). This applies in particular for statistical recrystallization models that pursue the aim of predicting crystallographic texture, certain microstructure parameters (e.g. grain size), and even certain mechanical properties during processing with a precision that is sufficiently robust for industrial applications.

In the past, various statistical variants of the original JMAK approaches were suggested for the prediction of recrystallization textures (Kolmogorov, 1937; Johnson and Mehl, 1939; Avrami, 1939, 1940).

These models typically combine JMAK-type kinetic evolution equations with the texture dependence of grain nucleation and the misorientation dependence of the motion of grain boundaries (Humphreys, 1992a; Rollett, 1997; Gottstein and Shvindlerman, 1999). Examples of such orientation-dependent JMAK approaches for crystallographic texture prediction are the Bunge transformation model (Bunge and Köhler, 1992) and the Gottstein kinetic model variants (Crumbach et al., 2006).

This section on statistical texture models in the field of recrystallization is essentially inspired by these two formulations, particularly by the microgrowth selection model of Sebald and Gottstein, which is consistently formulated on the basis of nucleation and crystal growth kinetics while the Bunge–Köhler model essentially uses crystallographic transformations of the orientation distribution functions of the deformed samples without considering kinetics (Bunge and Köhler, 1992).

In the Sebald–Gottstein model, the crystallographic texture of the deformed material is discretized in terms of a large set of discrete single orientations that approximate a given orientation distribution function of a plastically deformed specimen using typically cold-rolled sheet material.

Sebald and Gottstein investigated several nucleation mechanisms with respect to the orientation and misorientation distribution they create at the incipient stages of recrystallization. The information that was provided by the submodels for nucleation are the orientation-dependent density of nuclei within the deformed crystals with a given crystallographic orientation. This means that the nucleation submodels initiate the orientation and misorientation distributions of the nuclei for primary

recrystallization. The different types of nucleation processes investigated so far were random nucleation creating both, a random nucleus texture and a random misorientation distribution, nucleation at shear bands forming a random nucleus texture with a nonrandom misorientation distribution; and nucleation due to preexisting nuclei creating a nucleus texture similar to the deformation texture in conjunction with a narrow misorientation distribution.

The growth rate of the nuclei corresponds to their grain-boundary velocity, which is given by the product of the grain-boundary mobility and the driving force. The mobility of a grain boundary depends on the misorientation between the growing and the deformed grain. The model can distinguish three categories of grain boundaries, namely, small angle, high-angle, and special boundaries. Small-angle grain boundaries are assumed to be essentially immobile. In the case of aluminum, it is generally accepted that grain boundaries with near $40^\circ<111>$ misorientation may show particularly high mobilities so that such interfaces are treated as special boundaries (Ibe and Lücke, 1966, 1972; Ibe et al., 1970; Gottstein and Shvindlerman, 1999; Aust and Rutter, 1959, 1960; Molodov, 2001; Lücke and Stüwe, 1963; Gottstein et al., 1995; Shvindlerman et al., 1995, Shvindlerman and Gottstein, 1999). This is realized in the simulations of Gottstein and Sebald by assigning higher mobilities to such grain boundaries. The mobility of an average high-angle grain boundary is typically set to 20% of the maximum occurring mobility. The driving force for primary static recrystallization is the difference of the stored energy density between the deformed matrix and the nucleus, which in such models typically approximated in terms of the Taylor factor. Growth of the newly formed nuclei is assumed to be isotropic, but it ceases when the nuclei impinge. This means that a growing nucleus can only grow into the nonrecrystallized volume fraction. This portion of the material can be calculated according to the JMAK theory, which provides a relation between the increase in the recrystallized volume fraction for unconstrained growth (the so-called expanded volume fraction) and the true or constrained increase under consideration of grain impingement for a random spatial distribution.

When compared to the Potts Monte Carlo (Anderson et al., 1984; Srolovitz et al., 1984, 1985, 1986b, 1988; Glazier et al., 1990; Anderson and Rollett, 1990; Tavernier and Szpunar, 1991a, 1991b; Rollett et al., 1989b, 1989c, 1992; Peczak, 1995), cellular automaton (Raabe et al., 2004b; Hesselbarth and Göbel, 1991; Pezzee and Dunand, 1994; Sheldon and Dunand, 1996; Davies, 1995, 1997; Marx et al., 1997, 1998; Davies and Hong, 1999; Raabe, 1999, 2002, 2001; Janssens, 2003), or vertex-type front-tracking models (Humphreys, 1992b; Maurice and Humphries, 1998; Maurice, 2001; Weygand et al., 2001; Kinderlehrer et al., 2004, 2001), statistical JMAK-type approaches such as exemplarily presented here are more efficient for physically based recrystallization texture predictions in the field of materials processing owing to their semistatistical formulation. On the other hand, statistical models neglect important local features of the microstructures such as grain topology, grain neighborhood, and the local curvature of an interface. This can be a disadvantage when applying statistical models to heterogeneous microstructures.

23.9.3 Spatially Discrete Models for Simulating Recrystallization

23.9.3.1 Introduction

The design of time and space discretized recrystallization models for predicting texture and microstructure in the course of materials processing, which predict kinetics and energies in a local fashion are of interest for two reasons. First, from a fundamental point of view, it is desirable to understand better the dynamics and the topology of microstructures that arise from the interaction of large numbers of lattice defects that are characterized by a wide spectrum of intrinsic properties and interactions in spatially heterogeneous materials under complex engineering boundary conditions. For instance, in the

field of recrystallization (and grain growth), the influence of local grain-boundary characteristics (mobility, energy), local driving forces, and local crystallographic textures on the final microstructure is of particular interest (Rollett, 1997; Humphreys, 1997). An important point of interest in that context, however, is the question how local such a models should be in its spatial discretization in order to really provide microstructural input that cannot be equivalently provided by statistical methods. In the worst case, a problem in that field may be that spatially discrete recrystallization models may have the tendency to pretend a high degree of precision without actually providing it. In other words, even in highly discretized recrystallization models the physics always lies in the details of the constitutive description of the kinetics and thermodynamics of the deformation structure and of the interfaces involved. The mere fact that a model is formulated in a discrete fashion does not, as a rule, automatically render it a sophisticated model per se. Second, from a practical point of view, it makes sense to predict microstructure parameters such as the crystal size or the crystallographic texture, which determines the mechanical and physical properties of materials subjected to industrial processes on a sound phenomenological basis (Raabe, 1998).

In this section on spatially discrete models particular attention is laid on cellular automata (Raabe et al., 2004b; Hesselbarth and Göbel, 1991; Pezzee and Dunand, 1994; Sheldon and Dunand, 1996; Davies, 1995, 1997; Marx et al., 1997, 1998; Davies and Hong, 1999; Raabe, 1999, 2002, 2001; Janssens, 2003), Potts-type Monte Carlo multispin models (Anderson et al., 1984; Srolovitz et al., 1984, 1985, 1986b, 1988; Glazier et al., 1990; Anderson and Rollett, 1990; Tavernier and Szpunar, 1991a, 1991b; Rollett et al., 1989b, 1989c, 1992; Peczak, 1995), and vertex (front-tracking) models (Humphreys, 1992b; Maurice and Humphries, 1998; Maurice, 2001; Weygand et al., 2001; Kinderlehrer et al., 2004, 2001) because those three have been used in the past successfully for the simulation of recrystallization textures and microstructures. Related spatially discrete models of recrystallization phenomena such as the phase-field model as metallurgically motivated derivative of the Ginzburg–Landau kinetic theory also represent elegant ways to predict the evolution of topology during recrystallization but they are up to now less well-established for predicting recrystallization textures (Raabe, 1998).

23.9.3.2 Cellular Automaton Models of Recrystallization

Cellular automata are algorithms that describe the discrete spatial and temporal evolution of complex systems by applying local transformation rules to lattice cells that typically represent volume portions. The state of each lattice site is characterized in terms of a set of internal state variables. For recrystallization models these can be lattice defect quantities (stored energy), crystal orientation, or precipitation density. Each site assumes one out of a finite set of possible discrete states. The opening state of the automaton is defined by mapping the initial distribution of the values of the chosen state variables onto the lattice (Hesselbarth and Göbel, 1991; Pezzee and Dunand, 1994; Sheldon and Dunand, 1996; Davies, 1995, 1997; Marx et al., 1997, 1998; Davies and Hong, 1999; Raabe, 1999, 2002, 2001; Janssens, 2003).

The dynamical evolution of the automaton takes place through the application of deterministic or probabilistic transformation rules (switching rules) that act on the state of each lattice point. These rules determine the state of a lattice point as a function of its previous state and the state of the neighboring sites. The number, arrangement, and range of the neighbor sites used by the transformation rule for calculating a state switch determines the range of the interaction and the local shape of the areas that evolve. Cellular automata work in discrete time steps. After each time-interval, the values of the state variables are updated for all points in synchrony mapping the new (or unchanged) values assigned to them through the transformation rule. Owing to these features, cellular automata provide a discrete

method of simulating the evolution of complex dynamical systems that contain large numbers of similar components on the basis of their local interactions.

Cellular automata are—like all other continuum models that work above the discrete atomic scale—not intrinsically calibrated by a characteristic physical length or time scale. This means that a cellular automaton simulation of continuum systems requires the definition of elementary units and transformation rules that adequately reflect the kinetics at the level addressed. If some of the transformation rules refer to different real-time scales (e.g. recrystallization and recovery, bulk diffusion, and grain-boundary diffusion) it is essential to achieve a correct common scaling of the entire system. The requirement for an adjustment of time scaling among various rules is due to the fact that the transformation behavior of a cellular automaton is sometimes determined by noncoupled Boolean routines rather than by local solutions of coupled differential equations.

The following examples on the use of cellular automata for predicting recrystallization textures are designed as automata with a probabilistic transformation rule (Raabe, 1999). Independent variables are time and space. The latter is discretized into equally shaped cells each of which is characterized in terms of the mechanical driving force (stored deformation energy) and the crystal orientation (texture). The starting data of such automata are usually derived from experiment (for instance from a microtexture map) or from plasticity theory (for instance from crystal plasticity finite element simulations). The initial state is typically defined in terms of the distribution of the crystal orientation and of the driving force. Grains or subgrains are mapped as regions of identical crystal orientation, but the driving force may vary inside these areas.

The kinetics of the automaton gradually evolve from changes in the state of the cells (cell switches). They occur in accord with a switching rule (transformation rule) that determines the individual switching probability of each cell as a function of its previous state and the state of its neighbor cells. The switching rule is designed to map the phenomenology of primary static recrystallization. It reflects that the state of a nonrecrystallized cell belonging to a deformed grain may change due to the expansion of a recrystallizing neighbor grain that grows according to the local driving force and boundary mobility. If such an expanding grain sweeps a nonrecrystallized cell the stored dislocation energy of that cell drops to zero and a new orientation is assigned to it, namely that of the expanding neighbor grain. The mathematical formulation of the automaton used in this report can be found in (Raabe, 2002). It is derived from a probabilistic form of a linearized symmetric rate equation, which describes grain-boundary motion in terms of isotropic single-atom diffusion processes perpendicular through a homogeneous planar grain-boundary segment under the influence of a decrease in Gibbs energy. This means that the local progress in recrystallization can be formulated as a function of the local driving forces (stored deformation energy) and interface properties (grain-boundary mobility). The most intricate point in such simulations consists in identifying an appropriate phenomenological rule for nucleation events.

Figure 54 shows an example of a coupling of a cellular automaton with a crystal plasticity finite element model for predicting recrystallization textures in aluminum (Raabe and Becker, 2000). The major advantage of such an approach is that it considers the inherited material deformation heterogeneity as opposed to material homogeneity.

This type of coupling the two models, therefore, seems more appropriate when aiming at the simulation of textures formed during materials processing. Nucleation in this coupled simulation works above the subgrain scale, i.e. it does not explicitly describe cell walls and subgrain coarsening phenomena. Instead, it incorporates nucleation on a more phenomenological basis using the kinetic and thermodynamic instability criteria known from classical recrystallization theory. The kinetic instability criterion means that a successful nucleation process leads to the formation of a mobile high-

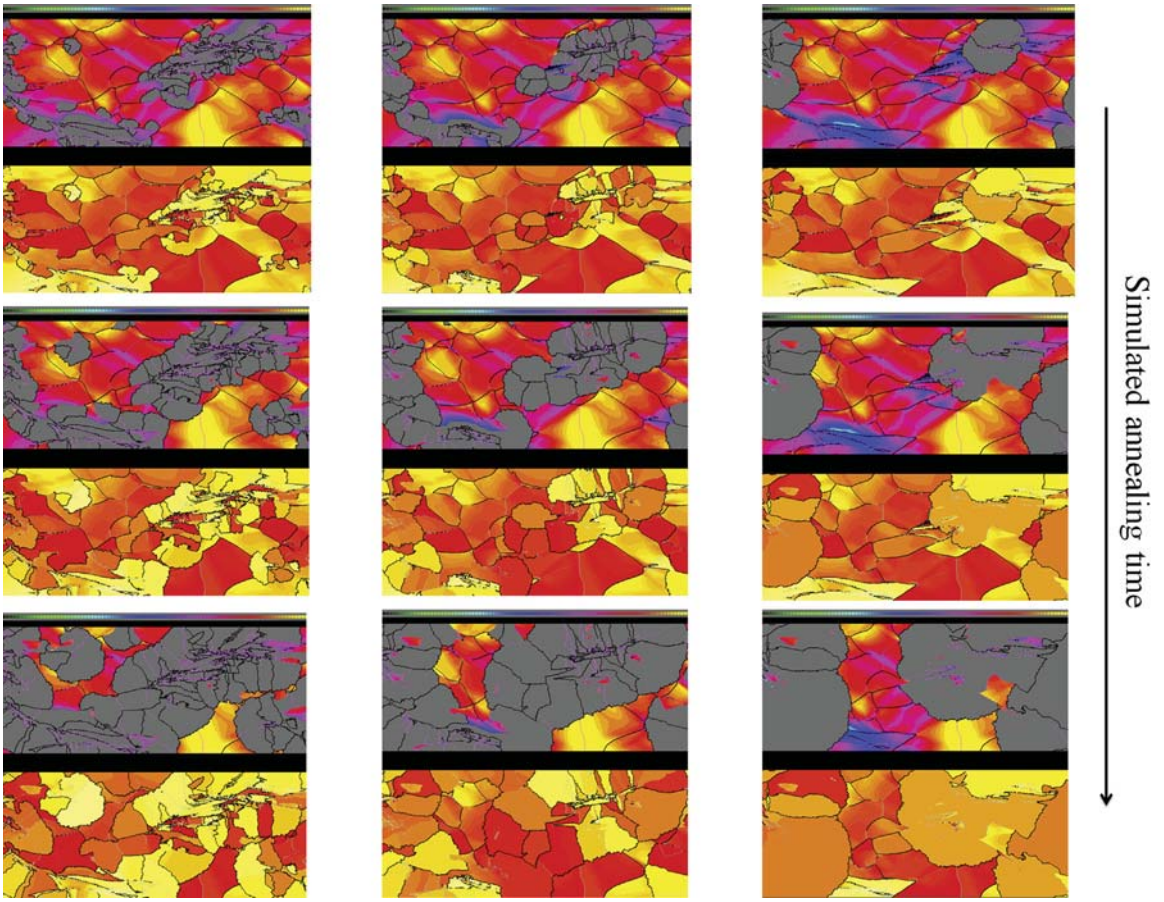

Figure 54 Series of subsequent stages of a 2D cellular automaton simulation of primary static recrystallization in a deformed aluminum polycrystal on the basis of crystal plasticity finite element data. The figure shows the change both in dislocation density (upper figures) and in microtexture (lower figures), as a function of the annealing time during isothermal recrystallization. The gray areas in the upper figures indicate a stored dislocation density of zero, i.e. these areas are recrystallized. The simulation parameters are: 800 K; thermodynamic instability criterion: site-saturated spontaneous nucleation in cells with at least 50% (left-hand series), 60% (middle series), or 70% (right-hand series) of the maximum occurring dislocation density (threshold value); kinetic instability criterion for further growth of such spontaneous nuclei: misorientation above 15°; activation energy of the grain-boundary mobility: 1.46 eV; preexponential factor of the grain-boundary mobility: $m_0 = 8.3.10 \pm 3$ m^3/(Ns); mesh size of the cellular automaton grid (scaling length): 61.9 μm per grid point (Raabe and Becker, 2000).

angle grain boundary that can sweep the surrounding deformed matrix. The thermodynamic instability criterion means that the stored energy changes across the newly formed high-angle grain boundary providing a net driving force pushing it forward into the deformed matter. Nucleation in this simulation is performed in accord with these two aspects, i.e. potential nucleation sites must fulfill both, the kinetic and the thermodynamic instability criterion. The used nucleation model does not create any new orientations. At the beginning of the simulation the thermodynamic criterion, i.e. the local value of

the dislocation density was first checked for all lattice points. If the dislocation density was larger than some critical value of its maximum value in the sample, the cell was spontaneously recrystallized without any orientation change, i.e. a dislocation density of zero was assigned to it and the original crystal orientation was preserved. In the next step, the conventional cellular growth algorithm was used, i.e. the kinetic conditions for nucleation were checked by calculating the misorientations among all spontaneously recrystallized cells (preserving their original crystal orientation) and their immediate neighborhood considering the first, second, and third neighbor shells. If any such pair of cells revealed a misorientation above 15°, the cell flip of the unrecrystallized cell was calculated according to its actual transformation probability. In case of a successful cell flip the orientation of the first recrystallized neighbor cell was assigned to the flipped cell.

23.9.3.3 Potts-type Monte Carlo Multispin Models of Recrystallization

The application of the Metropolis Monte Carlo method in microstructure simulation has gained momentum particularly through the extension of the Ising lattice model for modeling magnetic spin systems to the kinetic multistate Potts lattice model (Potts, 1952). The original Ising model is in the form of an $^1/_2$ spin lattice model where the internal energy of a magnetic system is calculated as the sum of pair-interaction energies between the continuum units that are attached to the nodes of a regular lattice. The Potts model deviates from the Ising model by generalizing the spin and by using a different Hamiltonian. It replaces the Boolean spin variable where only two states are admissible (spin up, spin down) by a generalized variable that can assume one out of a larger spectrum of discrete possible ground states, and accounts only for the interaction between *dissimilar* neighbors (Anderson et al., 1984; Srolovitz et al., 1984, 1985, 1986b, 1988; Glazier et al., 1990; Anderson and Rollett, 1990; Tavernier and Szpunar, 1991a, 1991b; Rollett et al., 1989b, 1989c, 1992; Peczak, 1995; Doherty et al., 1990; Miodownik et al., 1999). The introduction of such a spectrum of different possible spins enables one to represent domains discretely by regions of identical state (spin). For instance, in microstructure simulation such domains can be interpreted as areas of similarly oriented crystalline matter. Each of these spin orientation variables can be equipped with a set of characteristic state variable values quantifying the lattice energy, the dislocation density, the Taylor factor, or any other orientation-dependent constitutive quantity of interest. Lattice regions that consist of domains with identical spin or state are in such models translated as crystal grains. The values of the state variable enter the Hamiltonian of the Potts model. The most characteristic property of the energy operator when used for coarsening models is that it defines the interaction energy between nodes with like spins to be zero, and between nodes with unlike spins to be one. This rule makes it possible to identify interfaces and to quantify their energy as a function of the abutting domains.

According to Srolovitz et al. (Anderson et al., 1984; Srolovitz et al., 1984; Glazier et al., 1990; Anderson and Rollett, 1990; Glauber, 1963; Metropolis et al., 1953; Sahni et al., 1983; Hassold and Holm, 1993; Safran et al., 1983; Holm et al., 1998; Rollett et al., 1998) a typical energy operator for Potts-type grain growth and recrystallization simulations can be written

$$E = E^{\mathrm{GG}} + E^{\mathrm{El}} = \sum_{i=1}^{N} \left(\frac{J}{2} \sum_{j=1}^{nnn} \left(1 - \delta_{S_i S_j}\right) + H^{\mathrm{El}} f(Q_u - S_i) \right)$$

where E is a scaled energy proportional to the total excess energy associated with the presence of lattice defects, E^{GG} a scaled energy proportional to the excess energy associated with grain-boundary energy, E^{El} a scaled energy proportional to the excess energy associated with elastically stored energy, N the

number of discrete lattice sites, *nnn* the geometrically weighted number of neighbor sites in the first, second, and third neighbor shell, S the orientational state variable, δ_{SiSj} the Kronecker symbol, which assumes a value of 1 if $S_i = S_j$ and a value of 0 if $S_i \neq S_j$, J an energy proportional to the grain-boundary energy, and H^{El} an energy proportional to the stored elastic energy. J and H^{El} have a positive sign. Their respective proportionality factors relating them to realistic energies scale the simulation with respect to temperature. The factor $^1/_2$ in eqn (1) corrects that each interface segment is counted twice. The function $f(Q_u - S_i)$ describes whether a site is recrystallized or not. The variable Q_u is the number of distinct crystal orientations of unrecrystallized grains. The recrystallized sites are given orientation variables larger than Q_u. The step function $f(Q_u - S_i)$ assumes a value of 1 for arguments equal to or larger than 0 ($Q_u \geq S_i > 0$) and a value of 0 if the site is recrystallized, i.e. for arguments below 0 ($S_i > Q_u$).

The kinetic evolution of the Potts model, which occurs in the form of domain growth, is usually simulated using Metropolis or Glauber dynamics (Glauber, 1963; Metropolis et al., 1953), i.e. it proceeds by randomly selecting lattice sites, switching their orientational state randomly to a new one, and weighting the resulting energy change in terms of Metropolis Monte Carlo sampling. This means that an orientation flip is generally accepted if it leads to a state of lower or equal energy and is accepted with thermal probability if it leads to an energy increase. The switching probability W can be

$$W = \begin{cases} \exp(-\Delta E/k_B T) & \text{if} \quad \Delta E > 0 \\ 1 & \text{if} \quad \Delta E \leq 0 \end{cases}.$$

The evaluation of the thermal fluctuation, which leads to an energy increase, is conducted by generating a pseudorandom number between 0 and 1 and comparing it to the actual switching probability $\exp(-\Delta E/k_B T)$. If the random number is equal or lower than the thermal probability the switch is accepted (Anderson et al., 1984; Srolovitz et al., 1984, 1985, 1986b, 1988, Glazier et al., 1990; Anderson and Rollett, 1990; Tavernier and Szpunar, 1991a, 1991b; Rollett et al., 1989b, 1989c, 1992; Peczak, 1995). If it is larger the switch is rejected. If the new configuration is rejected, one counts the original position as a new one and repeats the process by switching another site. The microstructural evolution of the system is reflected by the development of the domain size and shape.

The Potts model is very versatile for describing coarsening phenomena. It takes a quasimicroscopic metallurgical view of grain growth or ripening, where the crystal interior is composed of lattice points (e.g. atom clusters) with identical energy (e.g. orientation) and the grain boundaries are the interfaces between different types of such domains (Holm et al., 2001; Miodownik et al., 2000). As in a real ripening scenario, interface curvature leads to increased wall energy on the convex side and thus to wall migration entailing local shrinkage. The discrete simulation steps in the Potts model, by which the system proceeds toward thermodynamic equilibrium, are typically calculated by randomly switching lattice sites and weighting the resulting interfacial energy changes in terms of Metropolis Monte Carlo sampling (Anderson et al., 1984; Srolovitz et al., 1984, 1985, 1986b, 1988; Glazier et al., 1990; Anderson and Rollett, 1990; Tavernier and Szpunar, 1991a, 1991b; Rollett et al., 1989b, 1989c, 1992; Peczak, 1995).

23.9.3.4 Vertex Models of Recrystallization

Vertex and related front tracking simulations are another alternative for engineering process models with respect to recrystallization phenomena (Humphreys, 1992b; Maurice and Humphries, 1998;

Maurice, 2001; Weygand et al., 2001; Kinderlehrer et al., 2004, 2001). Their use is currently less common when compared to the widespread application of Monte Carlo and cellular automaton models owing to their geometrical complexity and the required small integration time steps. Despite these differences to lattice-based recrystallization models they have an enormous potential for predicting interface dynamics at small scales also in the context of process simulations (Raabe et al., 2004b; Humphreys, 1997).

Topological network and vertex models idealize solid materials or soap-like structures as homogeneous continua that contain interconnected boundary segments that meet at vertices, i.e. boundary junctions (Humphreys, 1997; Humphreys, 1992b; Maurice and Humphries, 1998; Maurice, 2001; Weygand et al., 2001; Kinderlehrer et al., 2004, 2001). Depending on whether the system dynamics lies in the motion of the junctions or of the boundary segments, they are sometimes also referred to as boundary dynamics or, more generalized, as front-tracking models. The grain boundaries appear as lines or line segments in 2D and as planes or planar segments in 3D simulations. The dynamics of these coupled interfaces or interface portions and of the vertices determine the evolution of the entire network.

The dynamical equations of the boundary and node (vertex) motion can be described in terms of a damped Newtonian equation of motion that contains a large frictional portion or, mathematically equivalent, in terms of a linearized first-order rate equation. Using the frictional form of the classical equation of motion with a strong damping term results in a steady-state motion where the velocity of the defect depends only on the local force but not on its previous velocity. The overdamped steady-state description is similar to choosing a linearized rate equation, where the defect velocity is described in terms of a temperature-dependent mobility term and the local driving pressure.

The calculation of the local forces in most vertex models is based on equilibrating the line energies of subgrain walls and high-angle grain boundaries at the interface junctions according to Herring's equation. The enforcement of the local mechanical equilibrium at these nodes is for obvious topological reasons usually only possible by allowing the abutting interfaces to curve.

These curvatures in turn act through their capillary force, which is directed toward the center of curvature, on the junctions. In sum, this may lead to their displacement. In order to avoid the artificial enforcement of a constant boundary curvature between two neighboring nodes, the interfaces are usually decomposed into sequences of piecewise straight boundary segments.

Most vertex and network models use switching rules that describe the topological recombination of approaching vertices when such neighboring nodes are closer than some critical spontaneous recombination spacing. This is an analogy to the use of phenomenological annihilation and lock-formation rules that appear in dislocation dynamics. As in all continuum models, the use of such empirical recombination laws replaces a more exact atomistic treatment.

It is worth noting in this context that the recombination rules, particularly the various values for the critical recombination spacing of specific configurations, can affect the topological results of a simulation. Depending on the underlying constitutive continuum description, vertex simulations can consider crystal orientation and, hence, misorientations across the boundaries, interface mobility, and the difference in elastic energy between adjacent grains. Due to the stereological complexity of grain boundary arrays and the large number of degrees of freedom encountered in such approaches, most network simulations are currently confined to the 2D regime. Topological boundary dynamics models are different from kinetic cellular automaton or Potts Monte Carlo models in that they are not based on minimizing the total energy but directly calculate the motion of the lattice defects, usually on the basis of capillary and elastic forces.

References

Adams, B.L., Wright, S.I., Kunze, K., 1993. Metall. Mater. Trans. 24A, 819.

Alterthum, H., 1922. Zur Theorie der Rekristallisation. Z. Metallkd. 14, 417–424.

Anderson, M.P., Rollett, A.D., 1990. Simulation and Theory of Evolving Microstructures. The Minerals, Metals and Materials Society. TMS Publication, Warrendale, PA.

Anderson, M.P., Srolovitz, D.J., Grest, G.S., Sahni, P.S., 1984. Acta Metall. 32, 783.

Ashby, M.F., Harper, J., Lewis, J., 1969. The interaction of crystal boundaries with second-phase particles. Trans. Metall. Soc. AIME 245 (8), 413–420.

Aust, K.T., Rutter, J.W., 1959. Grain boundary migration in high-purity lead and dilute lead–tin alloys. Trans. Metall. Soc. AIME 215 (1), 119–127.

Aust, K.T., Rutter, J.W., 1960. Kinetics of grain boundary migration in high-purity lead containing very small additions of silver and of gold. Trans. Metall. Soc. AIME 218 (4), 682–688.

Avrami, M., 1939. Kinetics of phase change I, general theory. J. Chem. Phys. 7 (12), 1103–1112.

Avrami, M., 1940. Kinetics of phase change. II. Transformation time relations for random distribution of nuclei. J. Chem. Phys. 8, 212–224.

Babcock, S.E., Balluffi, R.W., 1989. Acta Metall. 37, 2357–2367.

Bailey, J.E., Hirsch, P.B., 1962. The recrystallization process in some polycrystalline metals. Proc. R. Soc. London 267 (1328), 11–30.

Bailey, J.E., 1960. Electron microscope observations on the annealing processes occurring in cold worked silver. Philos. Mag. 5 (53), 485–497.

Bailey, J.E., 1963. In: Thomas, G., Washburn, J. (Eds.), Electron Microscope Observations on Recovery and Recrystallization Processes in Cold Worked Metals. Electron Microscopy and Strength of Crystals. Interscience, New York, pp. 535–564.

Bale, H.A., Hanan, J.C., Tamura, N., 2005. Average and grain specific strain of a composite under stress using polychromatic microbeam X-rays. Adv. X-Ray Anal., 49.

Bate, P., 1999. Modelling deformation microstructure with the crystal plasticity finite-element method. Philos. Trans. R. Soc., A 357, 1589–1601.

Beck, P., Hu, H., 1966. ASM Seminar on Recrystallization. Grain Growth and Texture, Met.Park, Ohio, USA.

Beck, P.A., Sperry, P.R., 1950. J. Appl. Phys. 21, 150.

Beck, P.A., Sperry, P.R., Hu, H., 1950. The orientation dependence of the rate of boundary migration. J. Appl. Phys. 21, 420–425.

Beck, P.A., 1949. The formation of recrystallization nuclei. J. Appl. Phys. 20 (6), 633–634.

Berger, A., Wilbrandt, P.-J., Ernst, F., Klement, U., Haasen, P., 1988. On the generation of new orientations during recrystallization: recent results on the recrystallization of tensile-deformed fcc single crystals. Prog. Mater. Sci. 32, 1–95.

Bernacki, M., Coupez, R.L.T., 2011. Level set framework for the finite-element modelling of recrystallization and grain growth in polycrystalline materials. Scr. Mater. 64, 525–528.

Bernacki, M., Chastel, Y., Digonnet, H., Resk, H., Coupez, T., Logé, R., 2007. Development of numerical tools for the multiscale modelling of the recrystallization in metals, based on a digital material framework. Comput. Methods Catal. Mater. Sci. 7, 142–149.

Bernacki, M., Chastel, Y., Coupez, T., Logé, R.E., 2008. Level set framework for the numerical modelling of primary recrystallization in polycrystalline materials. Scr. Mater. 58, 1129–1132.

Bernacki, M., Resk, H., Coupez, T., Logé, R.E., 2009. Finite element model of primary recrystallization in polycrystalline aggregates using a level set framework. Modell. Simul. Mater. Sci. Eng. 17, 1–22.

Bhatia, M.L., Cahn, R.W., 1978. Proc. R. Soc. London, Ser. A 302, 341.

Blum, W., Schlögl, C., Meier, M., 1995. Subgrain formation and subgrain boundary migration in Al–5Mg during high temperature deformation in the range of class – a behavior in comparison with pure aluminium. Z. Metallkd. 86 (9), 631–637.

Bunge, H.-J., Esling, C., 1982. Quantitative Texture Analysis. DGM, Oberursel.

Bunge, H.-J., Esling, C., 1991. Advances and Applications of Quantitative Texture Analysis. DGM, Oberursel.

Bunge, H.J., Köhler, U., 1992. Model calculations of primary recrystallization textures. Scr. Metall. Mater. 27, 1539–1543.

Bunge, H.-J., 1969. Mathematische Methoden der Texturanalyse. Akademie Verlag, Berlin.

Bunge, H.-J., 1982. Texture Analysis in Materials Science. Butterworths, London. (Reprint: Cuvillier Verlag, Göttingen 1993.).

Bunge, H.-J., 1986. Experimental Techniques of Texture Analysis. DGM, Oberursel.

Bunge, H.-J., 1987. Theoretical Methods of Texture Analysis. DGM, Oberursel.

Burgers, W.G., Louwerse, P.C., 1931. Über den Zusammenhang zwischen Deformationsvorgang und Rekristallisationstextur bei Aluminium. Z. Phys. 67, 605–678.

Burgers, W.G., 1941. Rekristallisation, verformter Zustand und Erholung. Akademischer Verlagsgesellschaft, Leipzig.

Burke, J.E., Turnbull, D., 1952. Recrystallization and grain growth. Prog. Met. Phys. 3, 220–292. (London: Pergamon Press).

Burwell, J.T., 1940. Trans. Metall. Soc. AIME 140, 353.

Cahn, R.W., 1950. A new theory of recrystallization nuclei. Proc. Phys. Soc. London, Sect. A 63 (364), 323–336.

Cahn, J.W., 1962. Acta Metall. 10, 789.

Cahn, R.W. (Ed.), 1965. Physical Metallurgy. North-Holland Publishing Co., Amsterdam. Also 2nd, 3rd and 4th editions.

Cahn, I.R.W., 1966. In: Margohn, H. (Ed.), In Recovery, Recrystallization and Grain Growth. ASM, Metals Park, OH, pp. 99.
Calcagnotto, M., Ponge, D., Raabe, D., 2010. Mater. Sci. Eng., A 527, 2738–2746.
Carel, R., Thompson, C., Frost, H., 1996. Acta Mater. 44, 2419–2494.
Carpenter, H.C.H., Elam, C.F., 1920. Crystal growth and recrystallization in metals. J. Inst. Met. 24, 83–131.
Chawla, N., Ganesh, V.V., Wunsch, B., 2004. Three-dimensional (3D) microstructure visualization and finite element modeling of the mechanical behavior of SiC particle reinforced aluminum composites. Scr. Mater. 51, 161–165.
Chen, N., Zaefferer, S., Lahn, L., Günther, K., Raabe, D., 2002. In: Lee, S. (Ed.), Proceedings of the 13th International Conference on Textures of Materials (ICOTOM 13). Seoul, South Korea, pp. 949.
Choi, S.-H., 2003. Simulation of stored energy and orientation gradients in cold-rolled interstitial free steels. Acta Mater. 51, 1775–1788.
Christian, J.W., 1965. The theory of transformations in metals and alloys. In: Raynor, G.V. (Ed.), 1965. International Series of Monographs in Metal Physics and Physical Metallurgy, vol. 7. Pergamon Press, London, pp. 710–742.
Chung, J.-S., Ice, G.E., 1999. Automated indexing for texture and strain measurement with broad-band-pass X-ray microbeams. J. Appl. Phys. 86, 5249–5255.
Clarebrough, L.M., Haregraves, M.E., West, G.W., 1955. The release of energy during annealing of deformed metals. In: Proceedings of the Royal Society, A, vol. 232.
Cotterill, P., Mould, P.R., 1976. Recrystallization and Grain Growth in Metals. Surrey University, London. p. 85.
Crumbach, M., Goerdeler, M., Gottstein, G., Neumann, L., Aretz, H., Kopp, R., 2004. Through-process texture modelling of aluminium alloys. Modell. Simul. Mater. Sci. Eng. 12. S1.
Crumbach, M., Goerdeler, M., Gottstein, G., 2006. Modelling of recrystallisation textures in aluminium alloys: I. Model set-up and integration. Acta Mater. 54 (12), 3275–3289.
Czochralski, J., 1927. Geschichtlicher Beitrag zur Frage der Rekristallisation. Z. Metallkd. 19, 316–320.
Davies, C.H.J., Hong, L., 1999. Cellular automaton simulation of static recrystallization in cold-rolled AA1050. Scr. Mater. 40, 1145–1152.
Davies, C.H.J., 1995. The effect of neighbourhood on the kinetics of a cellular automaton recrystallisation model. Scr. Metall. Mater. 33, 1139–1154.
Davies, C.H.J., 1997. Growth of nuclei in a cellular automaton simulation of recrystallisation. Scr. Mater. 36, 35–46.
De Siqueira, R.P., Sandim, H.R.Z., Raabe, D., 2013. Particle stimulated nucleation in coarse-grained ferritic stainless steel. Metall. Mater. Trans. A 44A, 469–478.
Dillamore, I.L., Katoh, H., 1974. Met. Sci. 8, 73.
Dillamore, I.L., Smith, C.J.E., Watson, T.W., 1967. Met. Sci. J. 1, 49.
Dillamore, I.L., Roberts, J.G., Bush, A.C., 1979. Met. Sci. 13, 73.
Doherty, R.D., Baumann, S.F., 1993. In: Morris, J.G., et al. (Eds.), Aluminum Alloys for Packaging. TMS, Warrendale, PA, pp. 369.
Doherty, R.D., Cahn, R.W., 1972. Nucleation of new grains in recrystallization of cold worked metals. J. Less Common Met. 28 (2), 279–296.
Doherty, R.D., Martin, J.W., 1962–1963. The effect of a dispersed second phase on the recrystallization of aluminium–copper alloys. J. Inst. Met. 91, 332–338.
Doherty, R.D., Szpunar, J.A., 1984a. Kinetics of subgrain coalescence-a reconsideration of the theory. Acta Metall. 32 (10), 1789–1798.
Doherty, R.D., Szpunar, J.A., 1984b. Acta Metall. 32, 1789.
Doherty, R.D., Gottstein, G., Hirsch, J.R., Hutchinson, W.B., Lucke, K., Nes, E., Wilbrandt, P.J., 1988. In: Kallend, J.S., Gottstein, G. (Eds.), ICOTOM 8. TMS, Warrendale, PA, pp. 563.
Doherty, R.D., Li, K., Anderson, M.P., Rollett, A.D., Srolovitz, D.J., 1990. Proceedings of the International Conference on Recrystallization in Metallic Materials, Recystallization. In: Chandra, T. (Ed.), The Minerals, Metals and Materials Society. TMS Publication, Warrendale, PA, pp. 129.
Doherty, R.D., Kashyap, K., Panchanadeeswaran, S., 1993. Acta Metall. Mater. 41, 3029.
Doherty, R.D., Hughes, D.A., Humphreys, F.J., Jonas, J.J., Juul Jensen, D., Kassner, M.E., King, W.E., McNelley, T.R., McQueen, H.J., Rollett, A.D., 1997. Current issues in recrystallization: a review. Mater. Sci. Eng., A 238, 219–274.
Doherty, R.D., 1985. Scr. Metall. 19, 927.
Doherty, R.D., 2005. Primary recrystallization. In: Cahn, R.W., et al. (Eds.), Encyclopedia of Materials: Science and Technology. Elsevier, pp. 7847–7850.
Dorner, D., Zaefferer, S., -Lahn, L., Raabe, D., 2006. Overview of microstructure and microtexture development in grain-oriented silicon steel. J. Magn. Magn. Mater. 304, 183–186.
Dorner, D., Zaefferer, S., Raabe, D., 2007. Retention of the Goss orientation between microbands during cold rolling of an Fe3%Si single crystal. Acta Mater. 55, 2519–2530.
Drube, B., Stüwe, H.P., 1967. Z. Metallkd. 58, 799–804.
Duckham, A., Engler, O., Knutsen, R.D., June 28, 2002. Moderation of the recrystallization texture by nucleation at copper-type shear bands in Al–1Mg. Acta Mater. 50 (11), 2881–2893.
Duggan, B.J., Chung, C.Y., 1994. Mater. Sci. Forum 113–115, 1765.

Duggan, B.J., Hatherley, M., Hutchinson, W.B., Wakefield, P.T., 1978. Met. Sci. 12, 343.
Duggan, B.J., Lucke, K., Kohlhoff, G.D., Lee, C.S., 1993. Acta Metall. Mater. 41, 1921.
Eisenlohr, A., Gutierrez-Urrutia, I., Raabe, D., May 2012. Adiabatic temperature increase associated with deformation twinning and dislocation plasticity. Acta Mater. 60 (9), 3994–4004.
Engler, O., Vatne, H.E., 1998. Modeling the recrystallization textures of aluminum alloys after hot deformation. JOM 50, 23–27.
Engler, O., Hirsch, J., Lücke, K., 1989. Acta Metall. 37, 2743.
Engler, O., Vatne, H.E., Nes, E., 1996. The roles of oriented nucleation and oriented growth on recrystallization textures in commercial purity aluminium. Mater. Sci. Eng., A 205, 187–198.
Engler, O., 1997. Influence of particle stimulated nucleation on the recrystallization textures in cold deformed Al-alloys Part II—Modeling of recrystallization textures. Scr. Mater. 37, 1675–1683.
Ewing, J.A., Rosenhain, W., 1899. The crystalline structure of metals. Proc. R. Soc. 65, 85–90.
Ewing, J.A., Rosenhain, W., 1900a. The crystalline structure of metals. Philos. Trans. R. Soc., A 193, 353–372.
Ewing, J.A., Rosenhain, W., 1900b. The crystalline structure of metals. Philos. Trans. R. Soc., A 195, 279–301.
Faivre, P., Doherty, R.D., 1979. Nucleation of recrystallization in compressed aluminium – studies by electron microscopy and Kikuchi diffraction. J. Mater. Sci. 14 (4), 897–919.
Ferry, M., Humphreys, F.J., 1996. Discontinuous subgrain growth in deformed and annealed {110} (001) aluminium single crystals. Acta Mater. 44, 1293–1308.
Ferry, M., 2002. Mechanism of discontinuous subgrain growth in as-deformed aluminum single crystals. Mater. Sci. Forum 408–412, 979–984.
Fritzmeier, L., Luton, M.J., McQueen, H.J., 1979. Strength of Metals and Alloys. In: ICSMA 5, vol. 1. Pergamon Press, Frankfurt. pp. 95.
Fujita, N., Ohmura, K., Kikuchi, M., Suzuki, T., Funaki, S., Hiroshige, I., 1996. Scr. Metall. Mater. 35, 705–710.
Furtkamp, M., Gottstein, G., Molodov, D.A., Semenov, V.N., Shvindlerman, L.S., 1998. Grain boundary migration in Fe3.5%Si bicrystals with <001> tilt boundaries. Acta Mater. 46, 4103–4110.
Furu, T., Marthinsen, K., Nes, E., 1993. Mater. Sci. Forum 113–115, 41.
Gifkins, R.C., Coe, H.C., 1951. Metallurgia 43, 47.
Glauber, R.J., 1963. J. Math. Phys. 4, 294.
Glazier, J.A., Anderson, M.P., Grest, G.S., 1990. Philos. Mag. B 62, 615.
Godara, A., Raabe, D., Van Puyvelde, P., Moldenaers, P., 2006. Polym. Test. 25, 460–469.
Goss, N.P., 1935. Trans. Am. Soc. Met. 23, 511.
Gottstein, G., Shvindlerman, L.S., 1999. Grain Boundary Migration in Metals – Thermodynamics, Kinetics, Applications. CRC Press, Boca Raton.
Gottstein, G., Molodov, D.A., Czubayko, U., Shvindlerman, L.S., 1995. J. Phys. IV, colloque C3, supplément au Journal de Physique III 5, 9.
Gottstein, G., Shvindlerman, L.S., Molodov, D.A., Czubayko, U., 1997. In: Duxbury, P.M., Pence, T.J. (Eds.), Dynamics of Crystal Surfaces and Interfaces. Plenum Press, New York, pp. 109.
Gottstein, G., Molodov, D.A., Shvindlerman, L.S., 1998. Interface Sci. 6, 7.
Grewen, J., Huber, J., 1978. In: Haessner, F. (Ed.), Recrystallization of Metallic Materials, second ed. Dr. Riederer-Verlag, Stuttgart, pp. 111.
Gutierrez-Urrutia, I., Raabe, D., 2011. Dislocation and twin substructure evolution during strain hardening of an Fe-22 wt.% Mn-0.6 wt.% C TWIP steel observed by electron channeling contrast imaging. Acta Mater. 59, 6449–6462.
Gutierrez-Urrutia, I., Zaefferer, S., Raabe, D., 2009. Electron channeling contrast imaging of twins and dislocations in twinning-induced plasticity steels under controlled diffraction conditions in a scanning electron microscope. Scr. Mater. 61, 737–740.
Gutierrez-Urrutia, I., Zaefferer, S., Raabe, D., 2010. The effect of grain size and grain orientation on deformation twinning in a Fe-22 wt.% Mn-0.6 wt.% C TWIP steel. Mater. Sci. Eng., A 527, 3552–3560.
Gutierrez-Urrutia, I., Zaefferer, S., Raabe, D., 2013. Coupling of Electron Channeling with EBSD: toward the quantitative characterization of deformation structures in the SEM. JOM 65, 1229–1236.
Haessner, F. (Ed.), 1978. Recrystallization. Dr. Riederer Verlag, Stuttgart.
Hallberg, H., 2011. Metals 1, 16–48.
Hansen, N., Bay, B., 1981. Acta Metall. 29, 65.
Hartig, Ch., Feller-Kniepmeier, M., May 1985. Electron microscopic investigation of the microstructure of rolled and annealed Ni-single crystals. Acta Metall. 33 (5), 743–752.
Harun, A., Holm, E.A., Clode, M.P., Miodownik, M.A., Jul 2006. On computer simulation methods to model Zener pinning. Acta Mater. 54 (12), 3261–3273.
Hashimoto, S., Baudelet, B., 1989. Scr. Metall. 23, 1855.
Hassold, G.N., Holm, E.H., 1993. Comput. Phys. 7, 7.
Hayakawa, Y., Szpunar, J.A., 1997. Acta Mater. 45, 1285.
Heidenreich, R.D., 1949. Electron microscope and diffraction study of metal crystal textures by means of thin sections. J. Appl. Phys. 20 (10), 993–1010.

Heinrich, M., Haider, F., 1996. Primary recrystallization in slightly tensile deformed aluminium single crystals. Philos. Mag. 74, 1047–1057.
Hesselbarth, H.W., Göbel, I.R., 1991. Simulation of recrystallization by cellular automata. Acta Metall. 39, 2135–2144.
Hillert, M., 1965. Acta Metall. 13, 227.
Hillert, M., 1988. Acta Metall. 36, 3177.
Himmel, L. (Ed.), 1962. Recovery and Recrystallization of Metals. AIME. published by Interscience Publishers (1963).
Hjelen, J., Orsund, R., Nes, E., 1991. Acta Metall. Mater. 39, 1377.
Holm, E.A., Battaile, C.C., 2001. The computer simulation of microstructural evolution. JOM 9, 20.
Holm, E.A., Zacharopoulos, N., Srolovitz, D.J., 1998. Acta Mater. 46, 953.
Holm, E.A., Miodownik, M.A., Rollett, A.D., 2003. On abnormal subgrain growth and the origin of recrystallization nuclei. Acta Mater. 51, 2701–2716.
Holm, E.A., Hassold, G.N., Miodownik, M.A., Sep 3, 2001. On misorientation distribution evolution during anisotropic grain growth. Acta Mater. 49 (15), 2981–2991.
Hölscher, M., Raabe, D., Lücke, K., 1991. Rolling and recrystallization textures of bcc steels. Steel Res. 62, 567–575.
Hu, H., Rath, B.B., Vandermeer, R.A., 1990. An historical perspective and overview of the annealing studies of cold worked metals. In: Chandra, T. (Ed.), Recrystallization '90. TMS, Warrendale, pp. 3–16.
Hu, Y., Miodownik, M.A., Randle, V., Jun 2008. Experimental and computer model investigations of microtexture evolution of non-oriented silicon steel. Mater. Sci. Technol. 24 (6), 705–710.
Hu, H., 1962. Direct observations on the annealing of Si–Fe crystals in the electron microscope. Trans. Metall. Soc. AIME 224 (1), 75–84.
Hu, H., 1963. Recrystallization by subgrain coalescence. In: Thomas, G., Washburn, J. (Eds.), Electron Microscopy and Strength of Crystals. Interscience, New York, pp. 564–573.
Huang, Y., Humphreys, F.J., Ferry, M., 2000. The annealing behavior of deformed cube-oriented aluminium single crystals. Acta Mater. 48, 2543–2556.
Huh, M.-Y., Lee, J.-H., Park, S.H., Engler, O., Raabe, D., 2005. Effect of through-thickness macro and micro-texture gradients on ridging of 17%Cr ferritic stainless steel sheet. Steel Res. 76, 797–806.
Humphreys, F.J., Ardakani, M.G., 1994. Acta Metall. 42, 749.
Humphreys, F.J., Chan, H.M., 1996. Discontinuous and continuous annealing phenomena in aluminium–nickel alloy. Mater. Sci. Technol. 12 (2), 143–148.
Humphreys, F.J., Ferry, M., 1997. Applications of electron backscattered diffraction to studies of annealing of deformed metals. Mater. Sci. Technol. 13 (1), 85–90.
Humphreys, F.J., Hatherly, M., 1995. Recrystallization and Related Annealing Phenomena, vol. 8. Pergamon Press, Oxford, 235.
Humphreys, F.J., Hatherly, M., 2004. Recrystallisation and Related Annealing Phenomena. Elsevier.
Humphreys, F.J., Kalu, P.N., 1987. Acta Metall. 35, 2815.
Humphreys, F.J., 1977a. Acta Metall. 25, 1323.
Humphreys, F.J., 1977b. Acta Metall. 25, 1323–1344.
Humphreys, F.J., 1979. Acta Metall. 27, 1801.
Humphreys, F.J., 1992a. Modelling mechanisms and microstructures of recrystallisation. Mater. Sci. Technol. 8, 135–143.
Humphreys, F.J., 1992b. A network model for recovery and recrystallisation. Scr. Metall. 27, 1557–1562.
Humphreys, F.J., 1997. A unified theory of recovery, recrystallisation and grain growth, based on the stability and growth of cellular microstructures-i the basic model. Acta Meter. 45, 4231–4240.
Hurley, P.J., Humphreys, F.J., 2003. Acta Mater. 51, 3779–3793.
Hutchinson, W.B., Ryde, L., 1995. Microstructural and crystallographic aspects of recrystallization. In: Hansen, N., et al. (Eds.), Proc. 16th Riso Symposium. Riso National Lab, Roskilde, Denmark, pp. 105.
Hutchinson, W.B., Oscarsson, A., Karlsson, 1989. Mater. Sci. Technol. 5, 1118.
Hutchinson, W.B., 1989. Acta Metall. 37, 1047.
Hutchinson, B., 1999. Philos. Trans. R. Soc., A 357, 1471–1485.
Ibe, G., Lücke, K., 1966. Recrystallization, Grain Growth and Textures. American Society for Metals, Metals Park, Ohio. pp. 434.
Ibe, G., Lücke, K., 1972. Texture 1, 87.
Ibe, G., Dietz, W., Fraker, A.-C., Liicke, K., 1970. Z. Metallkd. 6, 498.
Inagaki, H., 1987. Z. Metallkd. 78, 630–638.
Inokuti, Y., Doherty, R.D., 1977. Texture 2, 143.
Inokuti, Y., Doherty, R.D., 1978. Acta Metall. 26, 61.
Inokuti, Maeda, C., Itoh, Y., Shimanaka, H., 1981. ICOTOM6. Tokyo 948.
Jägle, E.A., Mittemeijer, E.J., April 2012. Metall. Mater. Trans. 43A, 1117.
Janssens, K.G.F., Raabe, D., Kozeschnik, E., Miodownik, M.A., Nestler, B., 2007. Computational Materials Engineering. Elsevier, London.

Janssens, K.G.F., 2003. Random grid, three-dimensional, space-time coupled cellular automata for the simulation of recrystallization and grain growth. Modell. Simul. Mater. Sci. Eng. 11, 157.
Jia, J., Raabe, D., 2006. Eur. Polym. J. 42, 1755–1766.
Jia, N., Roters, F., Eisenlohr, P., Kords, C., Raabe, D., 2012a. Acta Mater. 60, 1099–1115.
Jia, N., Eisenlohr, P., Roters, F., Raabe, D., Zhao, X., 2012b. Orientation dependence of shear banding in face-centered-cubic single crystals. Acta Mater. 60, 3415–3434.
Johnson, W.A., Mehl, R.F., 1939. Reaction kinetics in the process of nucleation and growth. Trans. Metall. Soc. AIME 135, 416–458.
Jonas, J.J., Sellars, C.M., Tegart, W.J.McG., 1969. Metall. Rev. 14, 1.
Jones, A.R., Ralph, B., Hansen, N., 1979. Nucleation of recrystallization in aluminium containing dispersions of alumina. Met. Sci. 13, 149–154.
Juntunen, P., Raabe, D., Karjalainen, P., Kopio, T., Bolle, G., 2001. Optimizing continuous annealing of if steels for improving their deep drawability. Metall. Mater. Trans. A 32, 1989.
Juul Jensen, D., Hansen, N., Liu, Y.L., 1991. Mater. Sci. Technol. 2, 369.
Juul Jensen, D., Bolingbroke, R.K., Shi, H., Shahani, R., Furu, T., 1994. Mater. Sci. Forum 157–162, 1991.
Juul-Jensen, D., Hansen, N., Humphreys, F.J., 1988. Acta Metall. 33, 2155.
Juul-Jensen, D., 1992. Scr. Metall. Mater. 27, 533.
Juul-Jensen, D., 1995. Acta Metall. Mater. 43, 4117.
Kalisher, S., 1881. Über den Einfluss der Wärme auf die Molekularstruktur des Zinks. Ber. Dtsch. Chem. Ges. XIV, 2727–2753.
Keh, A.S., Weissman, S., 1963. In: Thomas, G., Washburn, J. (Eds.), Deformation Structure in Body-centered Cubic Metals. Electron Microscopy and Strength of Crystals. Interscience, New York, pp. 231–300.
Kinderlehrer, D., Livshits, I., Manolache, F., Rollett, A.D., Ta'asan, S., 2001. An approach to the mesoscale simulation of grain growth, influences of interface and dislocation behavior on microstructure evolution. In: Aindow, M., et al. (Eds.). Mat. Res. Soc. Symp. Proc., 652, p. Y1.5.
Kinderlehrer, D., Livshits, I., Rohrer, G.S., Ta'asan, S., Yu, P., 2004. Mesoscale evolution of the grain boundary character distribution, recrystallization and grain growth. Mater. Sci. Forum 467–470, 1063–1068.
Klement, U., Haasen, P., April 1993. In situ HVEM-investigations of the early stages of recrystallization in Cu-0.2 at.% Mn-single crystals. Acta Metall. Mater. 41 (4), 1075–1087.
Klinkenberg, C., Raabe, D., Lücke, K., 1992. Influence of volume fraction and dispersion rate of grain boundary cementite on the cold rolling textures of low carbon steels. Steel Res. 63, 227.
Kolmogorov, A.N., 1937. Statistical theory of crystallization of metals. Izv. Akad. Nauk SSSR, Met. 1, 355–359.
Konrad, J., Zaefferer, S., Raabe, D., 2006. Investigation of orientation gradients around a hard Laves particle in a warm rolled Fe3Al-based alloy by a 3D EBSD-FIB technique. Acta Mater. 54, 1369–1380.
Korbel, A., Embury, J.D., Hatherley, M., Martin, P.L., Erblöh, H.W., 1986. Acta Metall. 34, 1999.
Köster, U., 1974. Recrystallization involving a second phase. Metal Sci. 8, 151–160.
Krill III, C.E., Chen, L.-Q., 2002. Computer simulation of 3-D grain growth using a phase field model. Acta Mater. 50, 3057–3073.
Kuo, J.-C., Zaefferer, S., Zhao, Z., Winning, M., Raabe, D., 2003. Deformation behaviour of aluminium-bicrystals. Adv. Eng. Mater. 5 (8), 563–566.
Larson, B.C., Yang, W., Ice, G.E., Budai, J.D., Tischler, J.Z., 2002. Three-dimensional X-ray structural microscopy with submicrometre resolution. Nature 415, 887–890.
Laue, M.V., 1913. Röntgenstrahlinterferenzen. Z. Phys. 14, 1075–1079.
Lee, C.S., Duggan, B.J., 1993. Acta Metall. Mater. 41, 2691.
Leslie, W.C., Michalak, J.T., Aul, F.W., 1963a. In: Spencer, et al. (Eds.), Iron and Its Dilute Solutions. Publ. Interscience, NY.
Leslie, W.C., Plecity, F.J., Michalak, J.T., 1963b. Acta Metall. 11, 561.
Leslie, W.C., Michalak, J.T., Aul, F.W., 1963c. In: Spencer, Wemer, (Eds.), 1963c. Iron and Its Dilute Solid Solutions, 119. Interscience, New York, pp. 1470.
Li, C.H., Edwards, E.H., Washburn, J., Parker, E.R., 1953. Stress-induced movement of crystal boundaries. Acta Metall. 1, 223–229.
Li, J.C.M., 1961. J. Appl. Phys. 32, 525.
Li, J.C.M., 1962. Possibility of subgrain rotation during recrystallization. J. Appl. Phys. 33 (10), 2958–2965.
Liebman, B., Lücke, K., Masing, G., 1956. Untersuchung über die Orientierungsabhängigkeit der Wachstumsgeschwindigkeit bei der primären Rekristallisation von Aluminium-Einkristallen. Z. Metallkd. 47 (2), 57–63.
Lin, P., Palumbo, G., Harase, J., Aust, K.T., 1996. Acta Mater. 44, 4677.
Lins, J.F.C., Sandim, H.R.Z., Kestenbach, H.-J., Raabe, D., Vecchio, K.S., 2007. A microstructural investigation of adiabatic shear bands in an interstitial free steel. Mater. Sci. Eng., A 457, 205–218.
Liu, J., Mato, M., Doherty, R.D., 1989. Scr. Metall. 23, 1811.
Liu, X., Solberg, J.K., Gjengedal, R., Kluken, A.O., 1995. Mater. Sci. Technol. 11, 469.

Logé, R., Bernacki, M., Resk, H., Delannay, L., Digonnet, H., Chastel, Y., Coupez, T., 2008. Linking plastic deformation to recrystallization in metals using digital microstructures. Philos. Mag. 88, 3691–3712.
Lücke, K., Detert, K., 1957. A quantitative theory of grain boundary motion and recrystallization in metals in the presence of impurities. Acta Metall. 5 (11), 628–637.
Lücke, K., Stüwe, H.P., 1963. In: Himmel, L. (Ed.), On the Theory of Grain Boundary Motion. Recovery and Recrystallization of Metals. Interscience, New York, pp. 171–210.
Luton, M.J., Sellars, S.M., 1969. Acta Metall. 17, S. 1033.
Mahin, K., Hanson, K., Morris, J., 1980. Acta Metall. 28, 443.
Margulies, L., Winther, G., Poulsen, H.F., 2001. In situ measurement of grain rotation during deformation of polycrystals. Science 291 (5512), 2392–2394.
Martin, J.W., Doherty, R.D., 1976. Stability of Microstructure in Metallic Systems. Cambridge University Press, Cambridge. pp. 7–10.
Marx, V., Raabe, D., Engler, O., Gottstein, G., 1997. Simulation of the texture evolution during annealing of cold rolled bcc and fcc metals using a cellular automaton approach. Textures Microstruct. 28, 211–218.
Marx, V., Reher, F.R., Gottstein, G., 1998. Stimulation of primary recrystallization using a modified three-dimensional cellular automaton. Acta Mater. 47, 1219–1230.
Matsuo, M.I., 1989. ISIJ Int. 29, 809.
Maurice, C., Humphries, J., 1998. 2- and 3-d curvature driven vertex simulations of grain growth. In: Grain Growth in Polycrystalline Materials III, vol. 1. The Minerals, Metals and Materials Society, Warrnedale, pp. 81–90.
Maurice, C., 2001. 2- and 3-d curvature driven vertex simulations of grain growth. In: Proceedings of the First Joint International Conference on Recrystallization and Grain Growth, vol. 1. Springer-Verlag, Berlin, pp. 123–134.
May, J.E., Turnbull, D., 1958. Trans. Metall. Soc. AIME 769, 781.
McQueen, H.J., Jonas, J.J., 1975. Plastic Deformation of Materials. Acadamic Press, New York. pp. 393–493.
McQueen, H.J., Petkovic, R.A., Weiss, H., Hinton, L.G., 1976. In: Balance, J.B. (Ed.), The Hot Deformation of Austenite. AIME, New York, pp. 113–139.
McQueen, H.J., Evangelist, E., Ryan, N.D., 1990. In: Chandra, T. (Ed.), Recrystallization ('90) in Metals and Materials. TMS-AIME, Warrendale, PA, pp. 89.
McQueen, H.J., 1968. J. Met. 20 (4), 31.
Merriman, B., Bence, J., Osher, S., 1994. Motion of multiple junctions: a level set approach. J. Comput. Phys. 112, 334–363.
Metropolis, N., Rosenbluth, A.W., Rosenbluth, M.N., Teller, A.T., Teller, E., 1953. J. Chem. Phys. 21, 1087.
Miodownik, M.A., Martin, J.W., Cerezo, A., 1999. Philos. Mag. 79, 203.
Miodownik, M.A., 2002. A review of microstructural computer models used to simulate grain growth and recrystallisation in aluminium alloys. J. Light Met. 2, 125–135.
Miodownik, M., Holm, E.A., Hassold, G.N., Jun 13, 2000. Highly parallel computer simulations of particle pinning: Zener vindicated. Scr. Mater 42 (12), 1173–1177.
Miyazaki, A., Takao, K., Furukimi, O., 2002. ISIJ Int. 42, 916.
Molodov, D.A., Straumal, B.B., Shvindlerman, L.S., 1984. Scr. Metall. 18, 207.
Molodov, D.A., Gottstein, G., Shvindlerman, L.S., 1998. Grain Growth in Polycrystalline Materials III: Proceedings of [the] Third International Conference on Grain Growth, ICGG-3, June 14-19, 1998, Carnegie Mellon University, Pittsburgh, PA, USA.
Molodov, D.A., 2001. Grain Grain boundary boundary character – a key factor for grain boundary control. In: Gottstein, G., Molodov, D.A. (Eds.), 2001. Recrystallization and Grain Growth, vol. 1. Springer Verlag, Aachen, pp. 21–38.
Morawiec, A., 2000. Scr. Metall. 43, 275.
Mughrabi, H., Ungár, T., Kienle, W., Wilkens, M., 1986. Long-range internal stresses and asymmetric X-ray line-broadening in tensile-deformed [001]-orientated copper single crystals. Philos. Mag. A 53 (6), 793–813.
Mullins, W.W., 1956. J. Appl. Phys. 27, 900.
Nagai, T., Ohta, S., Kawasaki, K., Okuzono, T., 1990. Computer simulation of cellular pattern growth in two and three dimensions. Phase Trans. 28, 177–211.
Nes, E., 1995. Recovery revisited. Acta Metall. Mater. 43 (6), 2189–2207.
Orowan, E., 1934. Zur Kristallplastizität: iii. Über den Mechanismus des Gleitvorganges. Z. Phys. 89, 634–659.
Peczak, P., 1995. Acta Metall. 43, 1297.
Peranio, N., Li, Y.J., Roters, F., Raabe, D., 2010. Microstructure and texture evolution in dual-phase steels: competition between recovery, recrystallization, and phase transformation. Mater. Sci. Eng., A 527, 4161–4168.
Pezzee, C.E., Dunand, D.C., 1994. The impingement effect of an inert, immobile second phase on the recrystallization of a matrix. Acta Metall. 42, 1509–1522.
Pimenta Jr., F.C., Arruda, A.C.F., Padilha, A.F., 1986. Resistance to recrystallization in Al-1%Mn alloys. Z. Metallkd. 77 (8), 522–528.
Polanyi, M., 1934. Über eine Art Gitterstörung die einen Kristall plastich machen könnte. Z. Phys. 89, 660–664.

Potts, R.B., 1952. Proc. Cambridge Philos. Soc. 48, 106.
Poulsen, H.F., Nielsen, S.F., Lauridsen, E.M., Schmidt, S., Suter, R.M., Lienert, U., Margulies, L., Lorentzen, T.D., Juul Jensen, D., 2001. Three-dimensional maps of grain boundaries and the stress state of individual grains in polycrystals and powders. J. Appl. Crystallogr. 34, 751–756.
Raabe, D., Becker, R., 2000. Coupling of a crystal plasticity finite element model with a probabilistic cellular automaton for simulating primary static recrystallization in aluminum. Modell. Simul. Mater. Sci. Eng. 8, 445–462.
Raabe, D., Hantcherli, L., 2005. 2D cellular automaton simulation of the recrystallization texture of an IF sheet steel under consideration of Zener pinning. Comput. Mater. Sci. 34, 299–313.
Raabe, D., Lücke, K., 1992. Annealing textures of bcc metals. Scr. Metall. 27, 1533.
Raabe, D., Lücke, K., 1993. Textures of ferritic stainless steels. Mater. Sci. Technol. 9, 302–312.
Raabe, D., Schlenkert, G., Weisshaupt, H., Lücke, K., 1994. Texture and microstructure of rolled and annealed tantalum. Mater. Sci. Technol. 10, 229–305.
Raabe, D., Sachtleber, M., Zhao, Z., Roters, F., Zaefferer, S., 2001. Micromechanical and macromechanical effects in grain scale polycrystal plasticity experimentation and simulation. Acta Mater. 49, 3433.
Raabe, D., Zhao, Z., Park, S.–J., Roters, F., 2002a. Theory of orientation gradients in plastically strained crystals. Acta Mater. 50, 421–440.
Raabe, D., Klose, P., Engl, B., Imlau, K.-P., Friedel, F., Roters, F., 2002b. Concepts for integrating plastic anisotropy into metal forming simulations. Adv. Eng. Mater. 4, 169–180.
Raabe, D., Chen, N., Chen, L., 2004a. Polymer 45, 8265–8277.
Raabe, D., Roters, F., Barlat, F., Chen, L.-Q. (Eds.), 2004b. Continuum Scale Simulation of Engineering Materials. WILEY-VCH, Weinheim.
Raabe, D., 1995a. On the orientation dependence of static recovery in low-carbon steels. Scr. Metall. 33, 735–740.
Raabe, D., 1995b. Investigation of the orientation dependence of recovery in low-carbon steel by use of single orientation determination. Steel Res. 66, 222–229.
Raabe, D., 1996. On the influence of the chromium content on the evolution of rolling textures in ferritic stainless steels. J. Mater. Sci. 31, 3839–3845.
Raabe, D., 1997. Texture and microstructure evolution during cold rolling of a strip cast and of a hot rolled austenitic stainless steel. Acta Mater. 45, 1137–1151.
Raabe, D., 1998. Computational Materials Science. Wiley-VCH, Weinheim.
Raabe, D., 1999. Introduction of a scaleable 3D cellular automaton with a probabilistic switching rule for the discrete mesoscale simulation of recrystallization phenomena. Philos. Mag. A 79, 2339–2358.
Raabe, D., 2000. Scaling Monte Carlo kinetics of the Potts model using rate theory. Acta Mater. 48, 1617.
Raabe, D., 2001. Mesoscale simulation of recrystallization textures and microstructures. Adv. Eng. Mater. 3, 745–752.
Raabe, D., 2002. Cellular automata in materials science with particular reference to recrystallization simulation. Annu. Rev. Mater. Res. 32, 53.
Raabe, D., 2004. Acta Mater. 52, 2653–2664.
Raabe, D., 2007. J. Strain Anal. Eng. Des. 42, 253–268.
Radhakrishnan, B., Sarma, G.B., Zacharia, T., 1998. Acta Mater. 46 (12), 4415–4433.
Radhakrishnan, B., Sarma, G.B., Weiland, H., Baggethun, P., 2000. Modell. Simul. Mater. Sci. Eng. 8 (5), 737–750.
Rajmohan, N., Szpunar, J.A., Hayakawa, Y., 1999. Acta Mater. 47, 2999.
Randle, V., 1992. Microtexture Determination and Its Applications. The Institute of Materials, London.
Randle, V., 2004. Application of electron backscatter diffraction to grain boundary characterisation. Int. Mater. Rev. 49 (1), 1–11.
Randle, V., Engler, O., Aug 7, 2000. Introduction to Texture Analysis: Macrotexture, Microtexture and Orientation Mapping. Crc Pr Inc.
Rath, B.B., Hu, H., 1969a. Effect of driving force on the migration of high-angle tilt grain boundaries in aluminum bicrystals. Trans. Metall. Soc. AIME 245 (7), 1577–1585.
Rath, B.B., Hu, H., 1969b. Trans. Metall. Soc. AIME 245, 1243–1577.
Ray, R.K., Hutchinson, W.B., Duggan, B.J., 1975a. A study of the nucleation of recrystallization using HVEM. Acta Metall. 23 (7), 831–840.
Ray, R.K., Hutchinson, W.B., Duggan, B., 1975b. Acta Metall. 23, 831.
Reeh, S., Music, D., Gebhardt, T., Kasprzak, M., Japel, T., Zaefferer, S., Raabe, D., Richter, S., Schwedt, A., Mayer, J., Wietbrock, B., Hirt, G., Schneider, J.M., 2012. Elastic properties of face-centred cubic Fe-Mn-C studied by nanoindentation and ab initio calculations. Acta Materialia 60, 6025–6032.
Ridha, A.A., Hutchinson, W.B., 1982a. Acta Metall. 30, 1925.
Ridha, A.A., Hutchinson, W.B., 1982b. Acta Metall. 30, 1929.
Rios, P.R., 1987. A theory for grain-boundary pinning by particles. Acta Metall. 35 (12), 2805–2814.
Roberts, W., 1982. In: Krauss, G. (Ed.), Deformation, Processing and Structure. ASM, Metals Park, OH, pp. 109.
Rollet, A.D., Gottstein, G., Shvindlerman, L., Molodov, D., 2004. Grain boundary mobility – a brief review. Z. Metallkd. 95 (4), 226–229.
Rollett, A.D., Raabe, D., 2001. A hybrid model for mesoscopic simulation of recrystallization. Comput. Mater. Sci. 21, 69.
Rollett, A.D., Srolovitz, D.J., Doherty, R.D., Anderson, M.P., 1989a. Computer simulation of recrystallization in non-uniformly deformed metals. Acta Metall. 37 (2), 627–639.

Rollett, A.D., Srolovitz, D.J., Doherty, R.D., Anderson, M.P., 1989b. Acta Metall. 37, 627.
Rollett, A.D., Srolovitz, D.J., Anderson, M.P., 1989c. Acta Metall. 37, 1227.
Rollett, A.D., Luton, M.J., Srolovitz, D.J., 1992. Acta Metall. 40, 43.
Rollett, A.D., 1998. In: Weiland, H. (Ed.), Proceedings of the Third International Conference on Grain Growth. The Minerals, Metals and Materials Society, TMS Publication, Warrendale, PA.
Rollett, A.D., 1997. Overview of modeling and simulation of recrystallization. Prog. Mater. Sci. 42, 79–99.
Rosenhain, W., 1914. An Introduction to Physical Metallurgy. Constable, London.
Rossard, C., Blain, P., 1960. Mem. Sci. Rev. Metall. 57, 173.
Rossard, C., 1963. Écrouissage, Restauration, Recrystalisation. Presses Universitaires de France, Paris. p. 111.
Roters, F., Eisenlohr, P., Hantcherli, L., Tjahjanto, D.D., Bieler, T.R., Raabe, D., 2010. Overview of constitutive laws, kinematics, homogenization and multiscale methods in crystal plasticity finite-element modeling: theory, experiments, applications. Acta Mater. 58, 1152–1211.
Ruder, W.E., 1935. Am. Soc. Microbiol. 23, 534.
Russel, K.C., Ashby, M.F., 1970. Acta Metall. 18, 891.
Ryan, N.D., McQueen, H.J., 1990. High Temp. Technol. 8, 185.
Saetre, T., Hunderi, O., Nes, E., 1986. Acta Metall. 34, 981.
Safran, B.A., Sahni, P.S., Grest, G.S., 1983. Phys. Rev. B28, 2693.
Sahni, P.S., Srolovitz, D.J., Grest, G.S., Anderson, M.P., Safran, B.A., 1983. Phys. Rev. B28, 2705.
Sakai, T., Jonas, J.J., 1984. Acta Metall. 32 (2), 189.
Sakai, T., Akben, M.G., Jonas, J.J., 1983. Acta Metall. 31, 631.
Samajdar, I., Doherty, R.D., 1994. Scr. Metall. Mater. 31, 527.
Samajdar, I., Doherty, R.D., 1995. Scr. Metall. Mater. 32, 845.
Samajdar, I., Doherty, R.D., Kunze, K., 1992. Scr. Metall. 27, 1459.
Sandim, H.R.Z., Renzetti, R.A., Padilha, A.F., Raabe, D., Klimenkov, M., Lindau, R., Möslang, A., 2010. Annealing behavior of ferritic–martensitic 9%Cr–ODS–eurofer steel. Mater. Sci. Eng., A 527, 3602–3608.
Sandström, R., Lehtinen, B., Hedman, E., Groza, I., Karlsson, S., 1978. Subgrain growth in Al and Al-1% Mn during annealing. J. Mater. Sci. 13 (6), 1229–1242.
Schmidt, S., Nielsen, S.F., Gundlach, C., Margulies, L., Huang, X., Juul Jensen, D., July 2004. Science 305 (9), 229–232.
Schwartz, A.J., Kumar, M., Field, D.P., Adams, B.L. (Eds.), June 30 2009. Electron Backscatter Diffraction in Materials Science, second ed, Springer, Berlin.
Schwarzer, R., Weiland, H., 1986. In: Bunge, H.J. (Ed.), Experimental Techniques of Texture Analysis. DGM Informationsgesellschaft, Oberursel.
Sebald, R., Gottstein, G., 2002. Modeling of recrystallization textures: interaction of nucleation and growth. Acta Mater. 50, 1587–1598.
Sellars, C.M., Tegart, W.J.McG., 1966. Mem. Sci. Rev. Metall. 63, 731–746.
Sellars, C.M., 1978. Philos. Trans. R. Soc., A 288, 147–158.
Sheldon, R.K., Dunand, D.C., 1996. Computer modeling of particle pushing and clustering during matrix crystallization. Acta Mater. 44, 4571–4582.
Shimizu, R., Harase, J., 1989. Acta Metall. 37, 1241.
Shvindlerman, L.S., Gottstein, G., 1999. Recrystallization and related phenomena. In: Sakai, T., Suzuki, H.G. (Eds.), The Japan Inst. of Metals, Proc, Grain Boundary and Triple Junction Migration – the Latest Advances, vol. 13, pp. 431–438.
Shvindlerman, L.S., Czubayko, U., Gottstein, G., Molodov, D.A., 1995. In: Hansen, N., Juul Jensen, D., Liu, Y.L., Ralph, B. (Eds.), Proceedings 16th RISØ International Symposium on Materials Science: Microstructural and Crystallographic Aspects of Recrystallization, pp. 545.
Siqueira, R.P., Sandim, H.R.Z., Oliveira, T.R., Raabe, D., 2011. Composition and orientation effects on the final recrystallization texture of coarse-grained Nb-containing AISI 430 ferritic stainless steels. Mater. Sci. Eng., A 528, 3513–3519.
Smith, C.S., 1948. Grains, phases and interfaces, an interpretation of microstructure. Trans. Metall. Soc. AIME 175, 15.
Sorby, H.C., 1886. The application of very high powers to the study of the microscopical structure of steel. J. Iron Steel Inst. 30 (1), 140–145.
Sorby, H.C., 1887. On the microscopical structure of iron and steel. J. Iron Steel Inst. 31 (1), 255–288.
Srolovitz, D.J., Anderson, M.P., Sahni, P.S., Grest, G.S., 1984. Acta Metall. 32, 793.
Srolovitz, D.J., Grest, G.S., Anderson, M.P., 1985. Acta Metall. 33, 2233.
Srolovitz, D.J., Grest, G.S., Anderson, M.P., 1986a. Computer simulation of recrystallization—I. Homogeneous nucleation and growth. Acta Metall. 34, 1833–1845.
Srolovitz, D.J., Grest, G.S., Anderson, M.P., 1986b. Acta Metall. 34, 1833.
Srolovitz, D.J., Grest, G.S., Anderson, M.P., Rollett, A.D., 1988. Acta Metall. 36, 2115.
Stead, J.E., 1898. The crystalline structure of iron and steel. J. Iron Steel Inst. 53 (1), 145–205.
Straub, S., Blum, W., Maier, H.J., Ungar, T., Borbély, A., Renner, H., November 1996. Long-range internal stresses in cell and subgrain structures of copper during deformation at constant stress. Acta Mater. 44 (11), 4337–4350.
Stüwe, H.P., Padilha, A.F., Siciliano Jr, F., 2002. Competition between recovery and recrystallization. Mater. Sci. Eng., A A233, 361–367.

Stüwe, H.P., 1968. Deformation Under Hot Working Conditions. Iron Steel Inst., London. pp. 1–6.
Stüwe, H.P., 1978. In: Haessner, F. (Ed.), Driving and Dragging Forces in Recrystallization. Recrystallization of Metallic Materials. Dr. Riederer Verlag, Stuttgart, pp. 11–21.
Swan, P.R., 1963. In: Thomas, G., Washburn, J. (Eds.), Dislocations Arrangements in Face Centered Cubic Metals. Electron Microscopy and Strength of Crystals. Interscience, New York, pp. 131–181.
Tamhankar, R., Plateau, J., Crussard, C., 1958. Rev. Metall. 55, 383.
Tamura, N., Spolenak, R., Valek, B.C., Manceau, A., Meier Chang, M., Celestre, R.S., MacDowell, A.A., Padmore, H.A., Patel, J.R., 2002. Submicron X-ray diffraction and its applications to problems in materials and environmental science. Rev. Sci. Instrum. 73, 1369–1372.
Tamura, N., MacDowell, A.A., Spolenak, R., Valek, B.C., Bravman, J.C., Brown, W.L., Celestre, R.S., Padmore, H.A., Batterman, B.W., Patel, J.R., 2003. Scanning X-ray microdiffraction with sub-micrometer white beam for strain/stress and orientation mapping in thin films. J. Synchrotron Radiat. 10, 137–143.
Tavernier, P., Szpunar, J.A., 1991a. Acta Metall. 39, 549.
Tavernier, P., Szpunar, J.A., 1991b. Acta Metall. 39, 557.
Taylor, G.I., 1934. The mechanism of plastic deformation of crystals. Part I-Theoretical. Proc. R. Soc. London 145 (A), 312–387.
Thomas, I., Zaefferer, S., Friedel, F., Raabe, D., 2003. High resolution EBSD investigation of deformed and partially recrystallized IF steel. Adv. Eng. Mater. 5, 566–570.
Tsuji, N., Matsubara, Y., Sakai, T., Saito, Y., 1997. ISIJ Int. 37, 797.
Turnbull, D., Fisher, J.C., 1949. Rate of nucleation in condensed systems. J. Chem. Phys. 17, 71–73.
Tytko, D., Choi, P., Klöwer, J., Kostka, A., Inden, G., Raabe, D., 2012. Microstructural evolution of a Ni-based superalloy (617B) at 700 °C studied by electron microscopy and atom probe tomography. Acta Mater. 60, 1731–1740.
Upmanyu, M., Srolovitz, D.J., Shvindlerman, L.S., Gottstein, G., 1999. Misorientation dependence of intrinsic grain boundary mobility: simulation and experiment. Acta Mater. 47, 3901–3914.
Ushioda, K., Schlippenbach, U. v., Hutchinson, W.B., 1987. The effect of carbon content on recrystallisation and texture development in steel. Textures Microstruct. 7, 11–28.
Vandermeer, R.A., Juul Jensen, D., 1993. The migration of high angle grain boundaries during recrystallization. Interface Sci. 6 (1–2), 95–104.
Vandermeer, R.A., Rath, B.B., 1990. Interface migration during recrystallization: the role of recovery and stored energy gradients. Metall. Trans. A 21 (A), 1143–1149.
Varma, K., Willitis, B.L., 1984. Subgrain growth in aluminum during static annealing. Metall. Trans. A 15, 1502–1503.
Viswanathan, R., Bauer, C.L., 1973. Kinetics of grain boundary migration in copper bicrystals with [001] rotation axes. Acta Metall. 21 (8), 1099–1109.
von Neumann, J., 1952. Metal Interface. ASM, Cleveland, Ohio. pp. 108.
Walter, J.L., Koch, E.F., 1963. Substructures and recrystallization of deformed (100) [001]-oriented crystals of high purity silicon–iron. Acta Metall. 11 (8), 923–938.
Wassermann, G., Grewen, J., 1962. Texturen metallischer Werkstoffe. Springer-Verlag, Berlin.
Weiland, H., Schwarzer, R., 1984. Proc. ICOTOM 7, 857.
Wever, F., 1924. Über die Walzstruktur kubisch kristallisierender Metalle. Z. Phys. 28, 69–90.
Weygand, D., Brechet, Y., Lepinoux, J., 1999. Zener pinning and grain growth: a two-dimensional vertex computer simulation. Acta Mater. 47, 961–970.
Weygand, D., Brechet, Y., Lepinoux, J., 2001. A vertex simulation of grain growth in 2d and 3d. Adv. Eng. Mater. 3, 67–71.
Wilbrandt, P.-J., Haasen, P., 1979. HVEM study of the development of the recrystallization texture in deformed copper single crystals. Krist. Tech. 14 (11), 1379–1384.
Wilbrandt, P.-J., Haasen, P., 1980a. Z. Metallkd. 71, 273.
Wilbrandt, P.-J., Haasen, P., 1980b. Z. Metallkd. 71, 385.
Wilbrandt, P.-J., 1980. Phys. Status Solidi 61, 411.
Winning, M., Gottstein, G., Shvindlerman, L.S., 2001. Stress induced grain boundary motion. Acta Mater. 49, 211–219.
Winning, M., Gottstein, G., Shvindlerman, L.S., 2002. On the mechanisms of grain boundary migration. Acta Mater. 50, 353–363.
Winning, M., 2003. Motion of <100> tilt grain boundaries. Acta Mater. 50, 6465–6475.
Yang, W., Larson, B.C., Ice, G.E., Tischler, J.Z., Budai, J.D., Chung, K.S., Lowe, W.P., 2003. Spatially resolved Poisson strain and anticlastic curvature measurements in Si under large deflection bending. Appl. Phys. Lett. 82, 3856–3858.
Zaafarani, N., Raabe, D., Singh, R.N., Roters, F., Zaefferer, S., 2006. Three dimensional investigation of the texture and microstructure below a nanoindent in a Cu single crystal using 3D EBSD and crystal plasticity finite element simulations. Acta Mater. 54, 1863–1876.
Zaefferer, S., Kuo, J.-C., Zhao, Z., Winning, M., Raabe, D., 2003. On the influence of the grain boundary misorientation on the plastic deformation of aluminum bicrystals. Acta Mater. 51, 4719–4735.
Zaefferer, S., Wright, S.I., Raabe, D., 2008. Three-dimensional orientation microscopy in a focused ion beam-scanning electron microscope: a new dimension of microstructure characterization. Metall. Mater. Trans. A 39, 374–389.

Zaefferer, S., 2005. In: Proceedings of the 14th International Conference on textures of materials ICOTOM 14, 2005, Leuven, Belgium, Materials Science Forum. Application of Orientation Microscopy in SEM and TEM for the Study of Texture Formation during Recrystallisation Processes, vol. 495–497. Trans Tech Publications, Switzerland, pp. 3–12.

Zambaldi, C., Roters, F., Raabe, D., Glatzel, U., 2007. Mater. Sci. Eng., A 454–455, 433–440.

Zener, C., Smith, C.S., 1948. Grains, phases and interfaces: an interpretation of microstructure. Trans. Metall. Soc. AIME 175, 11–51.

Zhao, H., Chan, T., Merriman, B., Osher, S., 1996. A variational level set approach to multiphase motion. J. Comput. Phys. 127, 179–195.

Zhao, Z., Roters, F., Mao, W., Raabe, D., 2001. Introduction of a texture component crystal plasticity finite element method for industry-scale anisotropy simulations. Adv. Eng. Mater. 3, 984–990.

Zhao, Z., Mao, W., Roters, F., Raabe, D., 2004. A texture optimization study for minimum earing in aluminium by use of a texture component crystal plasticity finite element method. Acta Mater. 52, 1003–1012.

Biography

Dierk Raabe holds a Ph.D. degrees in physical metallurgy anm etal physics from RWTH Aachen. Currently he is Chief Executive of the Max-Planck Institut für Eisenforschung in Düsseldorf and Professor at RWTH Aachen. His focus is in physical metallurgy and materials physics. Specifically he works on the simulation and mechanical properties of metallic alloys. The aim is the design of materials with superior properties (strength, elongation, damage tolerance) for the fields of energy, mobility and health from the atomic to the macro-scale under consideration of synthesis and processing. He received the Leibniz-Award and an ERC advanced grant. He is a member of the Science Advisory Board of the German Government and chairs the Governors Board of RWTH Aachen University. He is a member of the National Academy Leopoldina.